SOUTHERN CALIFORNIA BIGHT SEA LEVEL RESPONSE TO LOCAL ATMOSPHERIC FORCING

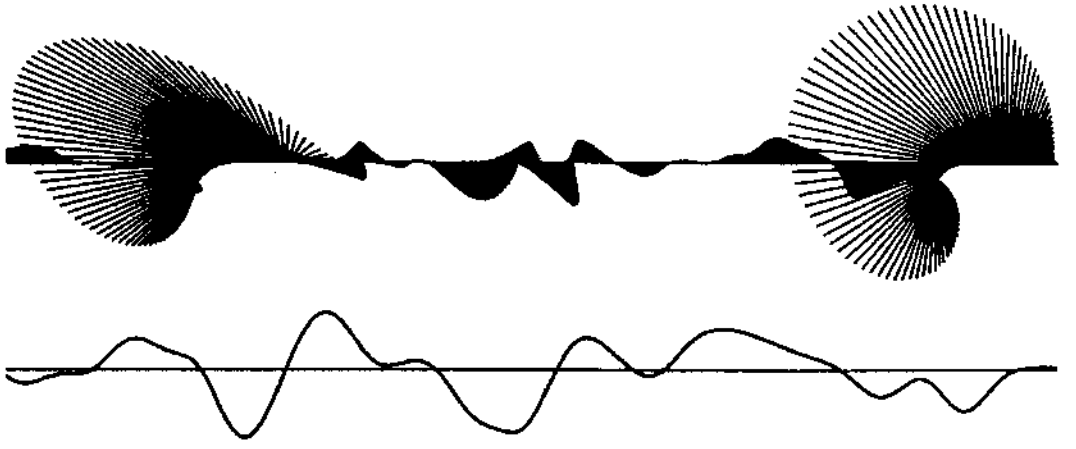

T. C-Y. FU

January 1988

UNIVERSITY OF CALIFORNIA, SAN DIEGO

Southern California Bight Sea Level Response to Local Atmospheric Forcing

A thesis submitted in partial satisfaction of the requirements for the degree Master of Science in Oceanography

by

Thomas Chung-Yee Fu

Committee in charge:

Professor Lynne D. Talley, Chairperson
Professor Myrl C. Hendershott
Professor Russ E. Davis
Professor Charles S. Cox
Professor Michael M. Mullin
Doctor Reinhard E. Flick

1988

The thesis of Thomas Chung-Yee Fu is approved:

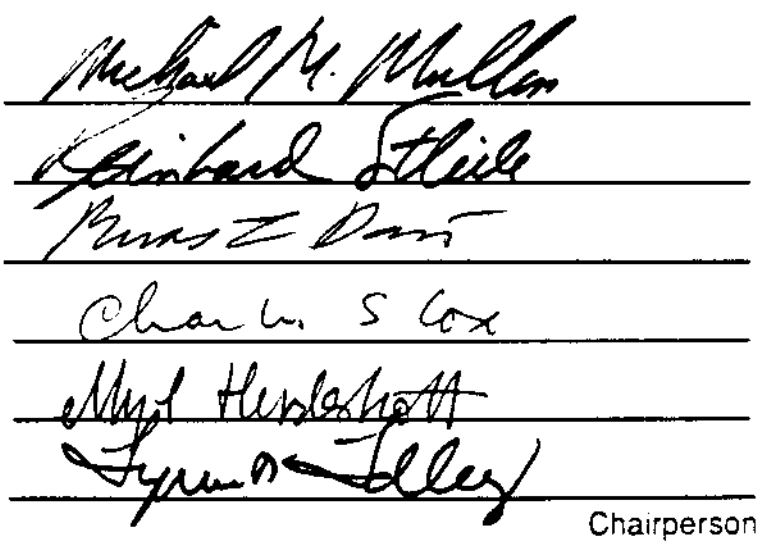

Chairperson

University of California, San Diego

1988

in memory of King-Sun Fu

Table of Contents

Page

List of Symbols

t	time
x	cross-shore coordinate
y	longshore coordinate
η	elevation of the sea surface
u,v	x, y components of the depth averaged current
τ_{sx}, τ_{sy}	x, y components of the wind stress on the sea surface
τ_{bx}, τ_{by}	x, y components of the bottom stress
P	atmospheric pressure
h	total water depth ($= D + \eta$, where D is the undisturbed water depth
ρ	density of sea water, assumed uniformed
g	acceleration due to gravity
f	coriolis parameter ($= 2\omega\sin\phi$, where ω is the angular speed of the Earth's rotation and ϕ is latitude)
K	bottom stress parameter
$H(t)$	Heavyside's Function
l	shelf width
a	arbitrary distance offshore, $a > l$

Page

List of Symbols

t	time
x	cross-shore coordinate
y	longshore coordinate
η	elevation of the sea surface
u,v	x, y components of the depth averaged current
τ_{sx}, τ_{sy}	x, y components of the wind stress on the sea surface
τ_{bx}, τ_{by}	x, y components of the bottom stress
P	atmospheric pressure
h	total water depth (= D + η, where D is the undisturbed water depth
ρ	density of sea water, assumed uniformed
g	acceleration due to gravity
f	coriolis parameter (= $2\omega\sin\phi$, where ω is the angular speed of the Earth's rotation and ϕ is latitude)
K	bottom stress parameter
$H(t)$	Heavyside's Function
l	shelf width
a	arbitrary distance offshore, $a > l$

b	arbitrary distance offshore, $b < l$
L	arbitrary distance offshore, $L > a$

List of Figures and Tables

Acknowledgements

During the past 18 months I've had the good fortune of working with Dr. Lynne D. Talley, Dr. Reinhard E. Flick and Daniel R. Cayan on the subject of this thesis. Dr. Talley was a source of great help and support, always taking the time to listen, discuss and teach. Dr. Flick deserves special thanks, for he got me started here at Scripps. His encouragement and help in the analysis of the data were essential to this study. His time and effort are much appreciated. Dan Cayan provided another set of ears to bend. His thoughts on the subject were always welcome and of great use.

The students and staff at the Center for Coastal Studies deserve much thanks for their support and contributions to this thesis. Mike Clark's fine work is displayed in the figures used in this thesis. Julio Candela, Mark Merrifield, Bill O'Reilly, Thomas Herbers and Karen May all deserve special thanks for their help and expertise in the analysis of the data sets.

This work would not have come to be, if not for the support and encouragement of my wife, Tracy. Her tolerance of my work habits and generous good nature are very much appreciated. As are

the encouragement and support shown to me by family and friends.

Finally, I would like to thank the people whose financial support made this possible. A portion of my financial support was provided by the California Department of Boating and Waterways. This work is the result of research sponsored by NOAA, National Sea Grant College Program, Department of Commerce, under grant number NA85AA-D-SG140, project number R/CZ-76, through the California Sea Grant College Program and in part by the California State Resources Agency. The U.S. Government is authorized to reproduce and distribute for governmental purposes.

ABSTRACT OF THE THESIS

Southern California Bight Sea Level Response

to Local Atmospheric Forcing

By

Thomas Chung-Yee Fu

Master of Science in Oceanography

University of California, San Diego, 1988

Professor Lynne D. Talley, Chairperson

The winter of 1982 -1983 was marked by the occurence of many extreme sea level events associated with strong North Pacific storms. A multiple - input linear statistical model, as well as direct examination of coastal and offshore sea level and meteorological data for five storm events were utilized in investigating the effects of the local atmospheric forcing on coastal sea level. The sea level variations under study were restricted to the frequency range 0.80 to 0.0333 cpd (periods of 1.25 to 30 days) to minimize tidal effects.

The statistical analysis revealed that local meteorological

forcing and sea surface temperature could explain approximately 80% of the variance of the sea level anomaly (measured sea level - predicted tide) in the winter, when storms were common. The amount of variance explained dropped to 45% the following summer.

Both the statistical analysis and case studies demonstrated that, at these time scales, longshore wind stress had a greater influence on coastal sea level than did cross-shore wind stress.

Examination of Santa Catalina and Newport Beach sea level records showed that the cross-shore spatial scale of the sea surface response was greater than the tide gauge spacing (~ 50 km). It also seen that Santa Catalina island did not act as a barrier to atmospherically forced water motions at these time scales (1.25 - 30 days).

Chapter 1 Introduction

In terms of loss of life and property damage, storm induced coastal flooding has become the world's foremost natural hazard. As atmospheric weather systems pass over ocean areas, water level oscillations are induced both by the wind stress and the horizontal gradients in atmospheric pressure associated with such systems. Storm surge is by definition restricted to the storm induced oscillations of water level with periods ranging from a few minutes to a few days. This definition excludes the wind waves which typically have periods on the order of a few to several seconds. These high frequency waves do play a significant role in the coastal flooding problem and can contribute directly to high coastal sea levels due to wave set-up, but these effects are not considered in this thesis. It is the combination of large amplitude storm surge, large amplitude wind waves and high tides which can cause enormous devastation to coastal areas.

One of the most destructive surges of the century occured in November 1970. Bangledesh, which has the Bay of Bengal as its southernmost border, was struck by a surge with an estimated

amplitude of over 7 m. Tide gauges were unable to measure the maximum sea level as the maximum recordable sea level was exceeded. This surge resulted in 200,000 to 300,000 deaths as well as hundreds of millions of dollars in damage.

Much of the work done on the study of storm surge has dealt with the large, highly destructive surges found in broad, shallow areas such as the continental shelf regions of the Bay of Bengal, the North Sea and the Gulf of Mexico. In those areas and many others storm surge can play a dominant role in coastal flooding. But often it is the coincidence of storm surge with high tides and other oceanographic factors which generates coastal flooding.

It was the occurence of many oceanographic and meteorological factors which caused the extensive (damage estimates totaled over $100,000,000) coastal floods of the winter of 1982-1983 along the California coast. In addition to wave attack (Seymour et al, 1984), Cayan and Flick (1985) identified four of these factors to be;

1) High predicted astronomical tides;

2) Storm surge due to strong North Pacific storms;

3) High sea level associated with the El Nino event of 1982-1983;

4) The cumulative effect of slow, secular rise in sea level.

Tides, which are the most predictable of all oceanic processes, contribute the largest amount of variance to the sea level signal. However, it has been suggested (Flick, 1986) that more than half of the variance of sea level anomaly (observed level minus predicted tide) at short (hours to days) time scales can be related to atmospheric forcing by pressure and wind. Secular sea level rise, though important for its long term effects on coastal regions, is negligible for day to day or even year to year variations. Similarly, the increased ocean temperatures associated with El Ninos generally influence sea surface variability on seasonal time scales. Monthly mean sea levels, in 1983, were on the order of 10 cm above the long term monthly means. This sea level rise played a significant role in the coastal flooding seen that year, but the influence of El Nino events on high frequency sea level anomalies is most likely due to enhanced storminess in the central North Pacific, which is attributed to El Nino episodes, not to above

normal water temperatures.

1.1 Storm surge dynamics

Storm surges, which are long gravity waves, belong to the same class of waves as tides and tsunamis. An important distinction though is that while tides and tsunamis occur on the oceanic scale, storm surges are a coastal phenomenon.

The dynamical theory of tides and storm surges is based primarily upon the one-layer shallow water equations. Depth averaging provides a useful simplification of the problem. This is justifiable since the main concern is with water level which is not directly influenced by details of the variation of current with depth. Stratification has been shown by Roed (1979) to have no appreciable effect on the surge at the coast. That is, the barotropic effects seem to be more strongly excited than the baroclinic modes. In cartesian coordinates (x, y) in the horizontal plane of the mean sea level, the depth averaged equations of motion and continuity are

$$\frac{\partial u}{\partial t} + u\frac{\partial u}{\partial x} + v\frac{\partial u}{\partial y} - fv = -g\frac{\partial \eta}{\partial x} - \frac{1}{\rho}\frac{\partial P}{\partial x} + \frac{1}{\rho h}(\tau_{sx} - \tau_{bx})$$

$$\frac{\partial v}{\partial t} + u\frac{\partial v}{\partial x} + v\frac{\partial v}{\partial y} + fu = -g\frac{\partial \eta}{\partial y} - \frac{1}{\rho}\frac{\partial P}{\partial y} + \frac{1}{\rho h}(\tau_{sy} - \tau_{by}) \qquad (1.1.1)$$

$$\frac{\partial \eta}{\partial t} + \frac{\partial (hu)}{\partial x} + \frac{\partial (hv)}{\partial y} = 0$$

where:

t = time,

u,v = x, y components of the depth-mean current,

η = elevation of the sea surface,

τ_{sx}, τ_{sy} = x, y components of the wind stress on the sea surface,

τ_{bx}, τ_{by} = x, y components of the bottom stress,

P = atmospheric pressure on the sea surface,

h = the total water depth (= D + η where D is the undisturbed depth),

ρ = the density of sea water, assumed uniform,

g = the acceleration due to gravity,

f = the coriolis parameter (= $2\omega \sin\phi$, where ω is the angular speed of the Earth's rotation and ϕ is latitude)

Equations (1.1.1) equate the acceleration of the water to the forces acting on it. It can be seen immediatly from equations (1.1.1) that since the wind stress is divided by the water depth, h, the wind stress is less effective in generating storm surge in deep

water (h large) than in shallow water (h small). This is not true of the pressure forcing, since the pressure terms in (1.1.1) are independent of depth.

1.2 Previous work

Fluctuations of sea level elevation along coastal regions are the result of many and varied processes. Tides dominate the shortest time scale changes (on the order of one day), with meteorological and steric effects usually becoming more important at time scales of days to months. High frequency fluctuations are also present and due to wind forced waves (Lisitzen, 1974).

Much work has been done in the area of tidal analysis and prediction. Tidal structure and variability in the Southern California Bight region has been described by Munk et al (1970) and Bratkovich (1985). Zetler and Flick (1985a,b) have discussed the factors controlling extreme tides and have published detailed predictions of peak tides in California up to the year 2000.

Studies of long - term secular trends in sea level have become the focus of much attention recently due to the concern over global atmospheric warming trends, and their effects on sea level. Much of the work in this area centers around the problem of

extracting a global trend from regional patterns and from tectonic and other "noise", which are all present in the sea level signal. Aubrey and Emery (1983) and Barnett (1983, 1984) have employed statistical methods to more objectively separate spacial and temporal patterns. Though studies of long - term trends are limited due to poor spacial coverage and insufficient record lengths, it is generally believed that a slow secular rise in sea level, about 10cm/century, along the California coast has been seen over the last 80 years (Flick and Cayan, 1985).

During the past ten years a considerable amount of work has been done in examining and describing the sea level variability with time periods on the order of one month. Anomalous sea levels along the west coast of North America have been shown to be strongly correlated with large Pacific Ocean scale meteorological and oceanographic events at this time scale (Wyrtki, 1985; Emery and Hamilton, 1985; Chelton and Davis, 1982; Christensen and Rodriguez, 1979; Reid and Mantyla, 1976; Roden, 1966). Simpson (1984) demonstrated the association between basin wide, tropical El Nino - Southern Oscillation (ENSO) events and elevated coastal sea levels in California at time scales of months to years.

It has been suggested that anomalous sea levels are due not to only local meteorological events, but that sea level variations with periods on the order of one month propagate poleward as coastally trapped, subinertial waves from sources as far south as the tropical east Pacific. The dynamics of these coastally trapped waves are discussed in Mysak (1980), Enfield and Allen (1980, !983) and many others. It also appears that the longshore component of the wind field plays an important role in creating monthly sea level variations (Lentz, 1984, Chelton and Davis, 1982).

Studies performed by Simpson (1983, 1984) suggest that surface and subsurface oceanic temperatures contributed to the anomalous sea levels during the winter of 1982 - 1983. Simpson also shows that upper ocean anomalous warming in 1982 - 1983 was associated with a positive anomaly of steric height in the Southern California Bight region.

1.3 Overview

Much of the theoretical work on storm surges has dealt with wind stress forcing on broad shelves and in shallow coastal regions. This has been motivated by the fact that the largest destructive

surges occur in these shallow, broad areas where the wind stress forcing term is large. The deeper and narrower continental shelf off the southern California coast suggests that pressure gradient forcing might play a more important role in sea level variability. Also due to the narrowness of the shelf, offshelf atmospheric forcing might contribute significantly to coastal sea level anomalies.

Southern California sea level and meteorological data allows for the investigation of both wind stress and pressure gradient forcing over deep water, and its effects on coastal and offshore island sea level.

The aim of this study is to explore the nature and mechanisms of storm surge generation on the California coast through analytical modelling
and statistical description of measured sea level anomalies. The emphasis is on examining the consequences of localized atmospheric forcing as well as on the time and spatial scale of the observed surge generation.

The thesis is divided into two parts. The first part, chapter 2, examines analytical models of storm surge. The second

part is concerned with data analysis. Meteorological and sea surface temperature data were used as inputs in a linear statistical model of sea level. Wind and atmospheric pressure data, for five winter storm events, were also examined.

Chapter 2 Mathematical Model

It has been shown that simple mathematical models describing wind-induced motion on a continental shelf can achieve first-order accuracy (McIntyre, 1979; Heaps, 1965). A mathematical model similar to those of Heaps (1965), Flather (1971) and McIntyre (1979) is employed to investigate the dynamic response of the water on an idealized shelf, of uniform depth and width, to offshelf wind stress fields.

Heaps examined the effects of wind stress over an idealized continental shelf, bounded by an infinitely long straight coast and connected with an infinite ocean. The boundary conditions Heaps imposed are that there is no normal flow at the coast, and that the sea level elevation is zero at the shelf edge. Flather and McIntyre extended Heaps work by considering an ocean of uniform depth and width instead of an infinite ocean. They relax the shelf edge condition and impose no normal flow at the ocean coast. The wind stress forcing is still limited to the continental shelf.

The objective of the present work is to modify the model further to examine the effects of offshelf wind stress on coastal

sea level elevation. The model uses the same geometry as Flather and McIntyre, with slightly different boundary conditions. No normal flow at the shelf coast and zero sea level elevation at an arbitrarily long distance from the wind stress forcing are employed. The wind stress forcing is imposed over an area between the shelf edge and an arbitrary offshore deep water boundary. The cross-sectional geometry of the model is shown in Figure 2.1.

The motivation for such a model is to examine the effects of an offshelf wind stress field on coastal sea level. Comparison with the earlier models can be made, including the effects of shelf width, shelf and ocean depth, rotation, and bottom friction on the sea level response.

2.1 Basic equations

The linearized vertically-integrated equations of motion and continuity are:

$$\frac{\partial u}{\partial t} - fv = -g\frac{\partial \eta}{\partial x} - \frac{1}{\rho}\frac{\partial P}{\partial x} + \frac{\tau_{sx}-\tau_{bx}}{\rho h}$$

$$\frac{\partial v}{\partial t} + fu = -g\frac{\partial \eta}{\partial y} - \frac{1}{\rho}\frac{\partial P}{\partial y} + \frac{\tau_{sy}-\tau_{by}}{\rho h} \qquad (2.1.1)$$

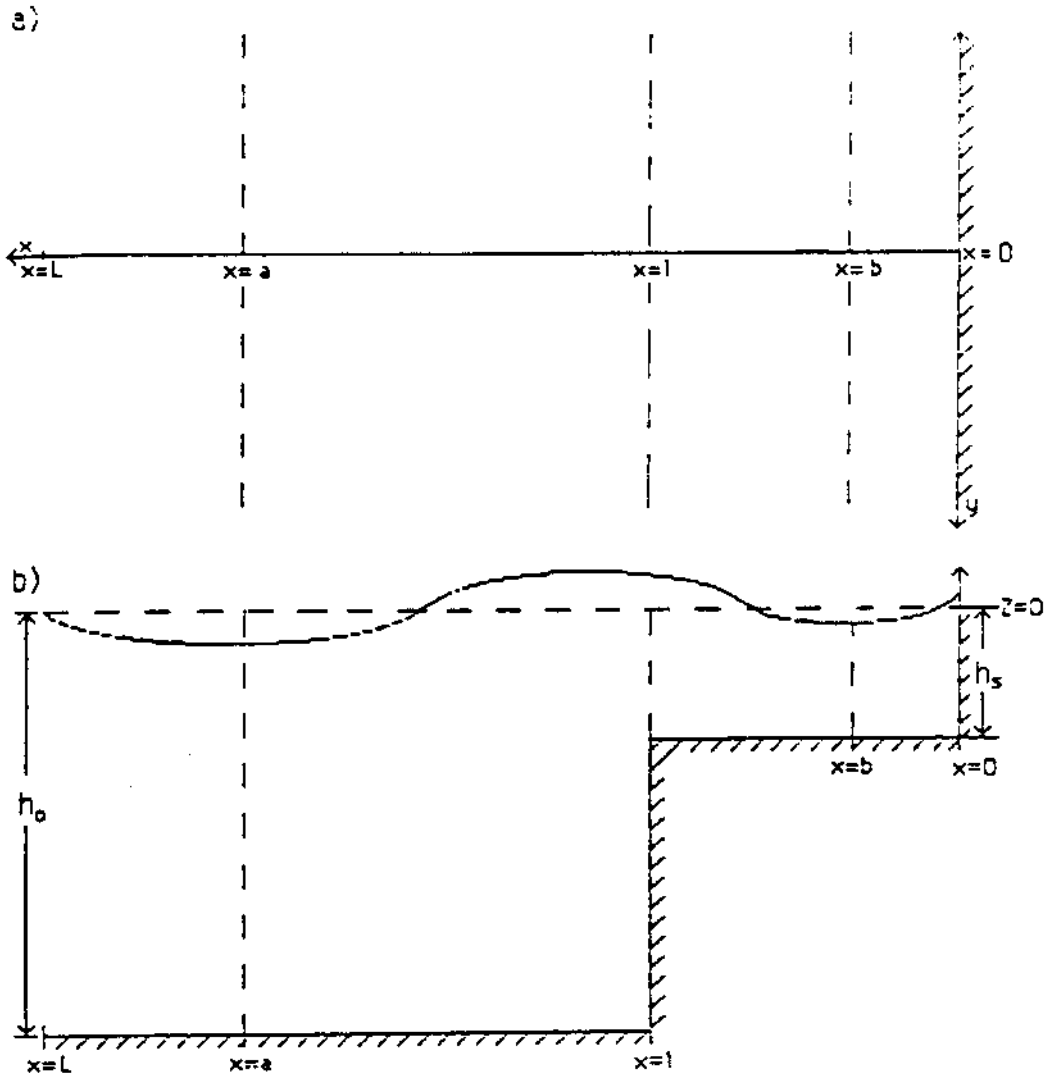

Figure 2.1: Geometry of the idealized shelf-ocean system a) plan view, b) cross-sectional view.

$$\frac{\partial u}{\partial x}+\frac{\partial v}{\partial y}+\frac{1}{h}\frac{\partial \eta}{\partial t}=0$$

Following Heaps (1965) and McIntyre (1979),it is assumed the bottom stress takes the form

$$\tau_{bx}= 2K\rho hu \qquad (2.1.2a)$$

$$\tau_{by}= 2K\rho hv\,, \qquad (2.1.2b)$$

where K is some constant. Then (2.1.1) becomes

$$\begin{aligned}
&\frac{\partial u}{\partial t}+2Ku-fv=-g\frac{\partial \eta}{\partial x}-\frac{1}{\rho}\frac{\partial P}{\partial x}+\frac{\tau_{sx}}{\rho h}\\
&\frac{\partial v}{\partial t}+2Kv+fu=-g\frac{\partial \eta}{\partial y}-\frac{1}{\rho}\frac{\partial P}{\partial y}+\frac{\tau_{sy}}{\rho h} \qquad (2.1.3)\\
&\frac{\partial u}{\partial x}+\frac{\partial v}{\partial y}+\frac{1}{h}\frac{\partial \eta}{\partial t}=0\,.
\end{aligned}$$

Now assuming that the motion on the shelf is the same for all sections normal to the coast, dependency on the alongshore coordinate y is eliminated and equations (2.1.3) reduce to

$$\frac{\partial u}{\partial t}+2Ku-fv=-g\frac{\partial \eta}{\partial x}-\frac{1}{\rho}\frac{\partial P}{\partial x}+\frac{\tau_{sx}}{\rho h}$$

$$\frac{\partial v}{\partial t} + 2Kv + fu = \frac{\tau_{sy}}{\rho h} \qquad (2.1.4)$$

$$\frac{\partial u}{\partial x} + \frac{1}{h}\frac{\partial \eta}{\partial t} = 0 .$$

Solutions to (2.1.4) are obtained yielding water motion over the shelf and in the ocean induced by a uniform wind stress field imposed at time t=0 over that part of the ocean lying between x=1 and x=a (Figure 2.1). The surface wind stress field is defined by

$$\frac{\partial P}{\partial x} = 0$$

$$\tau_{sx} = \tau_{sy} = 0 \quad , \qquad \text{for} \quad 0 < x < 1$$

$$\tau_{sx} = -PH(t) \quad , \quad \tau_{sy} = Qh(t) \qquad \text{for} \quad 1 < x < a$$

$$\tau_{sx} = \tau_{sy} = 0 \quad , \qquad \text{for} \quad a < x < L$$

where H(t) denotes the Heavyside unit function; P, Q are constants representing onshore and longshore stress components. Under these conditions equations (2.1.4) become, for $0 < x < 1$

$$\frac{\partial u}{\partial t} + 2Ku - fv = -g\frac{\partial \eta}{\partial x}$$

$$\frac{\partial v}{\partial t} + 2Kv + fu = 0 \qquad (2.1.5)$$
$$\frac{\partial u}{\partial x} + \frac{1}{h_s}\frac{\partial \eta}{\partial t} = 0$$

and for $1 < x < a$

$$\frac{\partial u}{\partial t} + 2Ku - fv = -g\frac{\partial \eta}{\partial x} - \frac{PH(t)}{\rho h_o}$$
$$\frac{\partial v}{\partial t} + 2Kv + fu = \frac{QH(t)}{\rho h_o} \qquad (2.1.6)$$
$$\frac{\partial u}{\partial x} + \frac{1}{h_o}\frac{\partial \eta}{\partial t} = 0$$

and for $a < x < L$

$$\frac{\partial u}{\partial t} + 2Ku - fv = -g\frac{\partial \eta}{\partial x}$$
$$\frac{\partial v}{\partial t} + 2Kv + fu = 0 \qquad (2.1.7)$$
$$\frac{\partial u}{\partial x} + \frac{1}{h_o}\frac{\partial \eta}{\partial t} = 0$$

Initially, the water is considered to be at rest so that, everywhere

$$u = v = 0 \qquad \text{at } t = 0. \qquad (2.1.8)$$

Boundary conditions of zero normal flow at the coastline

$$u = 0 \qquad \text{at } x = 0, \qquad (2.1.9)$$

and sea level elevation equal to zero far away from the wind stress field

$$\eta = 0 \qquad \text{at } x = L \tag{2.1.10}$$

must be satisfied. Similarly to the work by Heaps (1965) and Flather (1971), the equations are solved analytically using the Laplace transformation.

2.2 Review of previous models

The Heaps' shelf model is the simplest model, examining the coastal sea level response to a wind stress field, created suddenly, over a continental shelf. All motion is restrained to the shelf area, with all deep water and oceanic effects assumed to be small. The wind stress takes the following form

$$\frac{\partial P}{\partial x} = 0$$

$$\tau_{sx} = \tau_{sy} = 0 \ , \qquad \text{for} \quad 0 < x < b$$

$$\tau_{sx} = -PH(t) \ , \ \tau_{sy} = Qh(t) \qquad \text{for} \quad b < x < 1 \ ,$$

and the boundary conditions are,

$$u = 0 \qquad \text{at } x = 0 \tag{2.2.1}$$

$$\eta = 0 \qquad \text{at } x = 1 \ . \tag{2.2.2}$$

Using Laplace transformations, the solution to equations (2.1.4) for Heaps' shelf model is:

$$\eta = \left[P - \frac{fQ}{2K}\right] \frac{1-b}{\rho g h_s}$$

$$+\sum_{n=1}^{\infty} (-1)^n \frac{(2K-\lambda_n)\,[P(2K-\lambda_n) - fQ]}{\rho l \lambda_n \left[(K-\lambda_n)(2K-\lambda_n)^2 + Kf^2\right]}$$

$$x \sin\left[\frac{(2n-1)\pi(1-b)}{2l}\right] e^{-\lambda_n t} \tag{2.2.3}$$

$$+\sum_{n=1}^{\infty} (-1)^n \frac{2 I_n}{\rho l E_n} \sin\left[\frac{(2n-1)\pi(1-b)}{2l}\right]$$

$$x \cos\left(\nu_n t - \chi_n + \Phi_n\right) e^{-\mu_n t}$$

where

$$I_n = \left[\frac{P^2 - 2PQf(2K-\mu_n)/d_n^2 + f^2Q/d_n^2}{\mu_n^2 + \nu_n^2}\right]^{1/2}$$

$$E_n = \left\{ \left[K - \mu_n + (Kf^2/d_n^2) \cos 2\Theta_n \right]^2 + \left[\nu_n - (Kf^2/d_n^2) \sin 2\Theta_n \right]^2 \right\}^{1/2}$$

$$\chi_n = \tan^{-1} \left[\frac{\nu_n - (Kf^2/d_n^2) \sin 2\Theta_n}{K - \mu_n + (Kf^2/d_n^2) \cos 2\Theta_n} \right]$$

$$\Phi_n = \tan^{-1} \left[\frac{\nu_n (Qf/d_n^2)}{P - (Qf/d_n^2)(2K - \mu_n)} \right] + \tan^{-1} \left(\frac{\nu_n}{\mu_n} \right)$$

$$d_n = \left[(2K - \mu_n)^2 + \nu_n^2 \right]^{1/2}$$

$$\Theta_n = \tan^{-1} \left[\nu_n / (2K - \mu_n) \right]$$

and where

$$S = -\lambda_n \, , \quad -\mu_n \pm i\nu_n$$

are the roots of the cubic

$$S[\, S + 2K + f^2/(S+2K) \,] = -gh_s(2n-1)^2 \pi^2/4l^2 \quad . \qquad (2.2.4)$$

This gives the coastal sea surface elevation, at any time following

the sudden creation of a wind field between x = b and x = l, on the continental shelf.

McIntyre modifies the shelf edge boundary condition used by Heaps and considers the effects of an ocean of uniform depth and width connected to the shelf. The boundary conditions then become:

$$u = 0 \qquad \text{at } x = 0, L \ . \tag{2.2.5}$$

The wind stress field is the same as in the Heaps' model.

$$\frac{\partial P}{\partial x} = 0$$

$$\tau_{sx} = \tau_{sy} = 0 \qquad \text{for} \quad 0 < x < b$$

$$\tau_{sx} = -PH(t) \ , \ \tau_{sy} = Qh(t) \qquad \text{for} \quad b < x < 1$$

This leads to the following solution to equations (2.1.4)

$$\eta = \left[P - \frac{fQ}{2K}\right]\left(\frac{1-b}{\rho g h_s}\right)\left(1 - \frac{b+1}{2L}\right)$$

$$+ 2N \sum_{n=1}^{\infty} \frac{(2K - \lambda_n)\,[P(2K - \lambda_n) - fQ]}{\rho l \lambda_n \left[(2K - 2\lambda_n)(2K - \lambda_n)^2 + 2Kf^2\right]}$$

$$x \frac{\left\{\cos\left(\frac{m_n b}{l}\right) - \cos(m_n)\right\} \cos(m_n N) \cos\left(\frac{m_n x}{l}\right)}{\left\{\begin{matrix}(1 + MN)\sin(m_n)\sin(m_n N) \\ -(M+N)\cos(m_n)\cos(m_n N)\end{matrix}\right\}\cos(m_n)} e^{-\lambda_n t}$$

(2.2.6)

$$+ 4N \sum_{n=1}^{\infty} \frac{I_n}{\rho l E_n} \cos(\nu_n t + \phi_n - \psi_n)$$

$$x \frac{\left\{\cos\left(\frac{m_n b}{l}\right) - \cos(m_n)\right\} \cos(m_n N) \cos\left(\frac{m_n x}{l}\right)}{\left\{\begin{matrix}(1 + MN)\sin(m_n)\sin(m_n N) \\ -(M+N)\cos(m_n)\cos(m_n N)\end{matrix}\right\}\cos(m_n)} e^{-\mu_n t}$$

where

$$I_n = \left[\frac{P^2 - 2PQf(2K - \mu_n)/d_n^2 + f^2 Q/d_n^2}{\mu_n^2 + \nu_n^2}\right]^{1/2}$$

$$E_n = \left\{\left[2K - 2\mu_n + (2Kf^2/d_n^2)\cos 2\theta_n\right]^2 + \left[2\nu_n - (2Kf^2/d_n^2)\sin 2\theta_n\right]^2\right\}^{1/2}$$

$$\Phi_n = \tan^{-1}\left[\frac{\nu_n\,(Qf/\,d_n^2)}{P - (Qf/\,d_n^2)\,(2K - \mu_n)}\right] + \tan^{-1}\left(\frac{\nu_n}{\mu_n}\right)$$

$$\Psi_n = \tan^{-1}\left[\frac{2\nu_n - (2Kf^2/\,d_n^2)\,\sin 2\Theta_n}{2K - 2\mu_n + (2Kf^2/\,d_n^2)\cos 2\Theta_n}\right]$$

$$d_n = \left[(2K - \mu_n)^2 + \nu_n^2\right]^{1/2}$$

$$\Theta_n = \tan^{-1}\left[\nu_n \Big/ (2K - \mu_n)\right]$$

and where

$$M = \frac{L - l}{l}\left(\frac{h_s}{h_o}\right)^{1/2},\quad N = \left(\frac{h_s}{h_o}\right)^{1/2}. \qquad (2.2.7)$$

Here

$$S = -\lambda_n,\ -\mu_n \pm -i\nu_n .$$

are the roots of the cubic equation

$$S[\, S + 2K + f^2/(S+2K)\,] = -gh_s m_n^2 / l^2 \,, \qquad (2.2.8)$$

$m = m_n$ being the nth positive roots, in ascending order, of:

$$\tan(Mm) + N\tan(m) = 0 \,.$$

While the shelf modes in the Heaps solution equation (2.2.3) have a node at the shelf edge, the nodes of the shelf modes of the solution to McIntyre's model have moved seaward, away from the shelf edge. The relaxation of the Heaps' shelf edge boundary condition of $\eta = 0$ at x=1 allows for the inclusion of a deep water ocean, but with the wind stress field still confined to the shelf, the influence of the deep water ocean on coastal sea level elevation is found to be small.

2.3 Elevation of sea level at the coast in response to offshelf wind

The solution to equations (2.1.5) provides an expression for the elevation of the sea surface on the shelf produced by a steady uniform wind stress field, with onshore component P and longshore component Q, created suddenly at time t=0 over an area off the shelf between x=1 and x=a.

$$\eta = \left[P - \frac{fQ}{2K}\right]\left(\frac{1}{\rho g h_o}\right)(a - l)$$

$$+ \sum_{n=1}^{\infty} \frac{e^{\lambda_n t}}{\rho\sqrt{h_o}} \frac{(2K - \lambda_n)\,[P\,(2K - \lambda_n) - fQ]\,L_n \cosh\left(\frac{z_n x}{\sqrt{h_s}}\right)}{\lambda_n \left[(K - \lambda_n)\,(2K - \lambda_n)^2 + 2Kf^2\right] M_n'} \qquad (2.3.1)$$

$$+ \sum_{n=1} \frac{\exp\left[(\mu_n + i\nu_n)t\right]}{\rho\sqrt{h_o}} \frac{\left[2K + \mu_n + i\nu_n\right]\,[P\,(2K + \mu_n + i\nu_n) - fQ]\,L_n \cosh\left(\frac{z_n x}{\sqrt{h_s}}\right)}{(\mu_n + i\nu_n)\left[(K + \mu_n + i\nu_n)\,(2K + \mu_n + i\nu_n)^2 + 2Kf^2\right] M_n'}$$

where

$$L_n = \sinh\frac{z_n}{\sqrt{h_o}}(L - l) - \sinh\frac{z_n}{\sqrt{h_o}}(L - a)$$

$$M_n' = \left(\frac{\sqrt{h_o}}{h_s}l - \frac{l - L}{\sqrt{h_o}}\right)\cosh\frac{z_n l}{\sqrt{h_s}}\cosh\frac{z_n l}{\sqrt{h_o}}\sinh\frac{z_n L}{\sqrt{h_s}}$$

$$-\left(\frac{L}{\sqrt{h_s}}\right)\sinh\frac{z_n l}{\sqrt{h_s}}\sinh\frac{z_n l}{\sqrt{h_o}}\sinh\frac{z_n L}{\sqrt{h_o}}$$

$$+\left(\frac{L}{\sqrt{h_s}}\right)\sinh\frac{z_n l}{\sqrt{h_s}}\cosh\frac{z_n l}{\sqrt{h_o}}\cosh\frac{z_n L}{\sqrt{h_o}}$$

$$= \left(\frac{l - L}{\sqrt{h_o}} - \frac{\sqrt{h_o}}{h_s} l \right) \cosh \frac{z_n l}{\sqrt{h_s}} \sinh \frac{z_n l}{\sqrt{h_o}} \cosh \frac{z_n L}{\sqrt{h_o}}$$

$z = z_n$, being the nth positive root in ascending order of

$$\sqrt{\frac{h_o}{h_s}} \sinh \frac{z_n l}{\sqrt{h_s}} \cosh \frac{z_n l}{\sqrt{h_o}} \sinh \frac{z_n L}{\sqrt{h_o}}$$

$$- \cosh \frac{z_n l}{\sqrt{h_s}} \sinh \frac{z_n l}{\sqrt{h_o}} \sinh \frac{z_n L}{\sqrt{h_o}}$$

$$+ \cosh \frac{z_n l}{\sqrt{h_s}} \cosh \frac{z_n l}{\sqrt{h_o}} \cosh \frac{z_n L}{\sqrt{h_o}} \qquad (2.3.2)$$

$$- \sqrt{\frac{h_o}{h_s}} \sinh \frac{z_n l}{\sqrt{h_s}} \sinh \frac{z_n l}{\sqrt{h_o}} \cosh \frac{z_n L}{\sqrt{h_o}} = 0$$

Here

$$S = \lambda_n , \mu_n \pm i\nu_n$$

are the roots of the cubic

$$S[S + 2K + f^2/(S+2K)] = g z_n^2 \quad . \qquad (2.3.3)$$

The surge elevation solutions to all three models consists of a constant first term due to steady wind set-up, followed by two

infinite series. The first series represents a transient of pure exponential form present because of the rotation of the Earth. Its contribution to the coastal sea level elevation decreases steadily with time. The second infinite series is composed of exponentially -damped, due to bottom friction, periodic terms representing the free modes of oscillation.

The role of longshore and cross-shore wind stress, bottom friction, latitude (Coriolis parameter) and shelf depth can be examined. Examination of the solutions reveals some important facts. The first term in equations (2.2.3), (2.2.6) and (2.3.1) all show that the longshore component of the wind stress is multiplied by the coefficient f/(2K), where f is the Coriolis parameter and K is the bottom friction parameter. Heaps (1965), Flather (1976) and McIntyre (1979) chose 0.045/hr as an appropriate value for K. For this value of K, f/(2K) > 1 for all latitudes greater than 10 °, it can be seen that the longshore component of wind stress theoretically contributes a relatively greater effect on sea level variation than the cross-shore component. This factor also reveals the importance of rotation and the bottom stress

parameter in surge generation. The first term in the solutions of the three models, (equations (2.2.3), (2.2.6) and (2.3.1)), provides an expression for the sea level due to steady wind set-up. This is the long term value the sea level approaches. This term consists of the wind stress divided by the shelf depth, demonstrating that an increase in shelf depth would decrease the surge height, as expected.

2.4 Effects of offshelf wind stress and atmospheric pressure

Offshelf wind stress forcing may or may not contribute significantly to the coastal sea level anomaly. Non-dimensionalization of equations (2.1.4) reveals the importance of the geometry of the shelf region, (shelf depth, ocean depth and shelf width), on the magnitude of the surge generated. Defining the following non-dimensional parameters,

$$\eta = z\eta^{*}, \qquad h = Hh^{*},$$

$$t = Tt^{*}, \qquad P = pP^{*},$$

$$x, y = L(x^{*}, y^{*}), \qquad \tau_{sx} = s\tau$$

From continuity,

$$\frac{\partial u}{\partial x} + \frac{1}{h}\frac{\partial \eta}{\partial t} = 0,$$
$$u = \frac{L}{H}\frac{z}{T}u^*$$

is obtained. Then equation (2.1.4),

$$\frac{\partial u}{\partial t} + 2Ku - fv = -g\frac{\partial \eta}{\partial x} - \frac{1}{\rho}\frac{\partial P}{\partial x} + \frac{\tau_{sx}}{\rho h}$$

becomes

$$\left(\frac{1}{fT}\right)\frac{\partial u^*}{\partial t^*} + \left(\frac{2K}{f}\right)u^* - v^* = -\left[Fr\left(\frac{h}{z}\right)^2\frac{1}{fT}\right]\frac{\partial \eta^*}{\partial x^*} - \left[\frac{\rho T}{\rho f L^2}\left(\frac{h}{z}\right)\right]\frac{\partial P^*}{\partial x^*} + \frac{\tau T}{\rho f L z}\tau^*,$$

where

$$Fr = \text{Froude Number} = \frac{L^2 z}{gH^2T^2}.$$

Comparison of the two forcing terms shows the importance of the shelf depth, H, and the horizontal spatial scale, L. So it can be seen that increased depth decreases the effectiveness of wind

stress in generating surges.

It is generally thought that atmospheric pressure changes are the dominant forcing in deep water and wind stress forcing dominates in shallow water, but it is not clear whether the relatively deep Southern California Bight shelf region can be assumed to fall soley into either case. From the non-dimensionalization it can be seen that the horizontal spatial scale and water depth play a crucial role in storm surge generation. It is not clear what determines the horizontal spatial scale that is whether, it is the storm size or of the continental shelf width which determines the spatial scale.

3.1 General description

The Southern California Bight (Figure 3.1) extends from Point Conception southeastward to San Diego. The continental shelf in this region is very narrow, extending only five to ten kilometers from the shore. Seaward from the continental shelf to about 121° west longitude is a highly irregular borderland of intermediate depth (on the order of hundreds of meters) (Figure 3.2). Located within this borderland area are the Channel islands.

The mean current flow consists of a counter-clockwise gyre that occupies most of the Southern California Bight. The gyre is formed by the southward flowing California Current and the northward flowing California Counter current. Shoreward of the gyre, is a narrow reversing coastal current 15 to 20 km wide (Tsuchiya, 1980).

Winds in the bight are usually moderate. A subtropical high pressure system is present offshore at most times and dominates the atmosphere in the bight. This system generally causes onshore winds to be present throughout the bight.

Figure 3.1: Southern California Bight region with tide gauge and weather station locations.

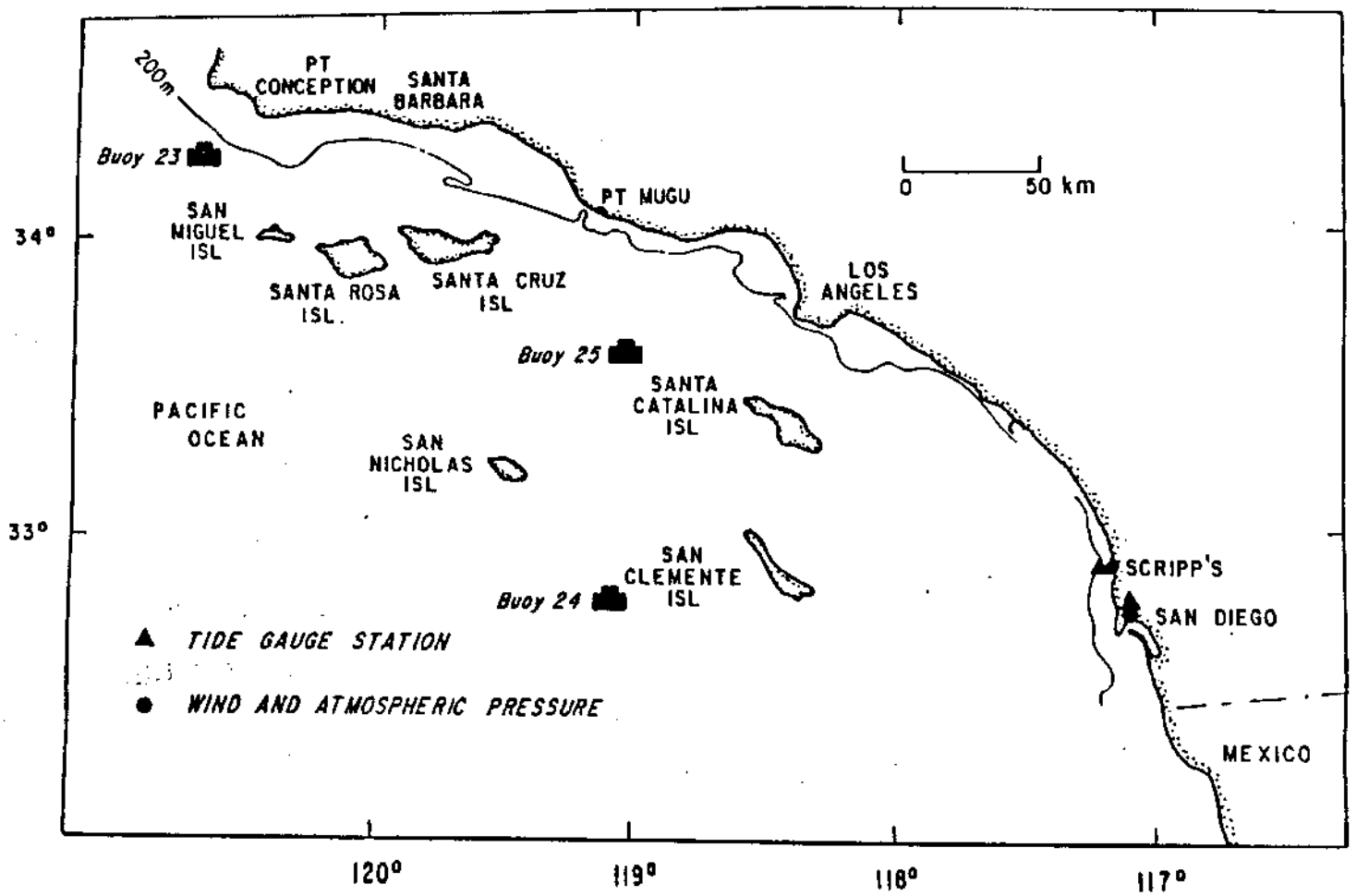
200m
PT CONCEPTION
SANTA BARBARA
Buoy 23
PT MUGU
0
50 km
SAN MIGUEL ISL
SANTA ROSA ISL.
SANTA CRUZ ISL
LOS ANGELES
34°
Buoy 25
SANTA CATALINA ISL
PACIFIC OCEAN
SAN NICHOLAS ISL
33°
SAN CLEMENTE ISL
SCRIPP'S
SAN DIEGO
Buoy 24
TIDE GAUGE STATION
WIND AND ATMOSPHERIC PRESSURE
MEXICO
120°
119°
118°
117°

Figure 3.2: Contour map of Southern California Bight bathymetry.

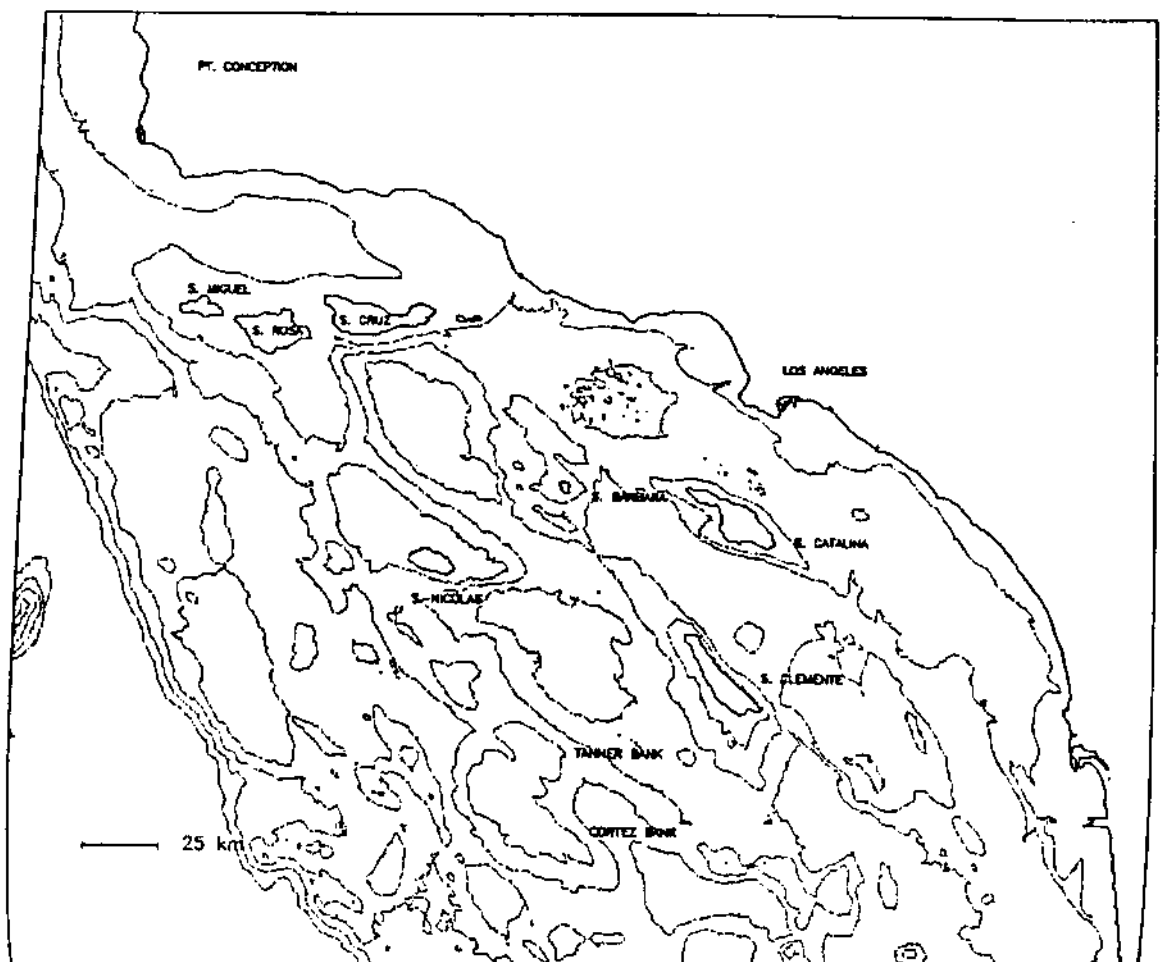

CONTOURS – 300m 900m 1500m 2100m 2700m

During the summer these onshore winds are reinforced by the presence of a thermal low pressure system over the California desert to the east of the coastal mountain range.

Another significant meteorological feature in the bight is the land/sea breeze. The land/sea breeze phenomenom has been studied extensively by Estoque (1961, 1962), Fisher (1961), Walsh (1974) and others. The land/sea breeze is due to differential heating and cooling of the land and water. It begins at the coast and extends only a few tens of kilometers from the coast. The larger scale synoptic conditions can also increase or decrease the strength and extent of the land/sea breeze (Estoque, 1962; Dorman, 1982).

Occasionally, the high pressure and sea/land breeze system is overridden by the passage of storm fronts and Santa Anas. Santa Anas are marked by reversal of the surface pressure gradient to offshore. They are characterized by dry, gusty easterly winds of considerable force. Frontal passages of storms are usually limited to the late fall, winter, and early spring. Associated with these fronts are strong winds from the southwest usually lasting for a few days. It is the passage of these storm fronts and their strong southwesterly winds which are associated with large sea level

anomalies.

3.2 Meteorological conditions for 1982 - 1983

Along the North American Pacific Coast, the winter of 1982 - 1983 was one of the most severe in several decades (Quiros, 1983; Namias and Cayan, 1984). The unusual storminess was associated with the El Nino - Southern Oscillation event of 1982 - 1983. The El Nino condition is associated with abnormally warm ocean temperatures which occur irregularly every three to seven years.

Studies of the atmospheric conditions in the northern hemisphere for the winter of 1982-1983 show a tendency for anomalously low barometeric pressure south of the Aleutian islands and higher than normal pressure in the North Pacific subtropics (Dickson and Livezey, 1984). Increased storm activity in the central North Pacific is usually associated with this type of pressure distribution.

One measure of storminess is average wind speed. The average westerly winds across the North Pacific Subtropics during the winter of 1982-1983 were found to be almost twice their normal (30 year average) speed. Other indications of the increased

storminess are the lower average surface pressure and increased precipitation found that winter (see Table 3.1) (Cayan and Flick, 1985).

3.3 Tidal cycle

Though sea level fluctations are due to the effects of wind, atmospheric pressure, waves, ocean temperature and currents, and long term secular trends, it is the gravitational tide producing forces which dominate sea level variability on the California coast. Tidal fluctuations in sea level are due to the periodic orbital changes in the position of the moon and the sun relative to the earth. Though these astronomical motions are very regular, highly accurate tide predictions are sometines difficult to obtain. This is due to the fact that the presence of continental land masses and ocean floor topography significantly alter the local response of the ocean to the gravitational tide-producing force. Because of the importance of coastal and ocean basin characteristics, the precise response to tidal forcing varies from location to location. The largest tidal fluctuations, regardless of location, occur semidiurnally (2 cycles per day and diurnally (1 cycle per day).

	Long Term Means (1941-1970)			Winter 1982-1983 Means		
	Surface press. (mb)	Wind speed (mph)	Precip. mo. Total (in.)	Surface press. (mb)	Wind speed (mph)	Precip mo. Total (in.)
Nov	1015.9	5.7	1.25	1014.2	7.1	2.10
Dec	1017.3	5.4	1.73	1015.9	7.5	1.43
Jan	1016.9	5.7	1.88	1015.9	6.1	2.10
Feb	1017.3	6.4	1.48	1014.9	7.7	3.88
Mar	1015.2	7.2	1.55	1013.2	9.3	6.57

Table 3.1: Monthly average meteorological parameters, long term means and winter 1982-1983 means (Cayan and Flick, 1985).

Tides in the Southern California Bight area are of the "mixed" type. This means that the diurnal constituents are of the same magnitude as the semidiurnal constituents. The mean tidal range for the bight varies from about 1.2 to 2 meters.

Chapter 4 Data Analysis

4.1 Data set description

Hourly sea level data for two coastal locations and one offshore island station within the Southern California Bight region and covering the period 26 November 1982 to 28 September 1983 were examined. The coastal stations are Newport Beach, California and La Jolla, California. Tide gauges are in place on San Clemente, San Nicholas and Santa Catalina islands, but only the Santa Catalina sea level record was of sufficient length and quality (only short gaps in the record) for an accurate tide prediction to be made. The offshore island station is located on the northeast side of Santa Catalina island facing the California coast. The sea level record from this station allows for the examination of the offshore spatial extent of the coastal surge, as well as the response of the island sea level to atmospheric forcing. The coastal stations are part of the tide gauge network maintained by NOAA/NOS. Sea level elevation is sampled every six minutes and the hourly values are those six minute data sampled on the hour. The time series record of sea level height obtained for Santa Catalina was six minute sampled data. This data

set was hourly averaged using a cosine taper to obtain a time series of hourly sea level elevations. The data sets of each station are divided into two time series, a winter series covering 26 November 1982 to 25 March 1983 and a summer series, including 29 May 1983 to 28 September 1983.

Hourly measurements of atmospheric pressure and wind velocity at three coastal stations and two offshore locations were examined. The three coastal stations from north to south are: Point Mugu, Long Beach and San Diego. The offshore data sets are from a station located on San Nicholas island and from NOAA buoy 24. Sea surface temperature at NOAA buoy 24 was also obtained.

A highly accurate tidal prediction was difficult to obtain due to the limited sea level time series avaialable. After this tidal prediction was removed from the sea level records, diurnal and semidiurnal variations, associated with the tides, remained in the anomaly record. To remove these tidal-variations as well as long period seasonal varialtions, all measurements were passed through a zero phase shift, Butterworth function bandpass panel filter with a low frequency cut-off of 0.033 cpd (30 day period) and a high frequency cut-off of 0.80 cpd (1.25 day period) (Kanasewich, 1981).

4.2 Sea level

An hourly time series of tidal predictions for the periods of interest were computed for each sea level station using extended harmonic analysis (for a description of extended harmonic analysis, see Cartwright, 1982). The sea level anomaly time series was computed as the difference between measured sea level and the tidal prediction. It is this anomaly that is of interest, as it is the portion of the sea level height which is not due to the tide-producing force but is thought to be forced by atmospheric pressure, winds and sea surface and subsurface temperatures.

Visual inspection of the time series plots (Figures 4.1 and 4.2) of sea level anomaly for the three stations shows periods of consistently high or low heights lasting from 3-10 days. These anomalies are on the order of a few cm with the largest variations being about 10 cm.

4.3 Atmospheric pressure and wind fields

Hourly atmospheric pressure and wind velocity measurements at five positions in the Southern California Bight region were examined. Three of these are coastal stations: Point Mugu, Long

Figure 4.1: Time series plots, 26 November 1982 - 30 March 1983: a) Station 24 - sea surface temperature, b) Station 24 - sea level pressure, c) Newport Beach - adjusted sea level anomaly, d) Santa Catalina - adjusted sea level anomaly, e) La Jolla - adjusted sea level anomaly.

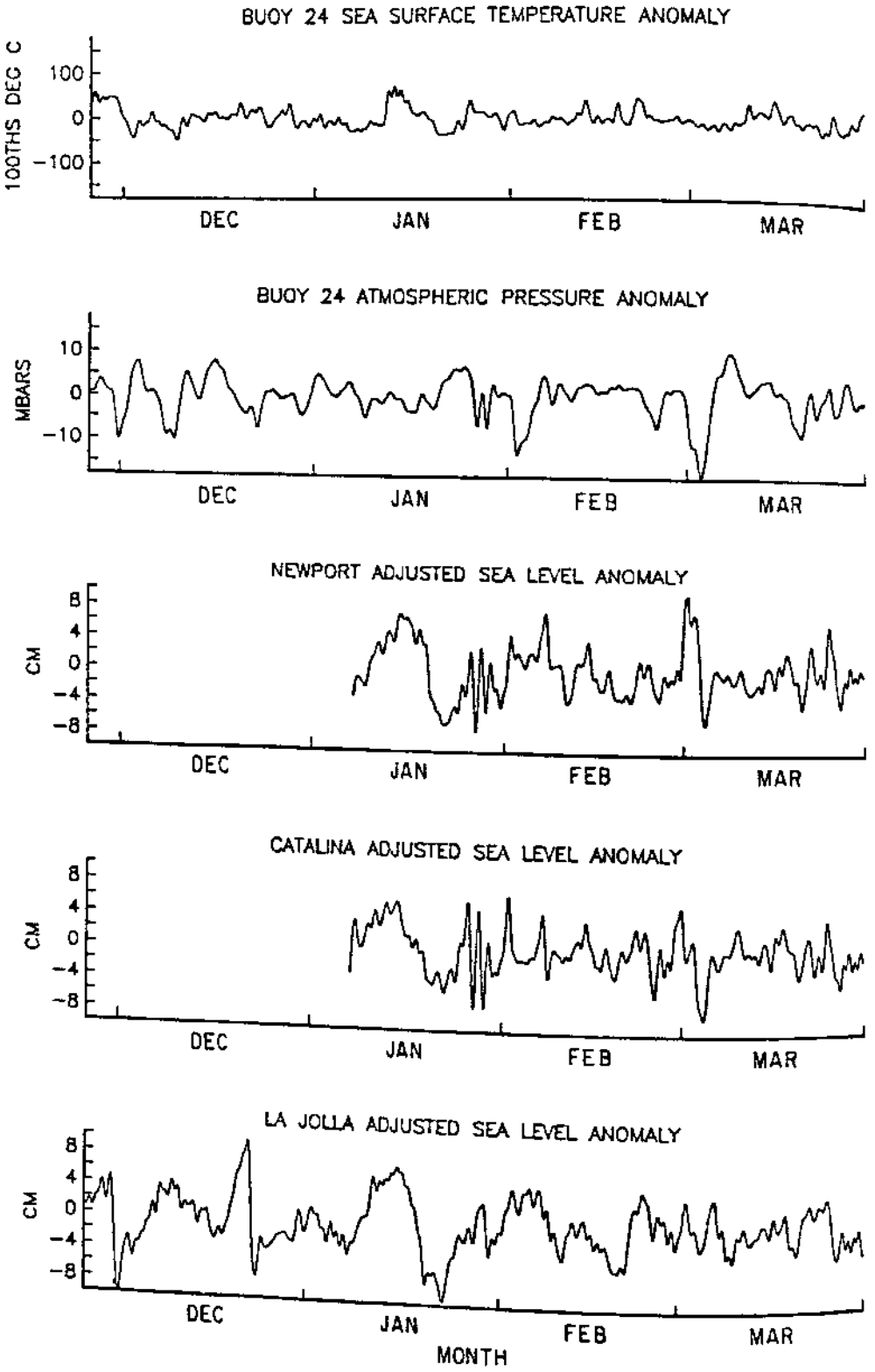
BUOY 24 SEA SURFACE TEMPERATURE ANOMALY
100THS DEG C
100
0
−100
DEC
JAN
FEB
MAR
BUOY 24 ATMOSPHERIC PRESSURE ANOMALY
MBARS
10
0
−10
DEC
JAN
FEB
MAR
NEWPORT ADJUSTED SEA LEVEL ANOMALY
CM
8
4
0
−4
−8
DEC
JAN
FEB
MAR
CATALINA ADJUSTED SEA LEVEL ANOMALY
CM
8
4
0
−4
−8
DEC
JAN
FEB
MAR
LA JOLLA ADJUSTED SEA LEVEL ANOMALY
CM
8
4
0
−4
−8
DEC
JAN
FEB
MAR
MONTH

Figure 4.2: Time series plots, 28 May 1982 - 29 September 1983: a) Station 24 - sea surface temperature, b) Station 24 - sea level pressure, c) Newport Beach - adjusted sea level anomaly, d) Santa Catalina - adjusted sea level anomaly, e) La Jolla - adjusted sea level anomaly.

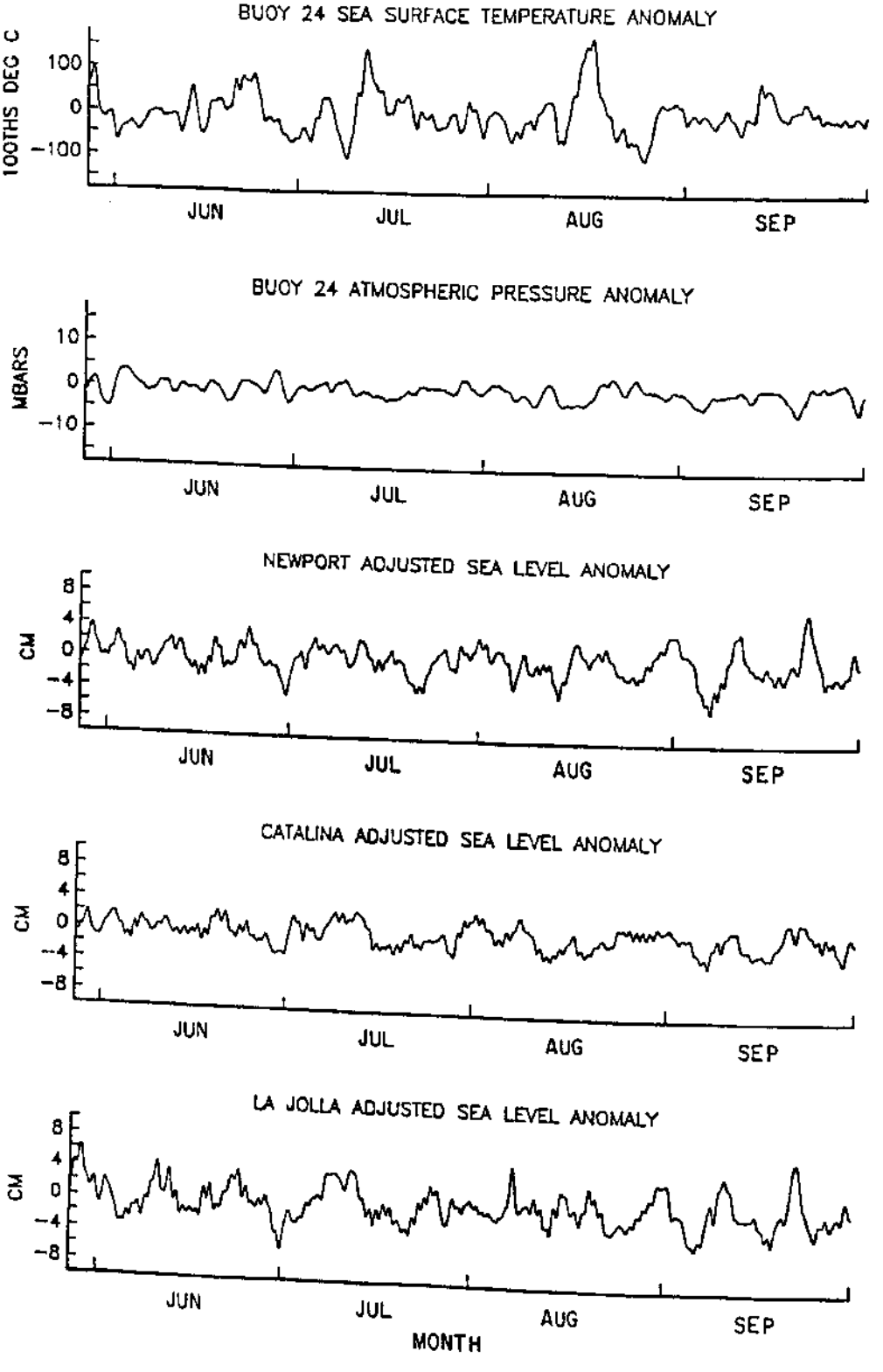
BUOY 24 SEA SURFACE TEMPERATURE ANOMALY
100THS DEG C
100
0
−100
JUN
JUL
AUG
SEP
BUOY 24 ATMOSPHERIC PRESSURE ANOMALY
MBARS
10
0
−10
JUN
JUL
AUG
SEP
NEWPORT ADJUSTED SEA LEVEL ANOMALY
CM
8
4
0
−4
−8
JUN
JUL
AUG
SEP
CATALINA ADJUSTED SEA LEVEL ANOMALY
CM
8
4
0
−4
−8
JUN
JUL
AUG
SEP
LA JOLLA ADJUSTED SEA LEVEL ANOMALY
CM
8
4
0
−4
−8
JUN
JUL
AUG
SEP
MONTH

Figure 4.3: Station 24 wind speed time series plots: a) East/West wind speed, 26 November 1982 - 30 March 1983; b) North/South wind speed, 26 November 1982 - 30 March 1983; c) East/West wind speed, 28 May 1983 - 29 September 1983; d) North/South wind speed, 28 May 1983 - 29 September 1983.

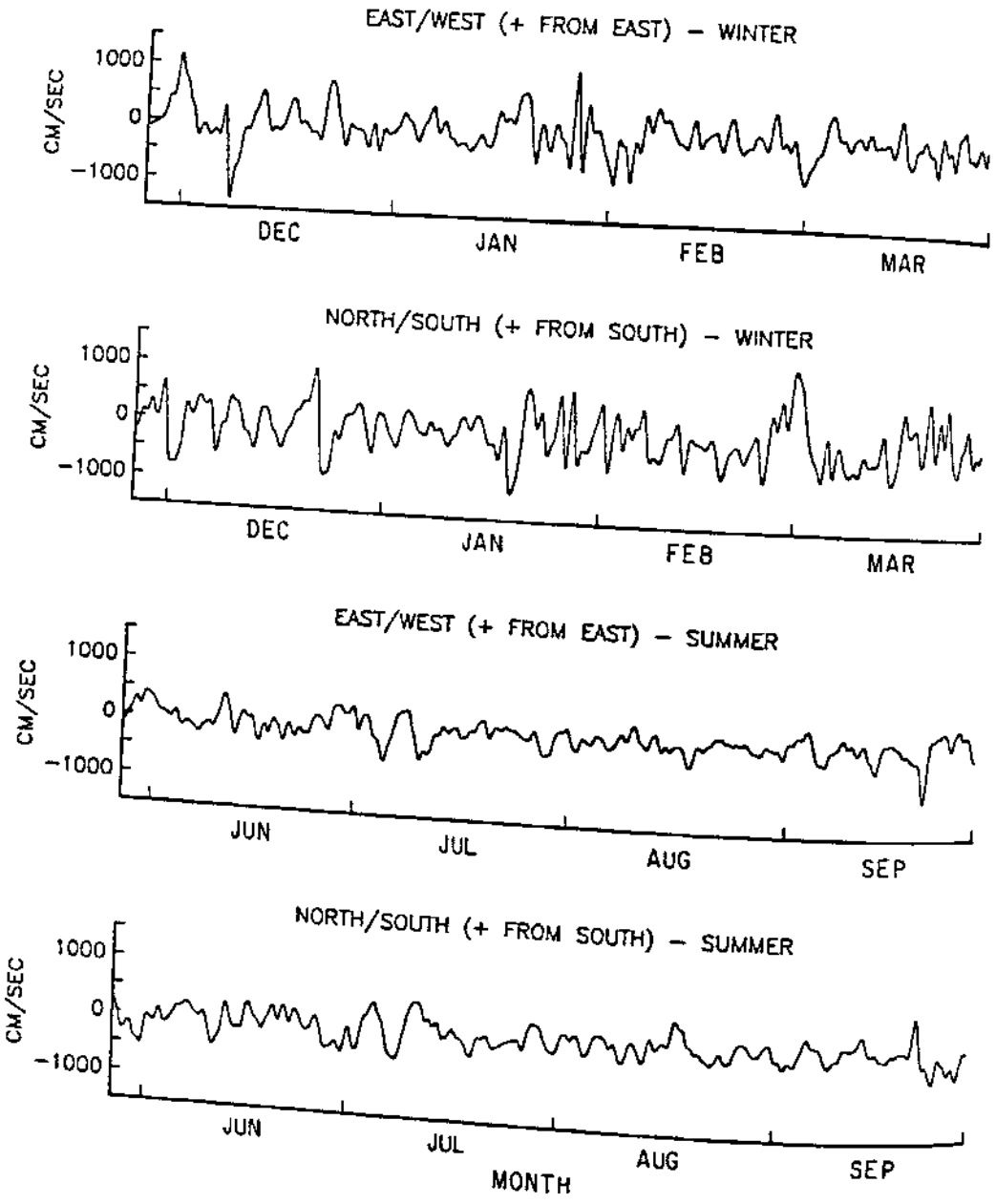
EAST/WEST (+ FROM EAST) – WINTER
CM/SEC
1000
0
−1000
DEC
JAN
FEB
MAR
NORTH/SOUTH (+ FROM SOUTH) – WINTER
CM/SEC
1000
0
−1000
DEC
JAN
FEB
MAR
EAST/WEST (+ FROM EAST) – SUMMER
CM/SEC
1000
0
−1000
JUN
JUL
AUG
SEP
NORTH/SOUTH (+ FROM SOUTH) – SUMMER
CM/SEC
1000
0
−1000
JUN
JUL
AUG
SEP
MONTH

Figure 4.4a: Sea level anomaly energy (sq cm hr) spectra, solid line - La Jolla, small dash - Newport Beach, large dash - Santa Catalina, 26 November 1982 - 30 March 1983. Degress of Freedom (DOF) = 72.

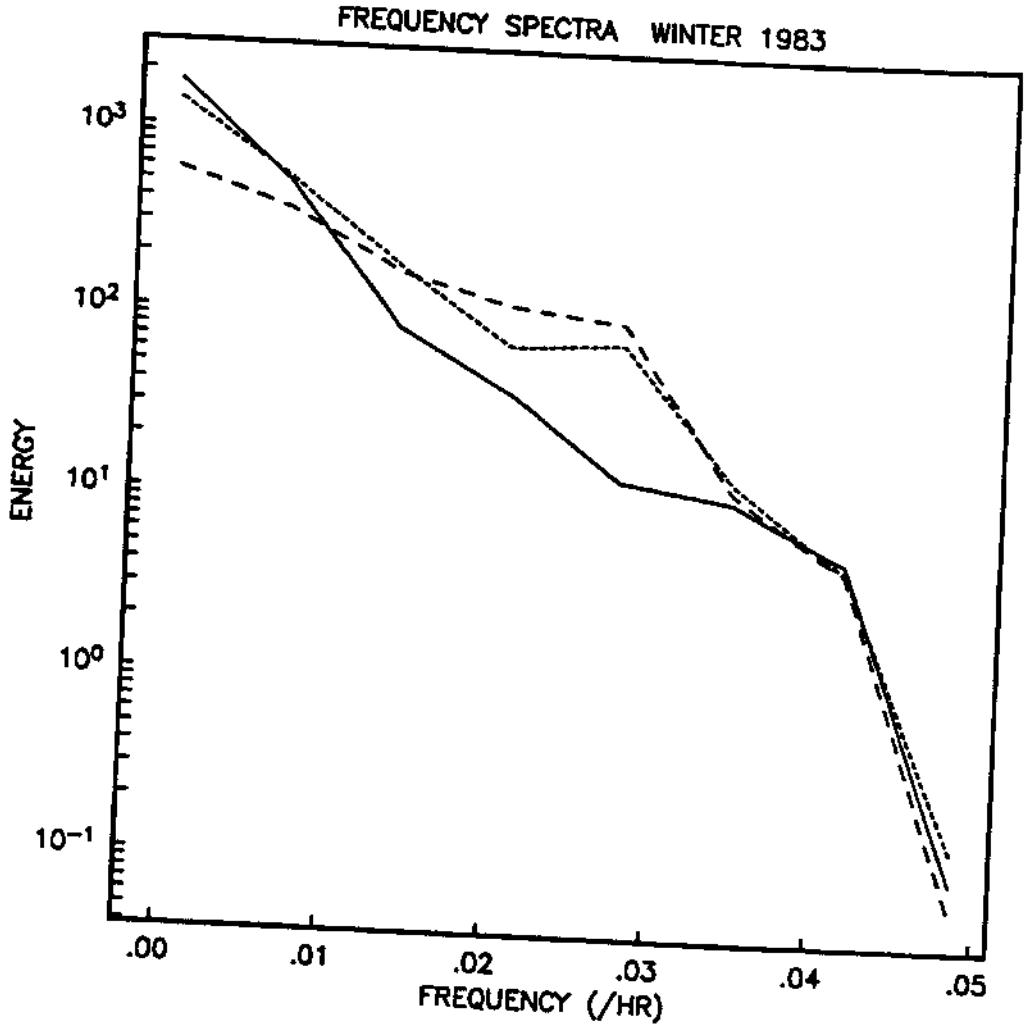
FREQUENCY SPECTRA WINTER 1983
ENERGY
10^3
10^2
10^1
10^0
10^{-1}
.00
.01
.02
.03
.04
.05
FREQUENCY (/HR)

Figure 4.4b: Sea level anomaly energy (sq cm hr) spectra, solid line - La Jolla, small dash - Newport Beach, large dash - Santa Catalina, 28 May 1983 - 29 September 1983. DOF = 72.

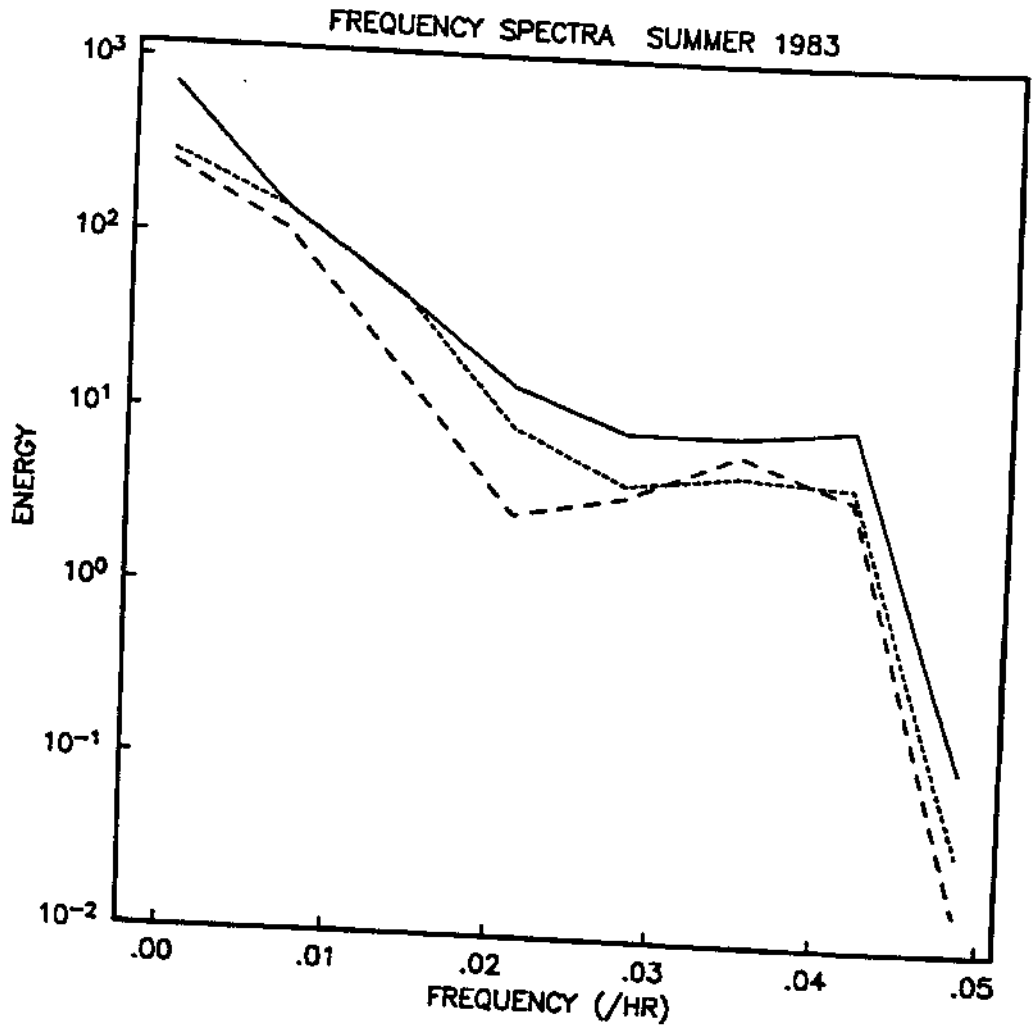
FREQUENCY SPECTRA SUMMER 1983
ENERGY
10^3
10^2
10^1
10^0
10^{-1}
10^{-2}
.00
.01
.02
.03
.04
.05
FREQUENCY (/HR)

Beach and San Diego, and the other two are offshore at San Nicholas island and at Buoy 24 (see Figure 3.1) Cross-spectral analysis was performed on the two time series of pressure measurements, beginning on 26 November 1982. The analysis (Figure 4.6) shows that the pressure field between each station pair is highly coherent in the frequency range of 0.033 cpd to 0.800 cpd. The pressure signal was also shown to be in phase at all stations. This is not surprising, since atmospheric pressure systems have spacial scales of similar to or larger than the station spacing. Similar analysis (Figures 4.8 and 4.9) performed on wind speeds broken into north-south and east-west components shows that the wind field too is highly coherent and in phase, though less so than the pressure field.

Figure 4.5a: Station 24 sea level pressure energy (sq mb hr) spectrum, 26 November 1982 - 30 March 1983. DOF = 72.

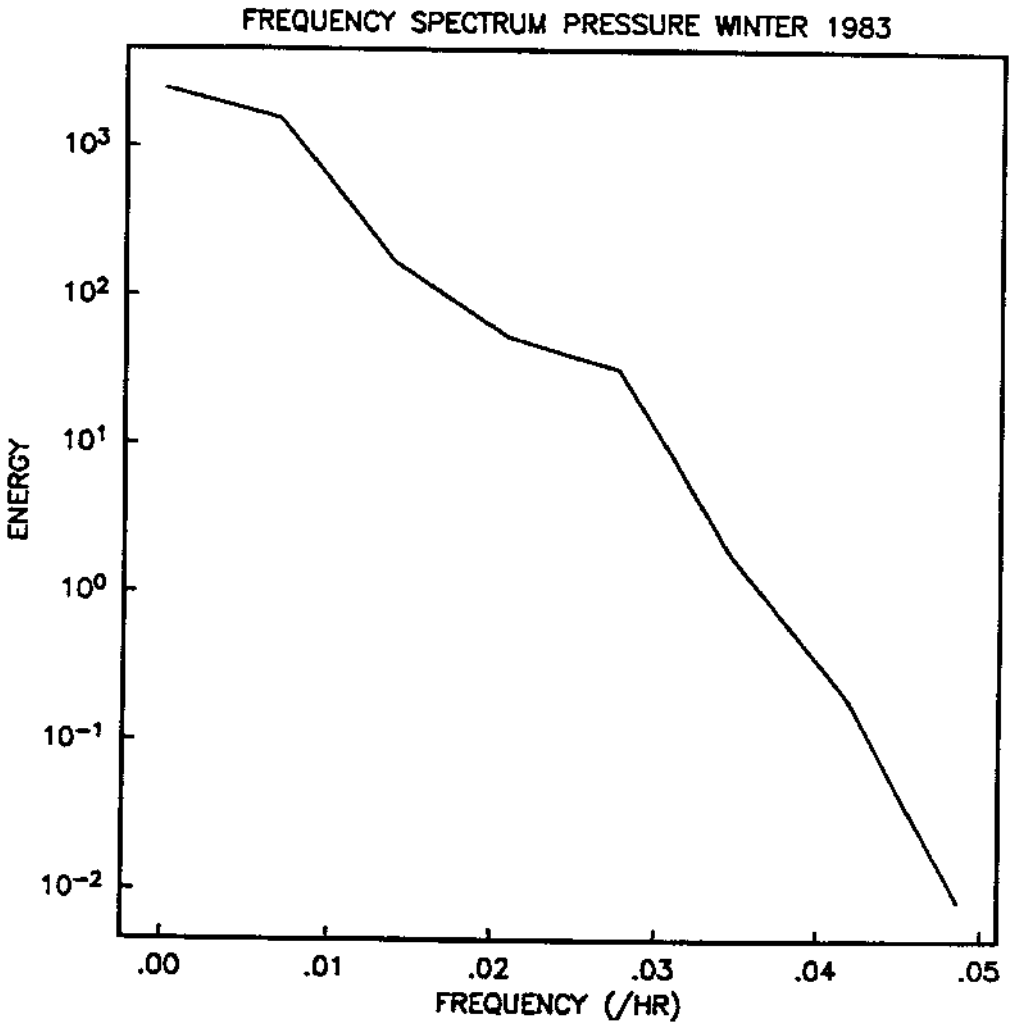
FREQUENCY SPECTRUM PRESSURE WINTER 1983
ENERGY
10^3
10^2
10^1
10^0
10^{-1}
10^{-2}
.00
.01
.02
.03
.04
.05
FREQUENCY (/HR)

Figure 4.5b: Station 24 sea level pressure energy (sq mb hr) spectra, 28 May 1983 - 29 September 1983. DOF = 72.

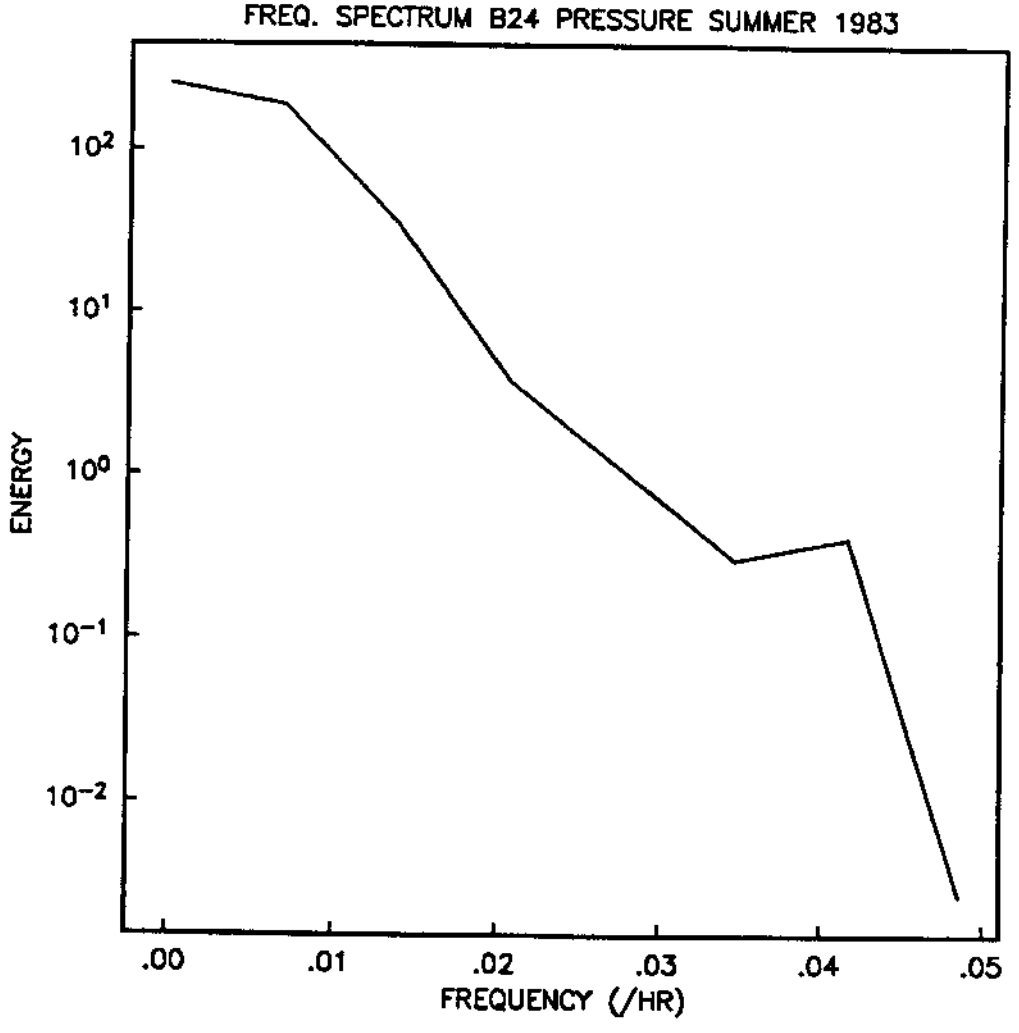
FREQ. SPECTRUM B24 PRESSURE SUMMER 1983
ENERGY
10^2
10^1
10^0
10^{-1}
10^{-2}
.00
.01
.02
.03
.04
.05
FREQUENCY (/HR)

Figure 4.6: Coherence and phase of sea level pressure at Pt. Mugu and San Nicholas island. When the phase < 0, Pt. Mugu leads San Nicholas island. Error bars provide 99% confidence limits. DOF = 120.

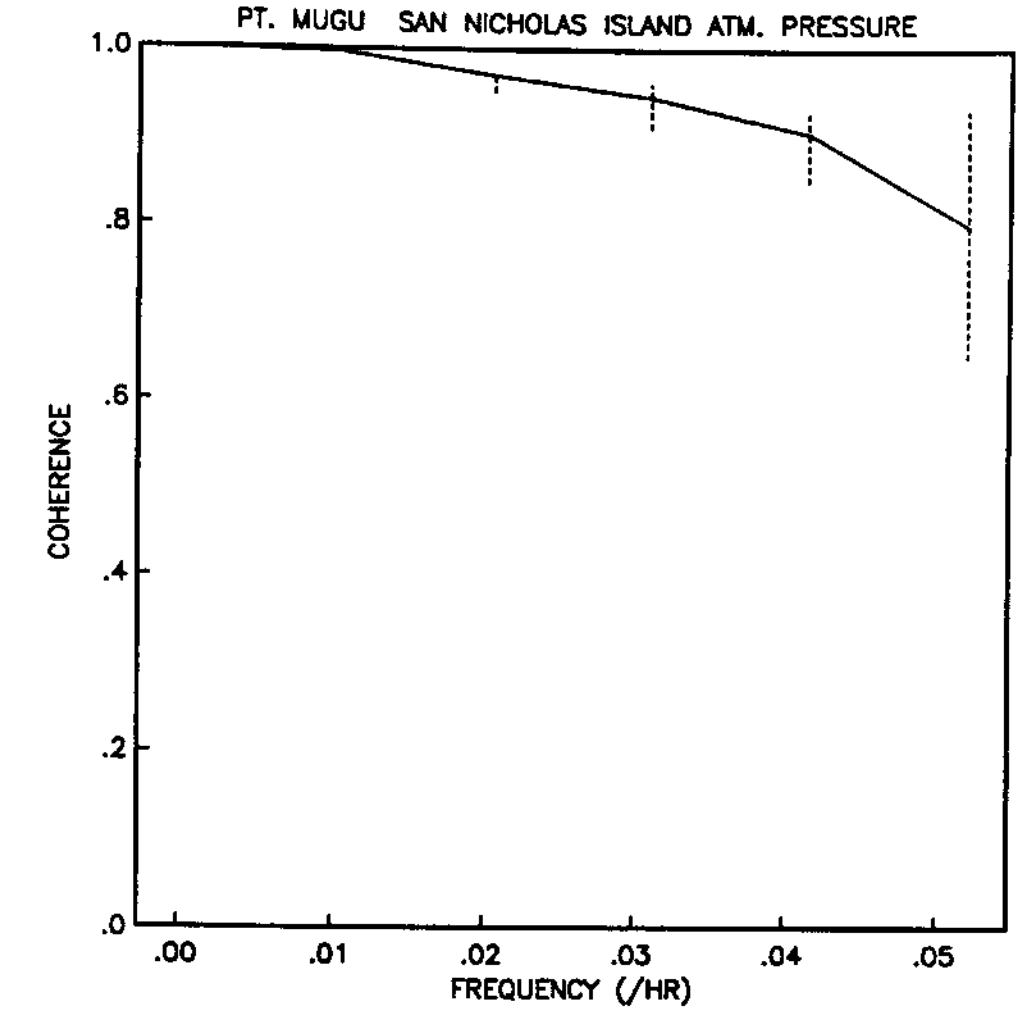
PT. MUGU SAN NICHOLAS ISLAND ATM. PRESSURE
COHERENCE
1.0
.8
.6
.4
.2
.0
.00
.01
.02
.03
.04
.05
FREQUENCY (/HR)

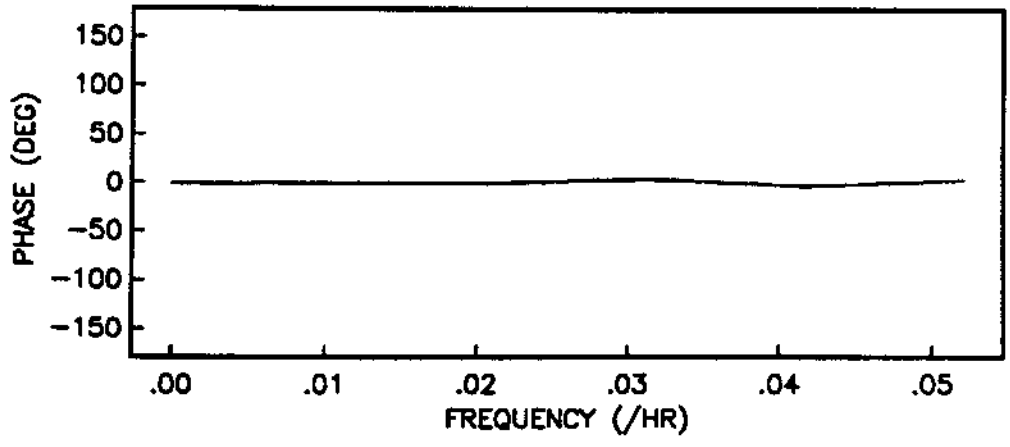
PHASE (DEG)
150
100
50
0
-50
-100
-150
.00
.01
.02
.03
.04
.05
FREQUENCY (/HR)

Figure 4.7a: Station 24, East/West wind speed energy (sq cm hr/sq sec) spectrum. DOF = 120.

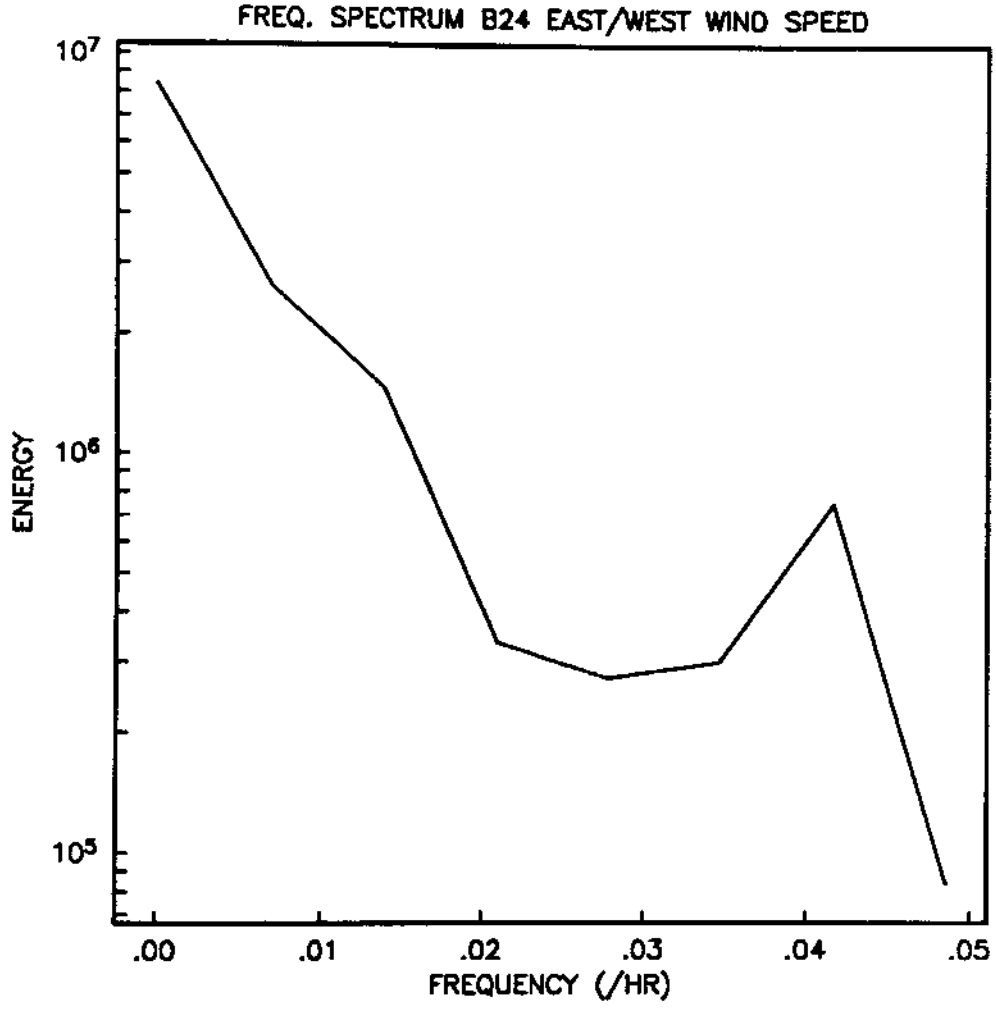
FREQ. SPECTRUM B24 EAST/WEST WIND SPEED
ENERGY
10^7
10^6
10^5
.00
.01
.02
.03
.04
.05
FREQUENCY (/HR)

Figure 4.7b: Station 24, North/South wind speed energy (sq cm hr/sq sec) spectrum. DOF = 120.

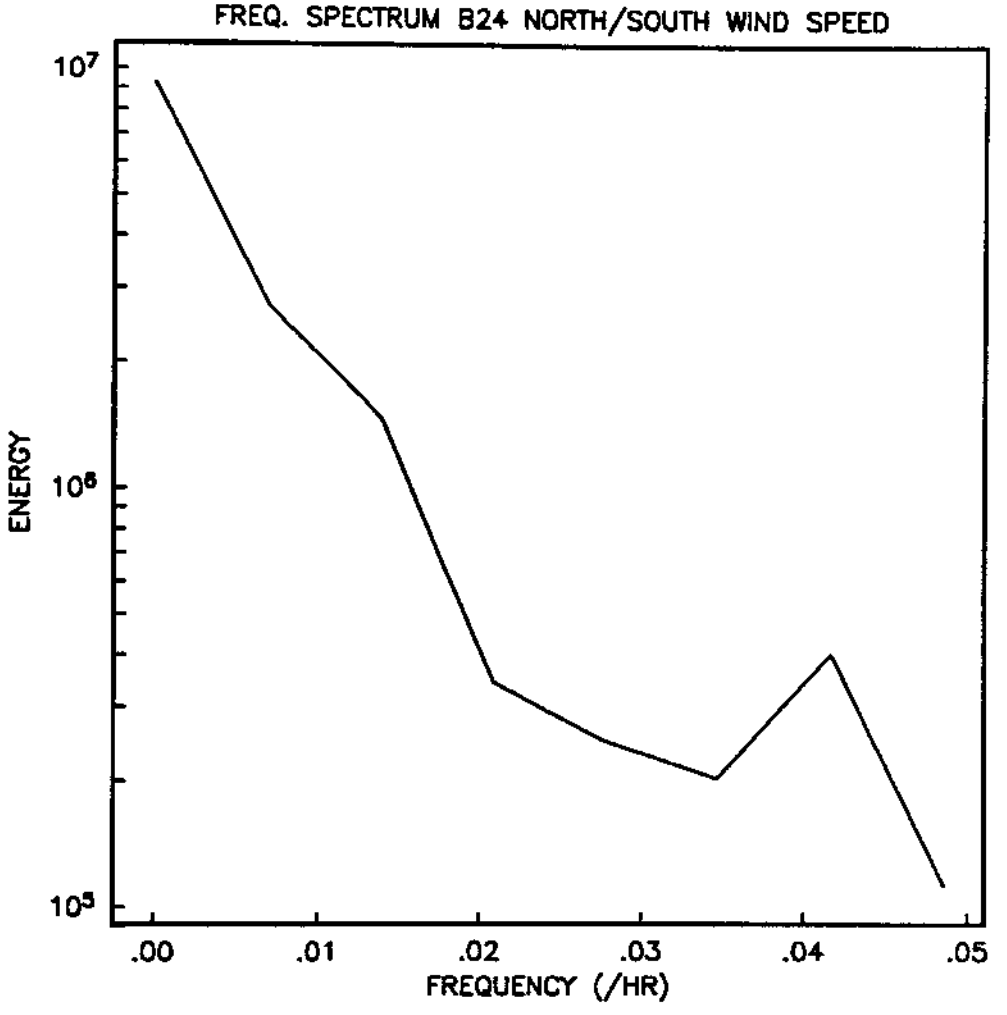
FREQ. SPECTRUM B24 NORTH/SOUTH WIND SPEED
ENERGY
10^7
10^6
10^5
.00
.01
.02
.03
.04
.05
FREQUENCY (/HR)

Figure 4.8: Coherence and phase of East/West wind at Station 24 and Station 25. When the phase < 0, Station 25 leads Station 24. Error bars provide 99% confidence limits. DOF = 120.

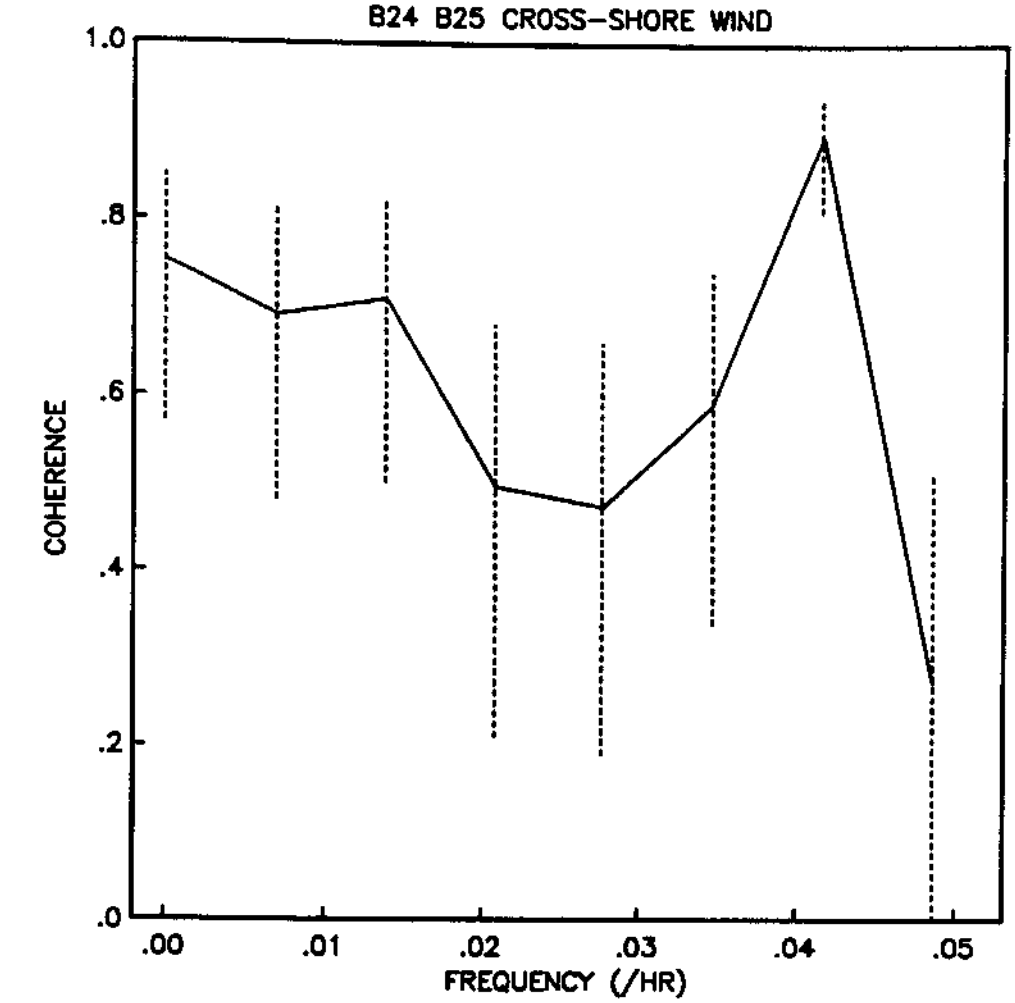
B24 B25 CROSS-SHORE WIND
COHERENCE
1.0
.8
.6
.4
.2
.0
.00
.01
.02
.03
.04
.05
FREQUENCY (/HR)

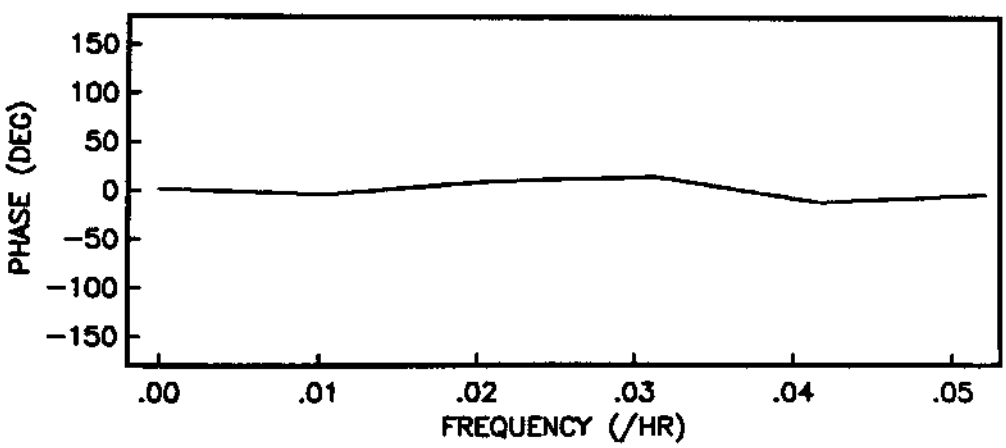
PHASE (DEG)
150
100
50
0
-50
-100
-150
.00
.01
.02
.03
.04
.05
FREQUENCY (/HR)

Figure 4.9: Coherence and phase of North/South wind at Station 24 and Station 25. When the phase < 0, Station 25 leads Station 24. Error bars provide 99% confidence limits. DOF = 120.

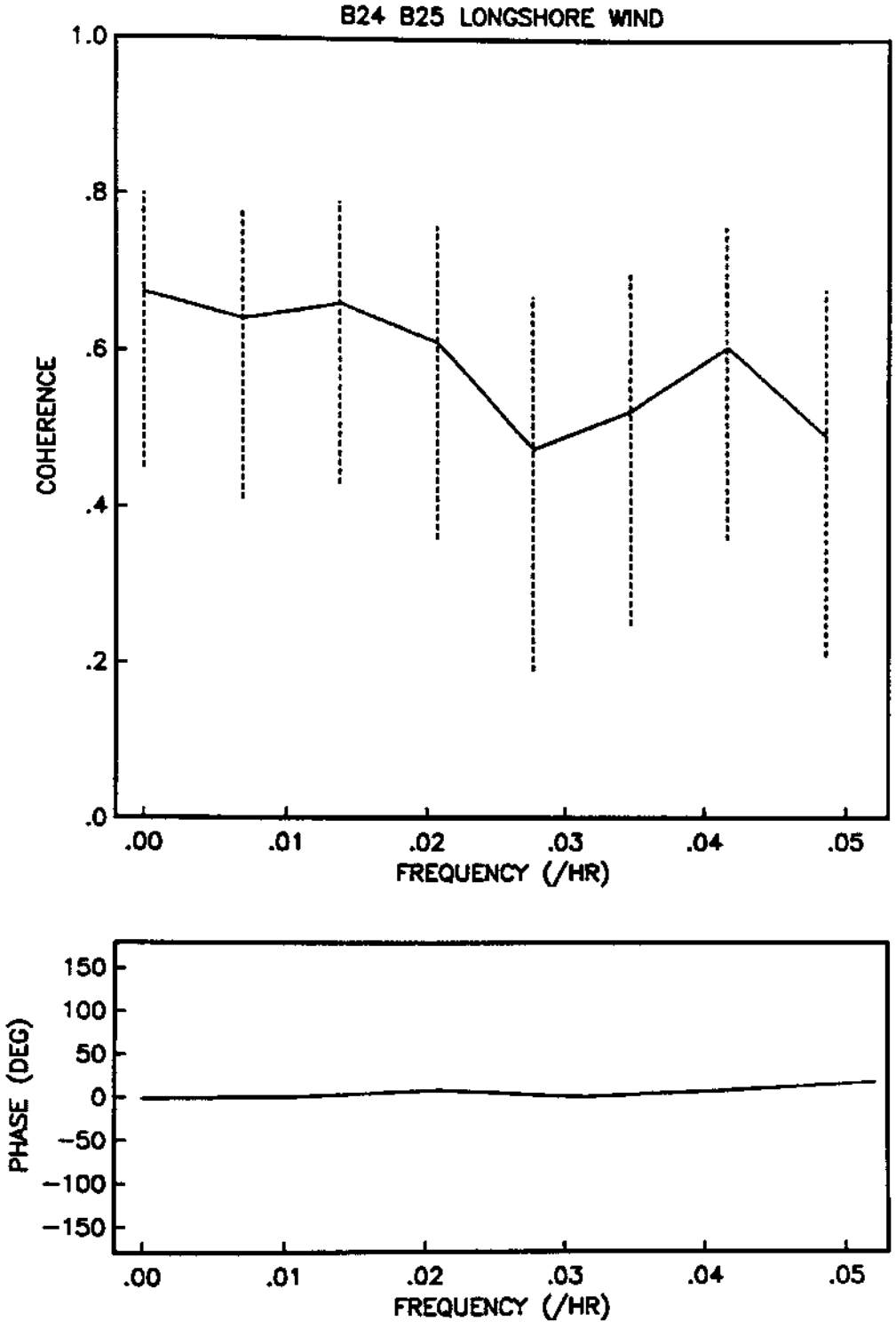
B24 B25 LONGSHORE WIND
COHERENCE
1.0
.8
.6
.4
.2
.0
.00
.01
.02
.03
.04
.05
FREQUENCY (/HR)
PHASE (DEG)
150
100
50
0
-50
-100
-150
.00
.01
.02
.03
.04
.05
FREQUENCY (/HR)

Chapter 5 Statistical Analysis

5.1 Linear statistical model

The statistical model used to examine the locally forced sea level variability is described in detail in Chelton (1983). It is an application of minimum mean square error estimation. A multiple - input statistical model is employed, since correlation between atmospheric pressure and wind could cause an apparent correlation between sea level elevation and wind resulting from each being correlated to atmospheric pressure. The estimand, sea level anomaly, denoted as η, is then assumed to be linearly related to M input variables, $d_1, d_2, \ldots, d_m$, so an estimate of the following form can be made

$$\hat{\eta} = \sum_{m=1}^{M} \alpha_m d_m(T_m) \tag{5.1.1}$$

where T_m is a time lag.

The response coefficients, α_n, that minimize the expected square error of the estimate are calculated over the finite record length. The estimate of the response coefficients is given by

$$\widehat{\alpha_m} = \sum_{n=1} \{ d_m d_n \}^{-1} \{ \eta d_n \} \qquad (5.1.2)$$

The brackets denote the sample mean value and $\{d_m d_n\}^{-1}$ is the m, n^{th} element of the inverse of the mean product matrix of the inputs. The skill of such an estimate can be expressed as the fraction of the variance explained by the estimator. Chelton (1982) showed that a multiple - input model effectively extracts only the effect of each input variable on the estimand from a true relation between the two, rather than from correlations of each to another input variable. If one assumes a process is governed by linear dynamics, the response coefficient, computed for each input variable, corresponds to the constant coefficient found in the linear dynamical equations for that input variable.

5.2 Atmospheric pressure forcing

To examine the effect of atmospheric pressure on sea level, linear regression analysis was performed. Since the pressure field over the area of investigation was coherent and in phase, pressure data at one station (NOAA Buoy 24) was all that was needed. The

analysis was performed on the three sea level stations (Newport Beach, La Jolla and Santa Catalina) for both winter and summer periods.

The effect of atmospheric pressure on sea level can be seen, from the equations of motion (equations 1.1.1). In the absence of fluid motion and wind stress, the steady state balance of terms in (1.1.1) becomes

$$\frac{\partial \eta}{\partial x} = -\frac{1}{\rho g}\frac{\partial P}{\partial x} \qquad (5.2.1)$$

$$\frac{\partial \eta}{\partial y} = -\frac{1}{\rho g}\frac{\partial P}{\partial y}\,, \qquad (5.2.2)$$

which can be integrated to get

$$\eta(x,y,t) = -\frac{1}{\rho g}\,P(x,y,t) + C\,. \qquad (5.2.3)$$

where C is the constant of integration, which is zero if the response to atmospheric pressure is assumed to be purely local.

Crepon (1976) showed that the asymptotic solution to the time dependent problem indicates that the static balance between atmospheric pressure gradient and sea surface slope as given in

(5.2.1) is consistent only if the pressure forcing length scale is smaller than the Rossby radius of deformation, $\sqrt{gd}/f$. The expression for the sea surface elevation is then given by

$$\eta(x,y,t) = -\frac{1}{\rho g} P(x,y,t) . \qquad (5.2.4)$$

This is the inverse barometer response and implies that a 1 mbar increase (decrease) in atmospheric pressure causes a 1.01 cm decrease (increase) in sea level. If the pressure forcing length scale is larger than the barotropic Rossby radius of deformation, the transient adjustment to the applied pressure forcing, which is accomplished by long gravity waves, is not carried out and the pressure gradient is balanced by geostrophic currents rather than sea surface tiltiing.

The results of the statistical analysis are given in Table 5.1. It can be seen that regression coefficients for the atmospheric pressure input variable are near the value of -1.01, which is what one would expect if the ocean responded as an inverse barometer. The mean of all six examples is in fact -0.985. Given the

Winter

		La Jolla	Newport	Catalina
Pressure.	Time Lag (hours):	0	0	0
	Weight (cm/mbar):	-1.114	-1.192	-0.957
Longshore Wind Stess	Time Lag (hours):	11	2	0
	Weight (sq. sec/cm):	0.244	0.272	0.199
Cross Shore Wind Stress	Time Lag (hours):	33	114	6
	Weight (sq.sec/cm):	-0.326	-1.356	-0.286
Sea Surface Temp.	Time Lag (hours):	0	0	0
	Weight (cm/deg. C):	6.564	4.925	6.510
	Skill of Estimate:	0.7583	0.8593	0.8186
	Artificial Skill:	0.140	0.242	0.244

Summer

		La Jolla	Newport	Catalina
Pressure	Time Lag (hours):	0	0	0
	Weight (cm/mbar):	-0.816	-0.767	-0.953
Longshore Wind Stess	Time Lag (hours):	21	27	19
	Weight (sq. sec/cm):	-0.098	0.014	0.119
Cross Shore Wind Stress	Time Lag (hours):	32	35	44
	Weight (sq. sec/cm):	-3.891	-3.224	-1.668
Sea Surface Temp.	Time Lag (hours):	0	0	0
	Weight (cm/deg C):	1.444	1.055	-0.071
	Skill of Estimate:	0.4474	0.4609	0.6164
	Artificial Skill:	0.041	0.041	0.039

Table 5.1: Statistical analysis results, for longshore and cross-shore defined by the general coastline of the bight a) Winter 82-83, b) Summer 83.

		Winter		
		La Jolla	Newport	Catalina
Pressure	Time Lag (hours):	0	0	0
	Weight (cm/mbar):	-1.109	-0.955	-0.969
Longshore Wind Stess	Time Lag (hours):	10	2	0
	Weight (sq. sec/cm):	0.220	0.259	0.262
Cross Shore Wind Stress	Time Lag(hours):	30	0	6
	Weight (sq. sec/cm):	-0.371	-0.090	-0.163
Sea Surface Temp.	Time Lag (hours):	0	0	0
	Weight (cm/deg C):	6.700	6.060	6.061
	Skill of Estimate:	0.7586	0.8289	0.8324

		Summer		
		La Jolla	Newport	Catalina
Pressure	Time Lag (hours):	0	0	0
	Weight (cm/mbar):	-0.832	-0.796	-0.966
Longshore Wind Stess	Time Lag (hours):	20	28	22
	Weight (sq. sec/cm):	-0.253	0.298	0.148
Cross Shore Wind Stress	Time Lag (hours):	31	12	0
	Weight (sq. sec/cm):	-2.520	-0.526	0.743
Sea Surface Temp.	Time Lag (hours):	0	0	0
	Weight (cm/deg C):	1.418	0.864	-0.221
	Skill of Estimate:	0.4483	0.4323	0.6068

Table 5.2: Statistical analysis results, for longshore and cross-shore defined by the local coastline of the bight a) Winter 82-83, b) Summer 83.

possible errors in measurement and sampling, it seems as if the sea surface in the bight responds as an inverse barometer. But by comparing the summer and winter values, it is noted that the winter values are consistently higher. This might imply that the ocean is in fact not behaving strictly as an inverse barometer. The barotropic Rossby radius of deformation in the Southern California Bight is approximately 1100 km which is less than the length scale of the pressure forcing. Crepon (1976) noted that the exact response can be greater or less than 1.01 cm/mbar depending upon the configuration of the forcing.

5.3 Sea surface temperature

The effect of temperature on sea surface elevation can be obtained from the hydrostatic equation, which for positive z upward is

$$\frac{dP_w}{dz} = -g\rho(z), \tag{5.3.1}$$

where P_w = pressure in the water,

g = gravitational acceleration,

ρ = water density.

Integrating from a reference pressure P_0 at depth z_0 to the surface z_s,where the water pressure is small compared to P_0, gives

$$(z_s - z_0) = -\frac{1}{g}\int_{P_0}^{0} \alpha \, dP \ , \qquad (5.3.2)$$

where α is the specific volume which is defined to be the reciprocal value of the density. The specific volume is a function of temperature, salinty and pressure. Warm or low salinity water displaces a larger volume, and hence causes a rise in sea surface elevation, relative to cold or high salinity water. The quantity $(z_s - z_0)$ is known as the steric height of the sea surface relative to the reference level P_0.

Statistical regression analysis, as outlined in section 5.1, revealed that the inclusion of sea surface temperature as an input variable increased the skill of the estimate of the sea level anomaly, adjusted for pressure, by up to 0.10, at the coast and 0.23 at Santa Catalina. Steric effects may play a larger role in forcing variations at longer time scales (seasonally).

Examination of the regression coefficients shows that there is little difference between stations with the values of similiar magnitude for a given season. However, there was a large difference between summer and winter coefficients at each station, as well as in the improvement of the skill of the estimate that inclusion of sea surface temperature provided. The winter values of the regression coefficient were about five times the summer values. And while the sea surface temperature anomalies were smaller in the winter than in the summer, the skill of the estimate for the winter increased by 0.10 at the coast and 0.23 at Santa Catalina, compared to 0.05 and less than 0.01, respectively for the summer. It seems the high sea surface temperatures, associated with the ENSO event that year, had a larger effect in the winter than in the summer. However this is a relatively small effect when compared to the atmospheric pressure effect, which was removed from the sea level anomaly record.

5.4 Wind stress forcing - spatial scale

Multiple - input statistical analysis was performed on sea level elevation anomalies with longshore and cross-shore wind stress,

atmospheric pressure and sea surface temperature as input variables. To identify the importance of local coastal morphology on the wind field, the wind velocity was broken into longshore and cross-shore components. An important question that must be considered is how are longshore and cross-shore defined. The precise direction is critical if the general idea that longshore wind forcing is of greater importance than cross-shore wind forcing is to be examined. In past works, the definitions of longshore and cross-shore have been arbitrarily chosen at each coastal location of interest by the general visual trend of the coastline. The implicit assumption made is that the winds feel the local coastal morphology, that is the coastline defines the spatial scale of the wind stress forcing rather than the meteorological systems. For many areas the coastline spatial scale and weather system spatial scales are similar, but this is not true for the Southern California Bight.

Three coordinate systems were chosen to attempt to identify the important spacial scaling and orientation. The coastline in the Southern California Bight area lies in a north - northwest line from San Diego to Dana Pt., but then turns abruptly to the west -

northwest, with the spatial scale of each coastal leg on the order of 100 km. So it is not clear how an appropriate coordinate system would be defined. The three coordinate sytems chosen represent the longshore and cross-shore orientations with respect to the local Newport Beach coastline, the local La Jolla coastline and the third with respect to the general coastline of the bight (Figure 5.2).

The longshore and cross-shore wind stresses for each coordinate system can be computed from the wind velocity. The wind stress components can be used as input variables in the statistical models giving three estimators with the only difference between them being the orientation of the coordinate system. The effects of different coordinate systems can be compared by the skill of the estimates. Also the regression coefficients for the longshore and cross-shore input variables, computed for each coordinate system, can be compared .

The results of the analysis show little difference at La Jolla between the local coordinate system and the regional coordinate system. The results at Newport Beach reveal that a small improvement in the skill of the estimate was achieved by defining longshore and cross-shore with respect to the general bight

Figure 5.1: Orientation of the local Newport, local La Jolla and regional coordinate systems.

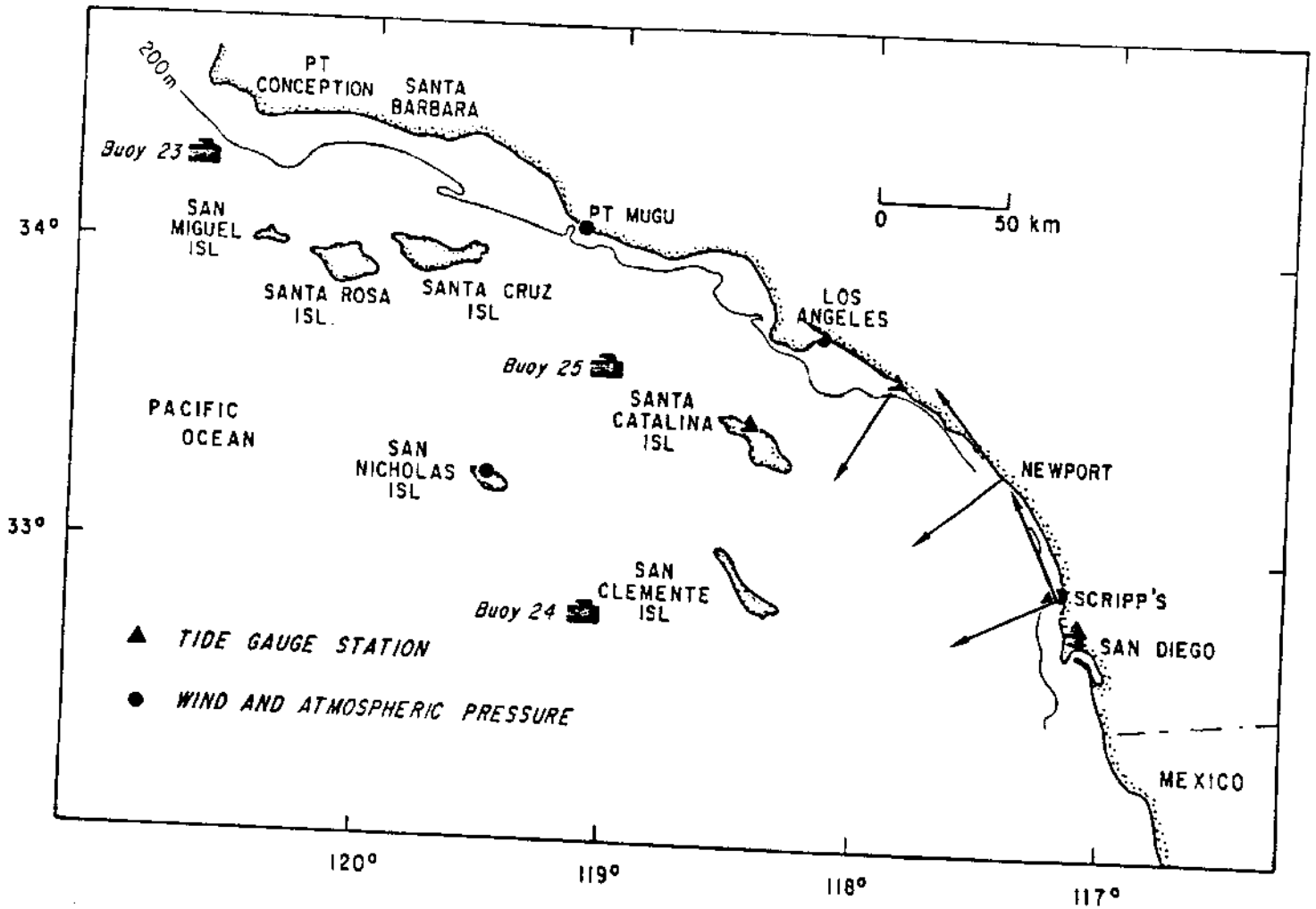
200m
PT CONCEPTION
SANTA BARBARA
Buoy 23
PT MUGU
0
50 km
SAN MIGUEL ISL
SANTA ROSA ISL.
SANTA CRUZ ISL
LOS ANGELES
Buoy 25
SANTA CATALINA ISL
PACIFIC OCEAN
SAN NICHOLAS ISL
NEWPORT
SAN CLEMENTE ISL
Buoy 24
SCRIPP'S
SAN DIEGO
TIDE GAUGE STATION
WIND AND ATMOSPHERIC PRESSURE
MEXICO
34°
33°
120°
119°
118°
117°

coastline. The results at Santa Catalina are similiar to those at La Jolla, with the coordinate system having only a small effect on the skill of the estimate. This suggests that the atmospheric forcing is at large spatial scales, which the regional coordinate system represents.

The response coefficients for the longshore wind stress input variable are similiar for the coastal stations as well as for the offshore island. This implies that the response to the longshore wind field does not "feel" the islands. Wind from the south piles up water at the coast through Ekman transport and this buildup extends offshore past Santa Catalina. This implies that the spatial scale of the sea level response is larger than the distance between Santa Catalina and Newport Beach. This is further reinforced by analysis of periods where the wind is from the north. Wind from the north does not pile up water on Santa Catalina , so the spatial scale of the sea level response must be large compared to the length of Santa Catalina Island. That is, Santa Catalina island does not act as a barrier to the atmospherically forced water motion. The weights of the cross-shore wind stress input variables, at each station, agree in sign and are similar in magnitude implying that the wind

field acts on a cross-shore spatial scale larger than the distance between Santa Catalina and Newport Beach.

5.5 Wind stress forcing - response adjustment time

Passage of storm fronts through the bight brings with them increasing wind velocities and a drop in the atmospheric pressure. The response of the sea level to atmospheric pressure forcing is immediate, while the response to the wind stress forcing would be expected to require an adjustment time. This is due to the fact that the pressure field acts across the whole bight uniformly displacing the water under it. The longshore wind stress acts on the water through Ekman transport. This water, when it meets a solid boundary piles up creating a sea surface tilt. A finite time, thought to be on the order of 1/f, is required for this pile up to occur since the water must be put in motion and rotation effects felt by the water mass. For shorter time scales, where rotation effects are slight, cross-shore wind stress is thought to force water directly in the cross-shore direction, and the wind stress forcing is balanced by bottom friction. When this flow meets a solid boundary again a sea surface tilt results.

The linear statistical model can be used to examine the adjustment times of longshore and cross-shore wind stresses. By repeatedly doing the statistical analysis on the cross-shore and longshore wind stresses at various time lags, a "best" adjustment time can be found. The criteria for "best" being the time lag which gives the best estimate skill.

The results of the analysis are shown in Figure 5.2. The winter results showed little similarity, between stations, of the "best" time lags for both longshore and cross-shore wind stress inputs, while the summer values were much more consistent. The summer is a period of less variable winds and few high wind events. This would imply that the adjustment time may be wind velocity dependent. The artificial skill calculation, assuming five day independent realizations, shows that the wind stress forcing contributes significantly in the winter, but has little effect in the summer.

The surprising result is that the spin-up time for the cross-shore wind stress input variable is consistently larger than for the longshore wind stress. The reasons for this have to do with the complexity of the mechanisms involved. From the analytical

Figure 5.2: Plots of skill vs. time lag; with artificial skill marked a) longshore windstress, 26 November 1982 - 30 March 1983; b) longshore windstress, 28 May 1983 - 29 September 1983; c) cross-shore windstress, 26 November 1982 - 30 March 1983; d) cross -shore windstress 28 May 1983 - 29 September 1983. Solid line - La Jolla, small dash - Newport Beach, large dash - Santa Catalina.

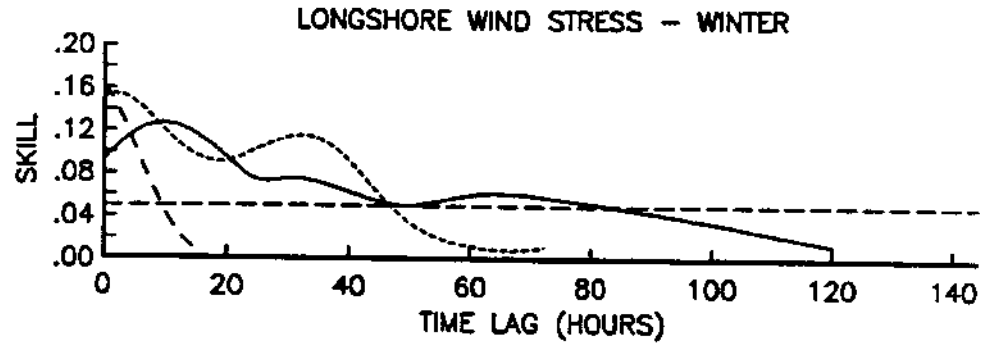
LONGSHORE WIND STRESS – WINTER
SKILL
.20
.16
.12
.08
.04
.00
0
20
40
60
80
100
120
140
TIME LAG (HOURS)

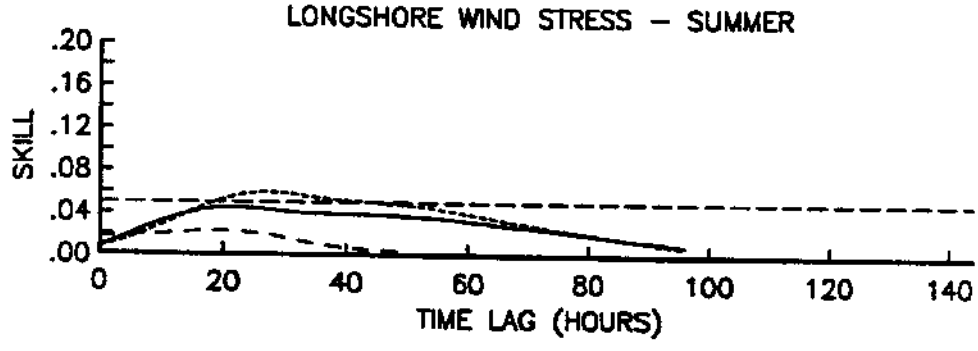
LONGSHORE WIND STRESS – SUMMER
SKILL
.20
.16
.12
.08
.04
.00
0
20
40
60
80
100
120
140
TIME LAG (HOURS)

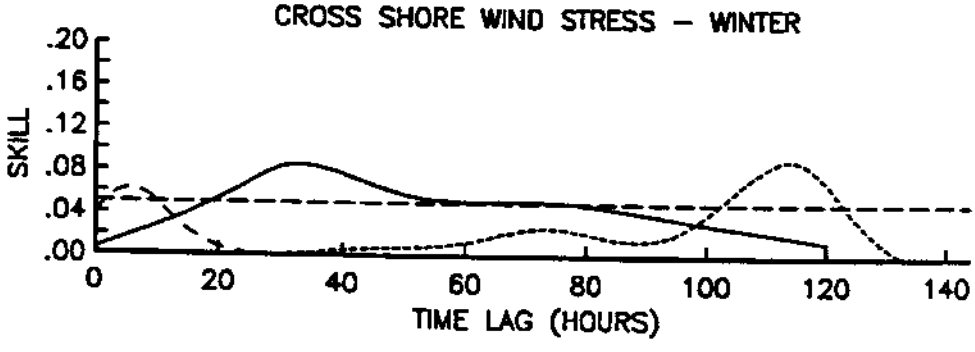
CROSS SHORE WIND STRESS – WINTER
SKILL
.20
.16
.12
.08
.04
.00
0
20
40
60
80
100
120
140
TIME LAG (HOURS)

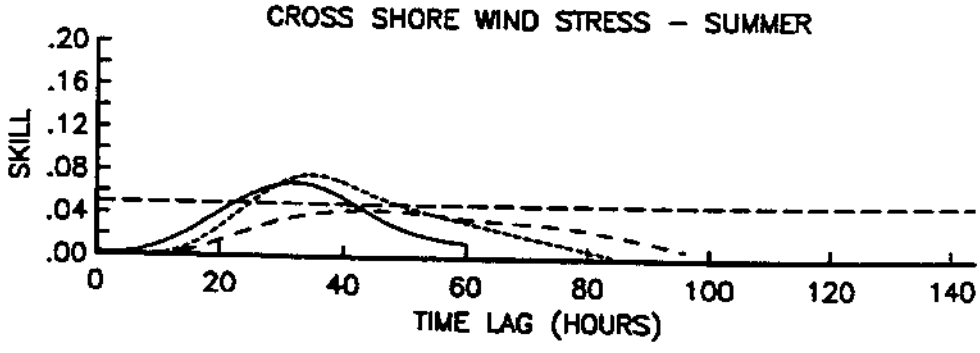
CROSS SHORE WIND STRESS – SUMMER
SKILL
.20
.16
.12
.08
.04
.00
0
20
40
60
80
100
120
140
TIME LAG (HOURS)

model solution (equations 2.3.1), it can be seen that bottom friction plays a dominant role in the adjustment of sea level to steady wind stress forcing. The bottom friction is very much velocity dependent. This is consistent with the summer results when winds are steady, but the model provides little dynamical insight in the winter when winds are inconsistent in strength. The analysis does reveal the importance of the duration (compared to 1/f) of the wind events in forcing sea level fluctuations.

Chapter 6 Storm Events

6.1 General description

With storm system spatial scales being much larger than the Southern California Bight, the position of the bight within the storm system as the storm passes over the bight region becomes of great importance. Most storm systems pass from the west to the east or from the northwest to the southeast. If the storm center passes to the north of the bight, the storm event begins with increasing winds to the north-northeast. The winds continue to increase in speed and begin to rotate to the east. The maximum wind speed is reached with the wind blowing in a northeasterly direction. The storm continues eastward as the storm center, marked by a distinct pressure drop, passes through the bight region, the winds decrease and abruptly turn to the south. The wind speeds then increase again in speed until the storm has passed.

Storms in which the center passes to the south of the bight are led by increasing winds to the northwest. Passage of the storm center is also marked by a drop in atmospheric pressure as well as a reversal in wind direction and decrease in wind speed.

The wind speeds begin to pick up again until the storm has passed and the wind returns to "normal".

An examination of five storm events during the winter of 1982-1983 reveals some general characteristics of the sea level response to storm forcing in the Southern California Bight. It was seen earlier that the sea level response to pressure forcing was very similiar to an inverse barometer. Assuming this is true, the sea level can be adjusted to remove the response due to atmospheric pressure forcing. It is this adjusted sea level response that iss examined in the following discussion.

6.2 28 November - 3 December 1982

The storm event at the end of November 1982 was marked by a atmospheric pressure drop over the bight of 10.2 mbars on 30 November. The wind conditions before the storm were light at 10 to 15 km/hr to the east. As the storm neared the wind speed increased and changed direction blowing to the southeast at 40 km/hr. As the front moved past the winds abruptly changed to the northwest and the speed decreased to close to 30 km/hr. The high winds persisted for just over a day, and then further decreased

Figure 6.1a: Daily weather map, 29 November 1982.

SAN DIEGO: HIGH SLP (T =-6) (1982 11 29 0)

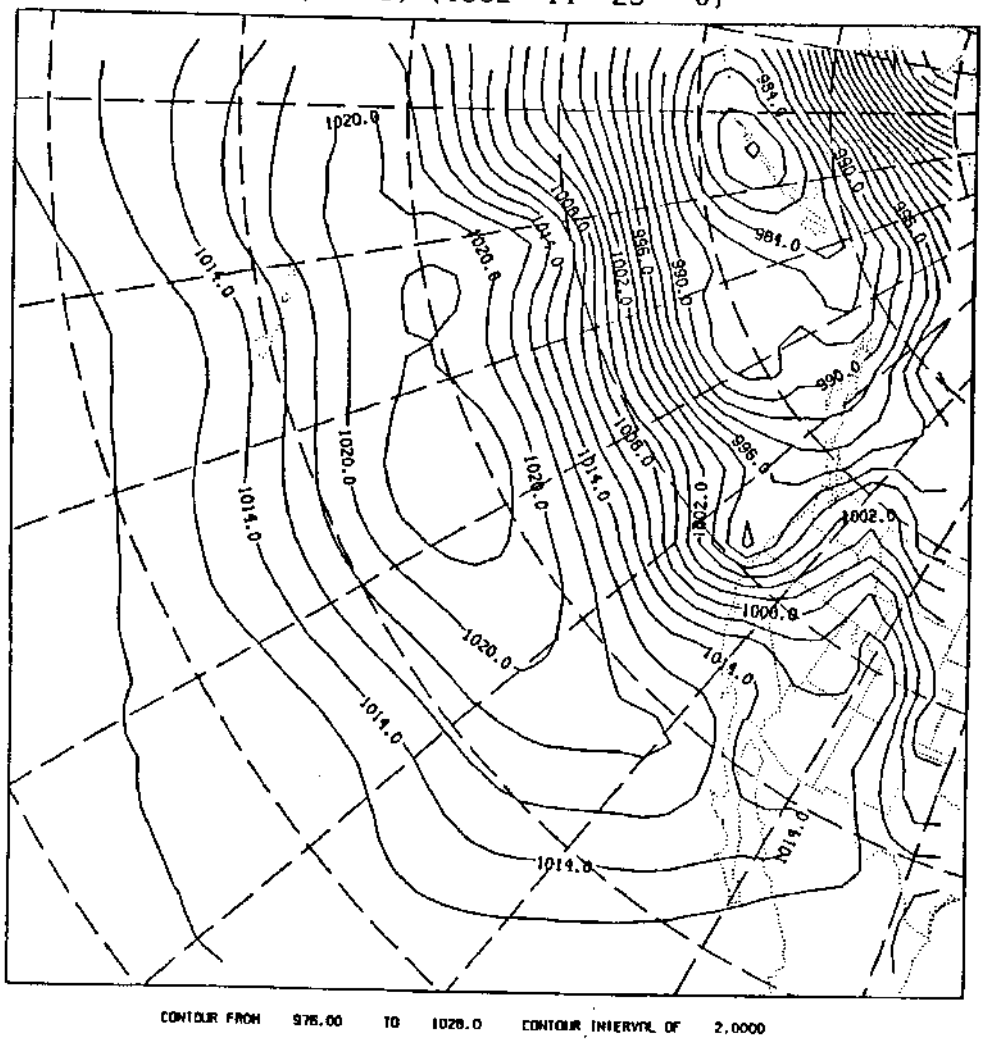

Figure 6.1b: Daily weather map, 30 November 1982.

SAN DIEGO: HIGH SLP (T =-2) (1982 11 30 0)

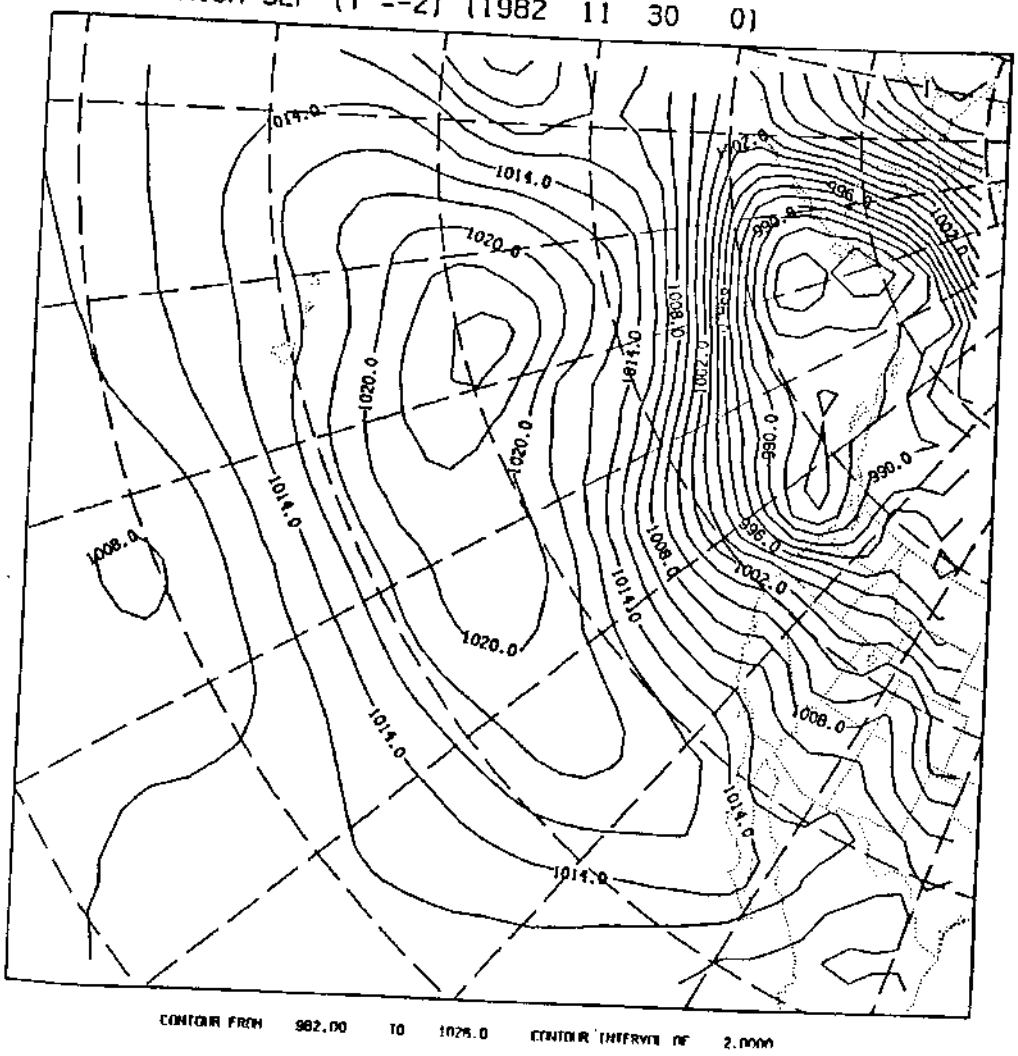

Figure 6.1c: Daily weather map, 1 December 1982.

SAN DIEGO: HIGH SLP (T = 2) (1982 12 1 0)

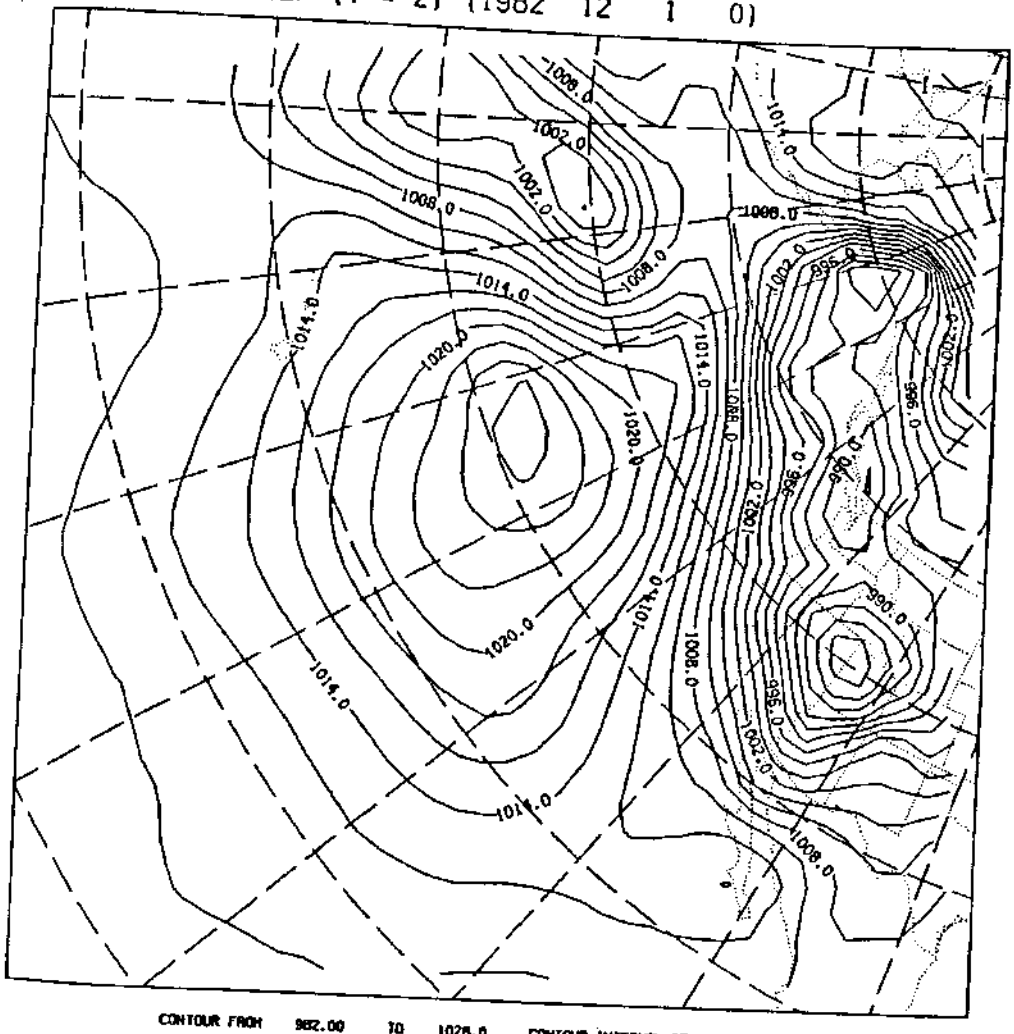

and rotated to back to their usual onshore state.

Examination of the wind stress time series for the storm showed a peak in both cross-shore and longshore stresses. The cross-shore wind stress peak preceeded the atmospheric pressure drop by about twelve hours. The longshore wind stress peak lagged the pressure drop by ten hours. The crosshore wind stress was directed in the offshore direction causing a sea level drop at La Jolla 31 hours later. The longshore wind stress was directed to the southeast. Ekman transport would be to the southwest, away from the coast. The adjusted sea level drop at La Jolla occured ten hours after the peak longshore wind stress. These numbers agree with the time lags found in the multiple input statistical analysisfor La Jolla.

6.3 20 December - 25 December 1982

This storm event was similiar to the 28 November - 3 December event, in that a peak in offshore wind stress followed by the maximum pressure drop, followed by the peak in longshore wind stress directed to the southeast. The storm was moving in a slightly different direction and speed, since the times between the

Figure 6.2a: Daily weather map, 22 December 1982.

SAN DIEGO: HIGH SLP (T =-6) (1982 12 22 0)

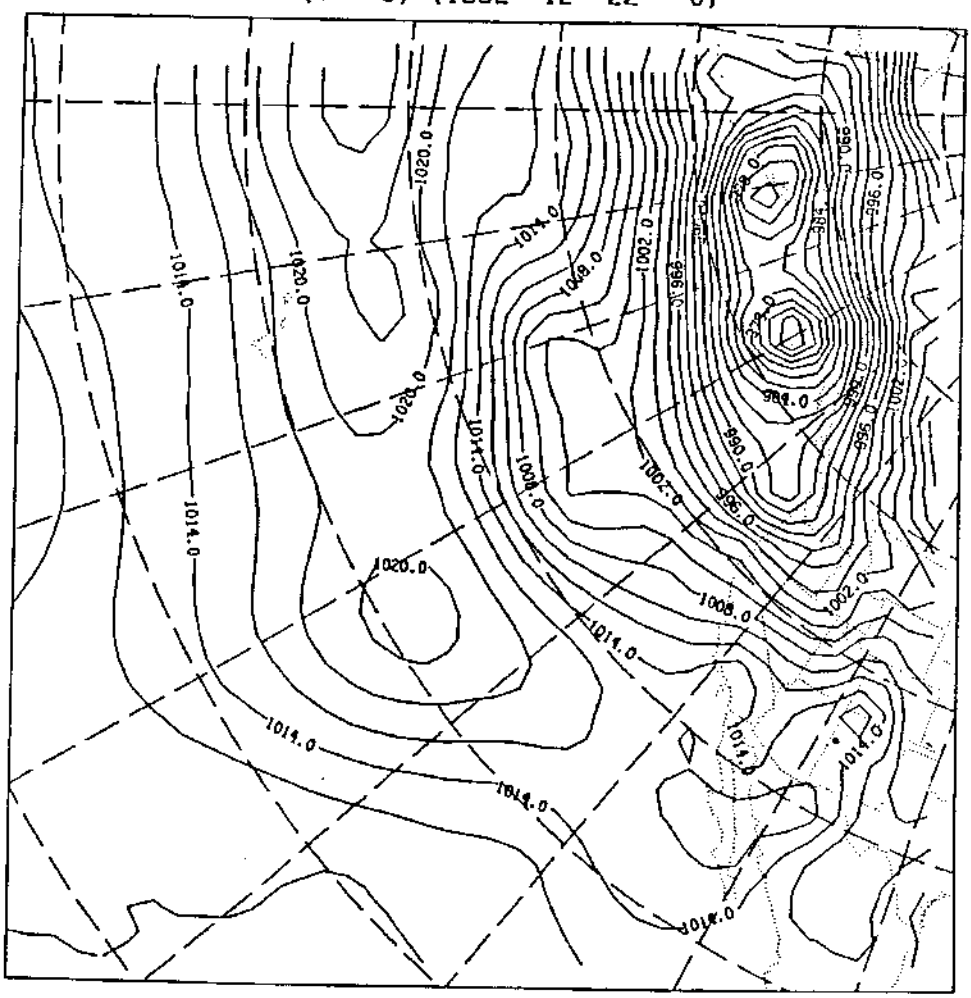

Figure 6.2b: Daily weather map, 23 December 1982.

SAN DIEGO: HIGH SLP (T =-2) (1982 12 23 0)

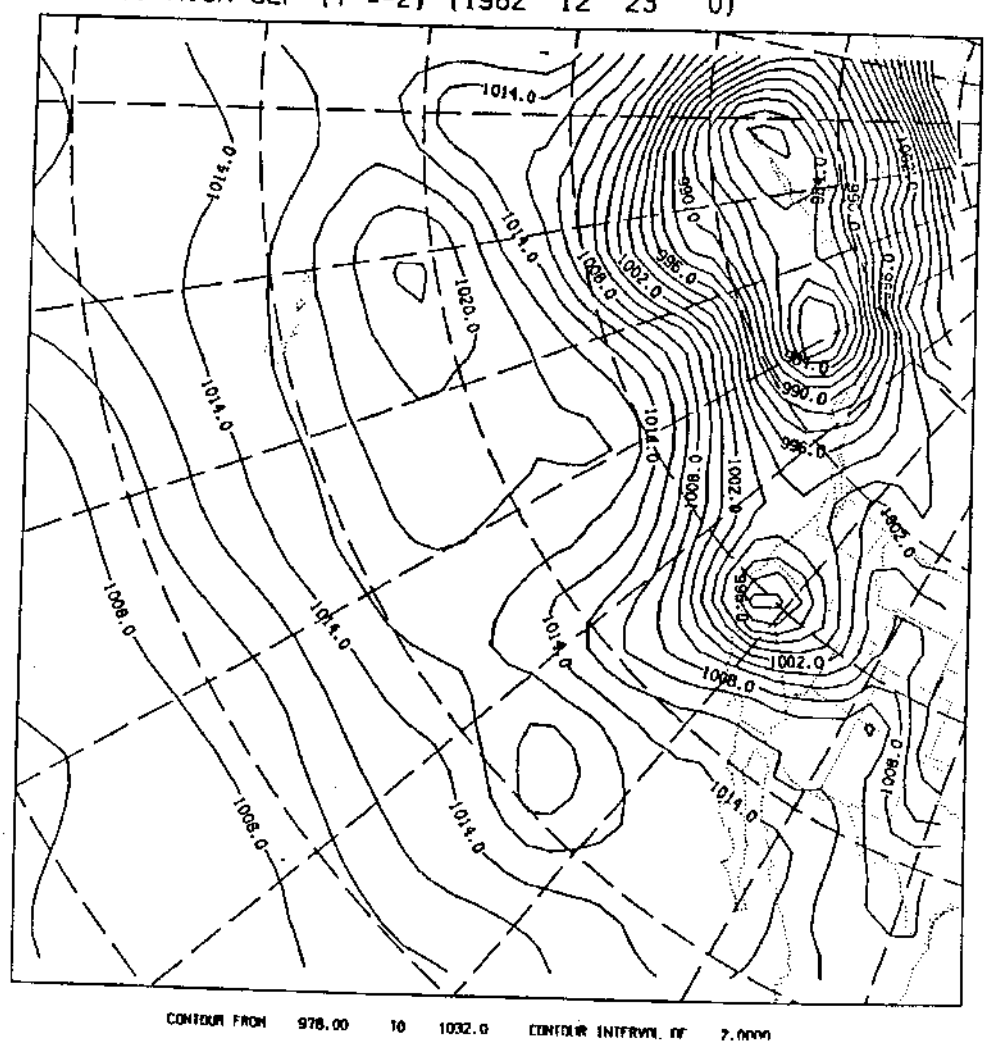

Figure 6.2c: Daily weather map, 24 December 1982.

SAN DIEGO: HIGH SLP (T = 2) (1982 12 24 0)

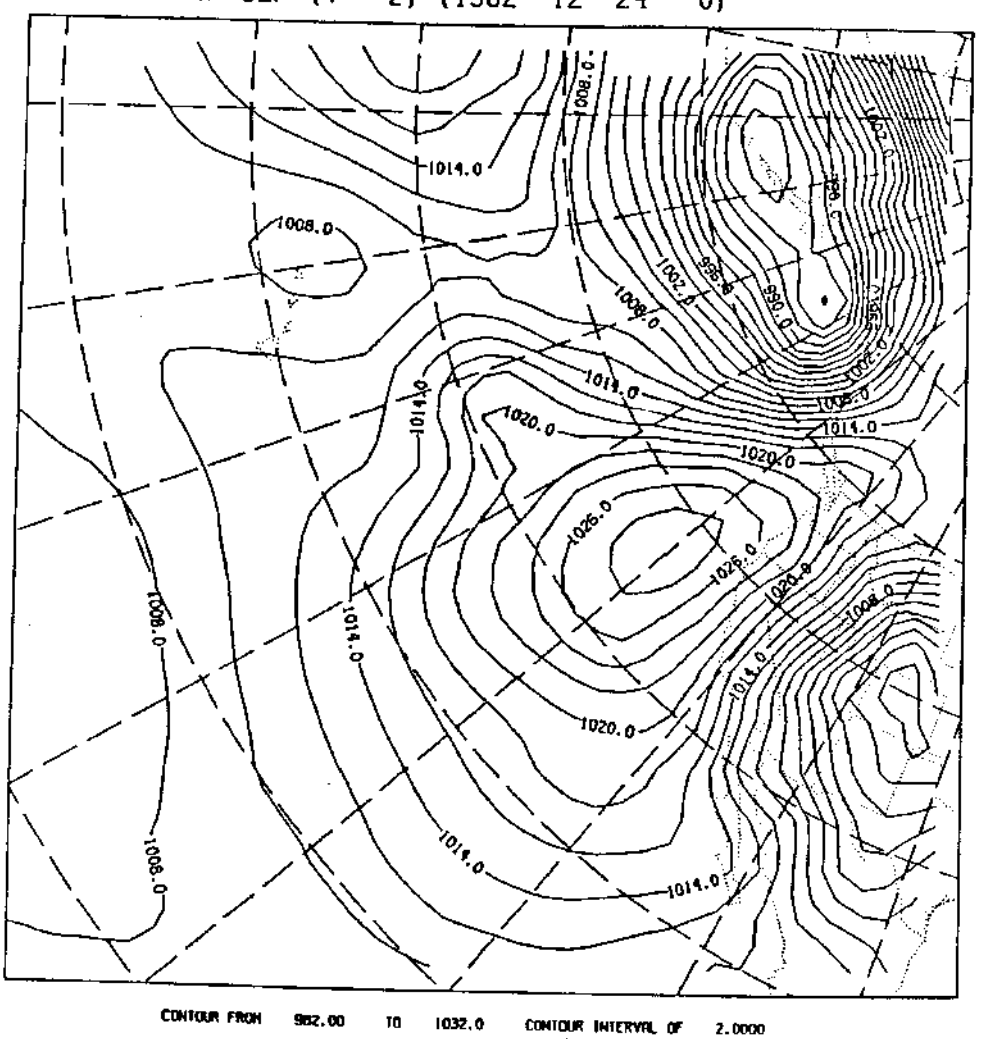

wind stress peaks and the pressure minimum were 5 and 20 hours compared to 14 and 10 hours respectively. The offshore and longshore wind stress preceded the adjusted sea level extreme by 32 and 8 hours. These too, are similiar to to the previous statistical results.

6.4 26 January - 29 January 1982

The period was marked by two low pressure occurences, one on 27 January 1982 and the other on 28 January 1982. Wind field similarities were evident between each event. These events were both marked by increases in the longshore wind stress followed by a weak offshore wind stress peak. The occurence of the weak offshore wind stress peak is coincident with the reversal in the longshore wind stress direction to the southeast. The time between wind stress extrema and adjusted sea level peaks were between 8 and 12 hours, which is consistent with the previous results. The time between the weak offshore wind stress peak and the adjusted sea level drop was about 24 hours. The adjusted sea level anomalies were much smaller than found in the previous events. This may be due to the fact that the January events were

Figure 6.3a: Daily weather map, 26 January 1983.

SAN DIEGO: HIGH SLP (T =-6) (1983 1 26 0)

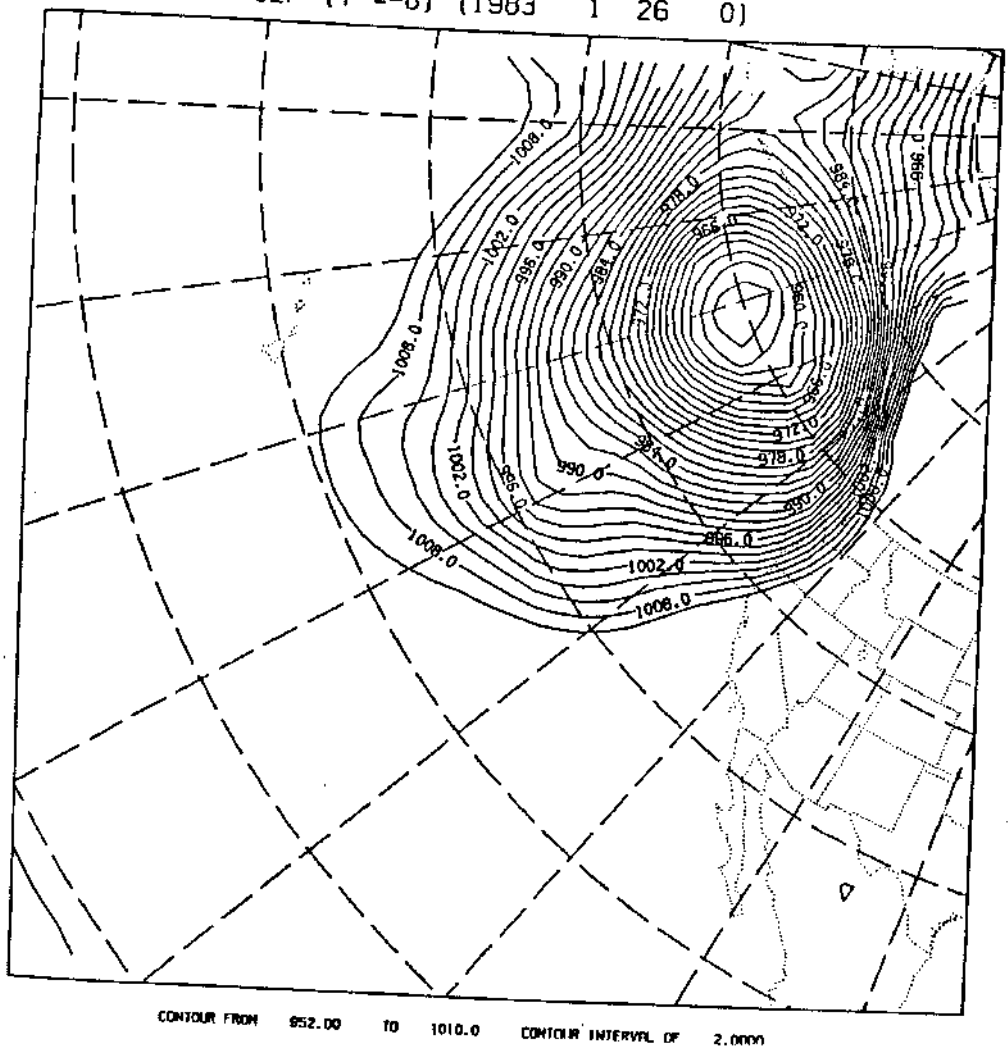

Figure 6.3b: Daily weather map, 27 January 1983.

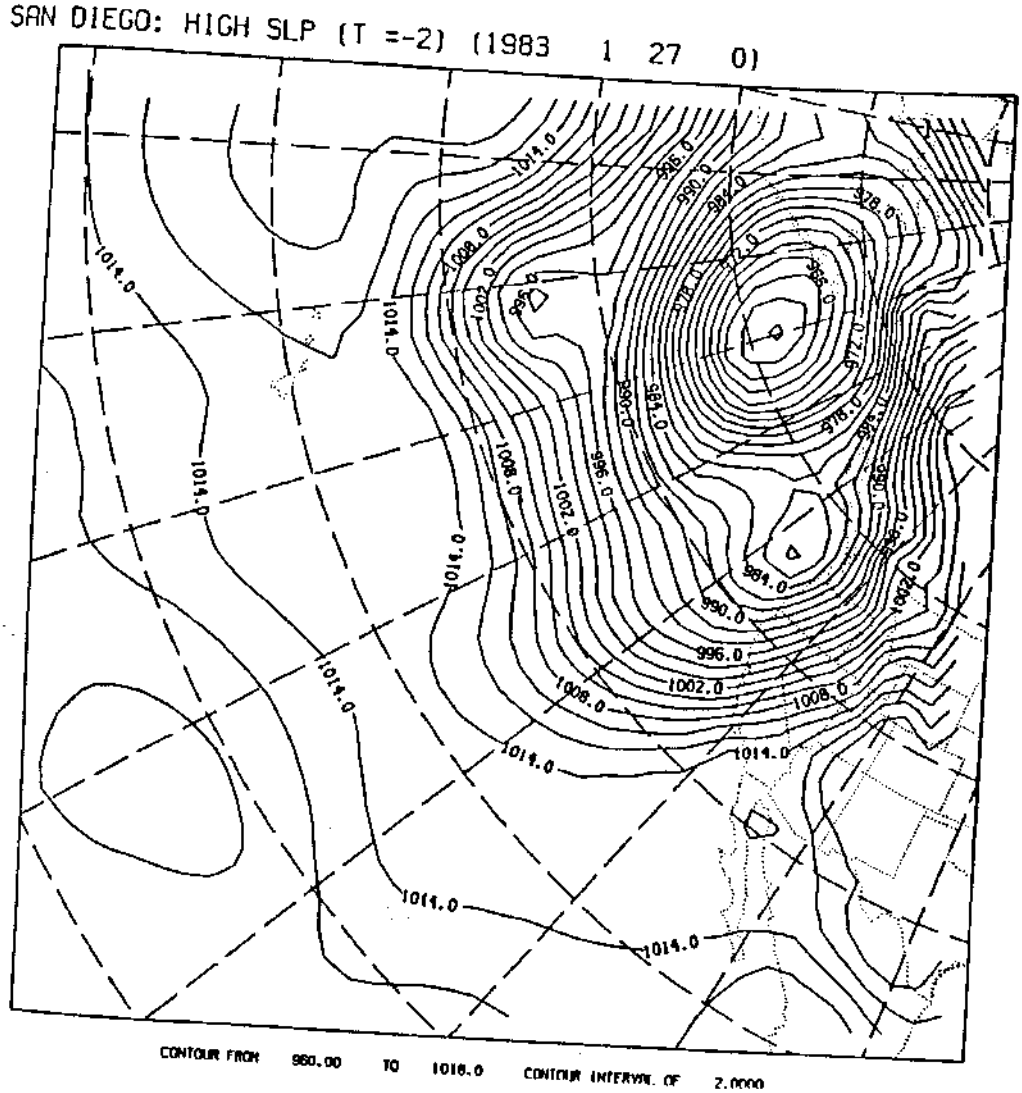
SAN DIEGO: HIGH SLP (T =-2) (1983 1 27 0)
CONTOUR FROM 960.00 TO 1018.0 CONTOUR INTERVAL OF 2.0000

Figure 6.3c: Daily weather map, 28 January 1983.

SAN DIEGO: HIGH SLP (T = 2) (1983 1 28 0)

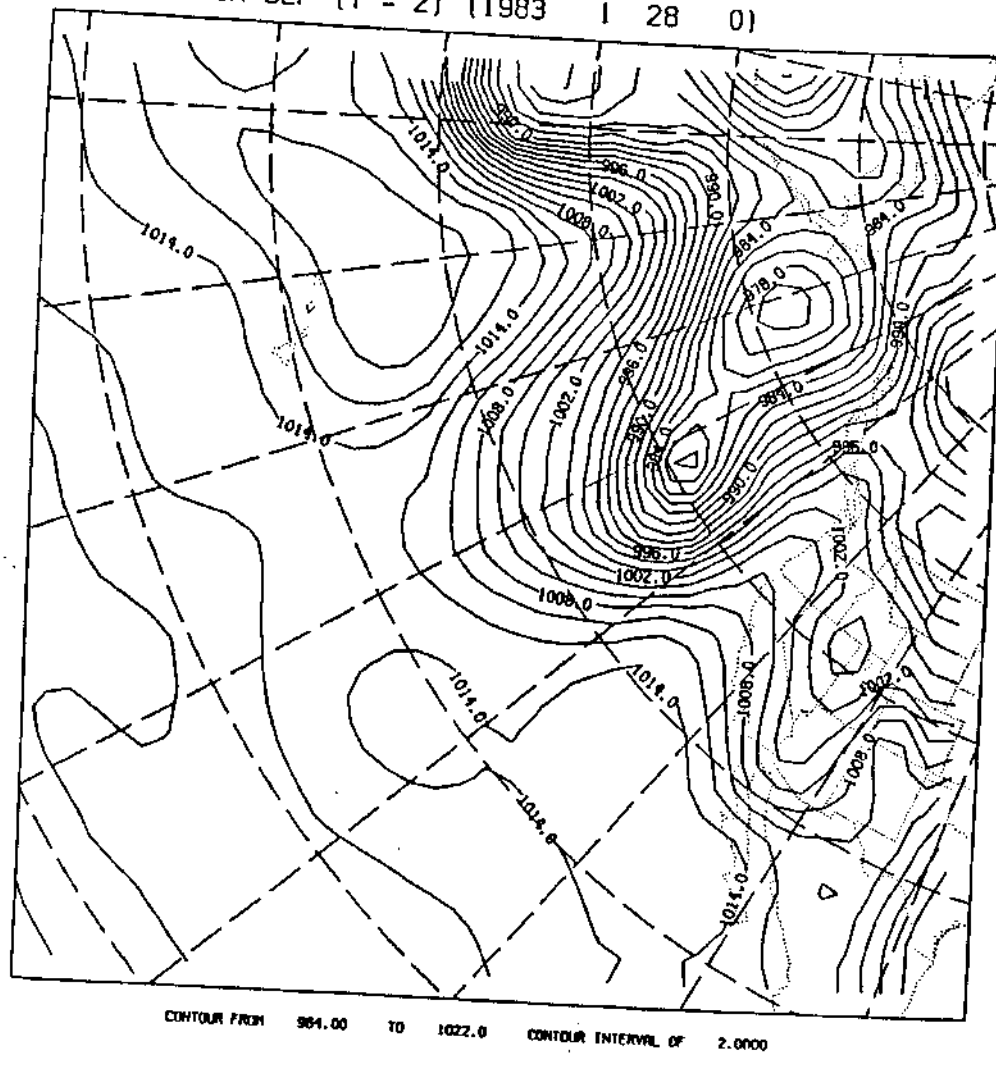

of much shorter duration with strong steady winds lasting for roughly a day while the earlier events had consistent winds for two or more days.

This storm event coincided with the occurance of peak tides, and absolute sea level elevation (above the 1960 -1978 average MLLW) reached 2.54 meters in San Diego on 27 January, the highest such value since 1906. High sea levels were recorded all along the California coast during this period, with San Francisco recording its all-time maximum sea level on 26 January. It was during this period of intense storm activity that most of the 1983 coastal flood damage occurred.

6.5 1 February - 3 February

This storm event was similiar to the January events but with inconsistent high winds. The inconsistent winds caused aa adjusted sea level rise of only 1 to 2 cm. Though the wind forcing caused only a small sea level change, the atmospheric pressure forcing caused sea level rises on the order of 10 cm.

6.6 28 February - 5 March

Figure 6.4a: Daily weather map, 2 February 1983.

SAN DIEGO: HIGH SLP (T =-6) (1983 2 2 0)

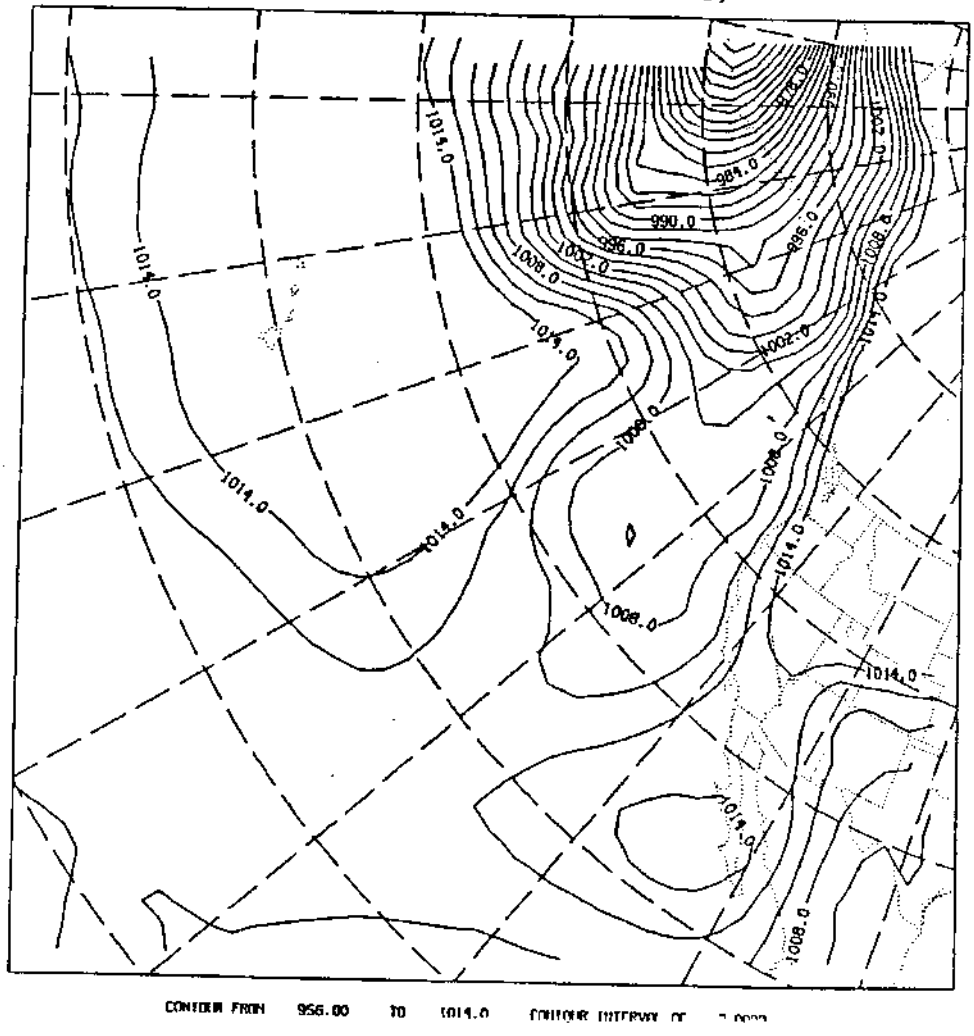

Figure 6.4b: Daily weather map, 3 February 1983.

SAN DIEGO: HIGH SLP (T =-2) (1983 2 3 0)

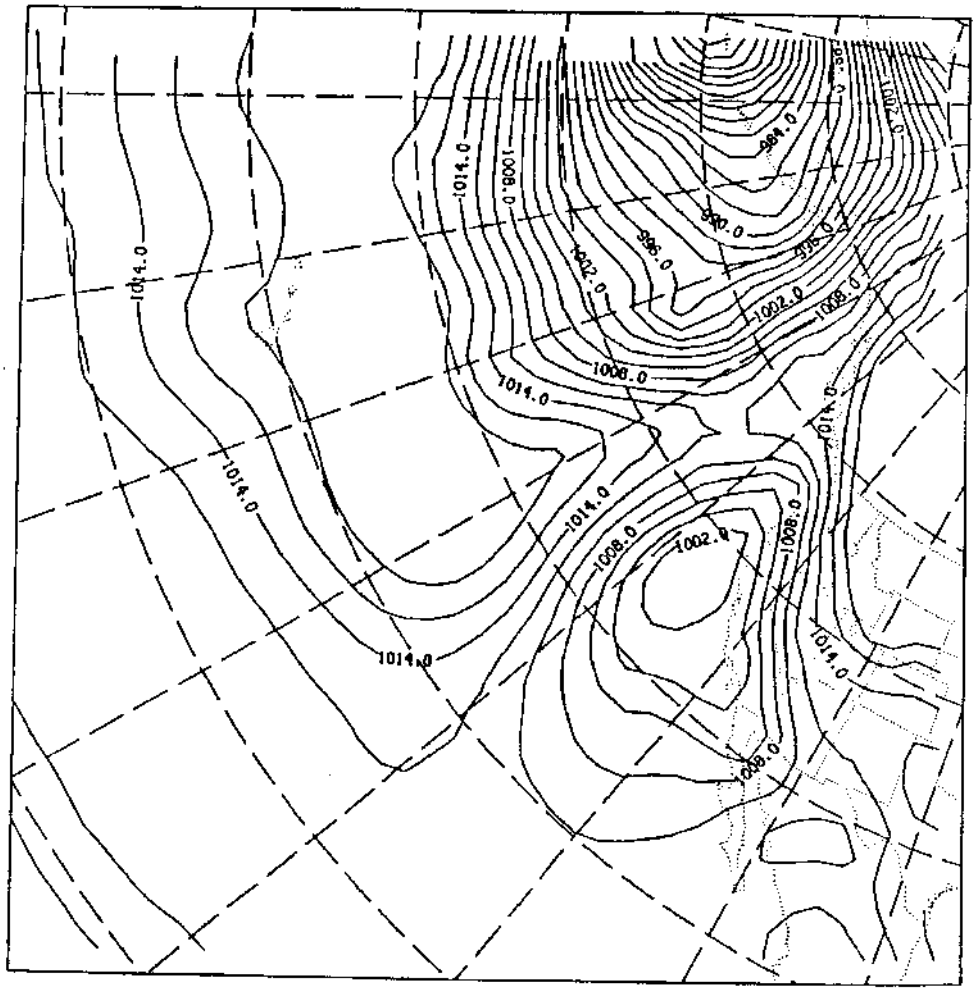

This was the strongest storm event of the winter of 1982 - 1983. The pressure drop was over 17 mbars with wind speeds over 40 km/hr. The storm path through the bight was different, having a more southerly direction, and the duration of the storm was longer than those of the earlier storms The offshore wind stress peak led the event as it has in earlier events. Forty-two hours later the maximum longshore windstress peak occured. This maximum peak corresponded to wind speeds close to 50 km/hr to the northeast. Forty-eight hours later the center of the storm had its closest approach to the bight. Another forty-two hours later the longshore wind stress field reversed and weakened as the storm moved out of the bight.

Adjusted sea level anomalies reached 5 cm with total sea level anomalies exceeding 15 cm. The offshore wind stress peak was followed 30 hours later by a drop in sea level. The longshore wind stress field was directed to the northwest, generating an increase in sea level at the coast 20 hours later. The time lag for the offshore wind stress corresponds with the values found in the statistical analysis for the winter period. The longshore wind stress time lag however was as much as twice as long as the

Figure 6.5a: Daily weather map, 1 March 1983.

SAN DIEGO: HIGH SLP (T =-6) (1983 3 1 0)

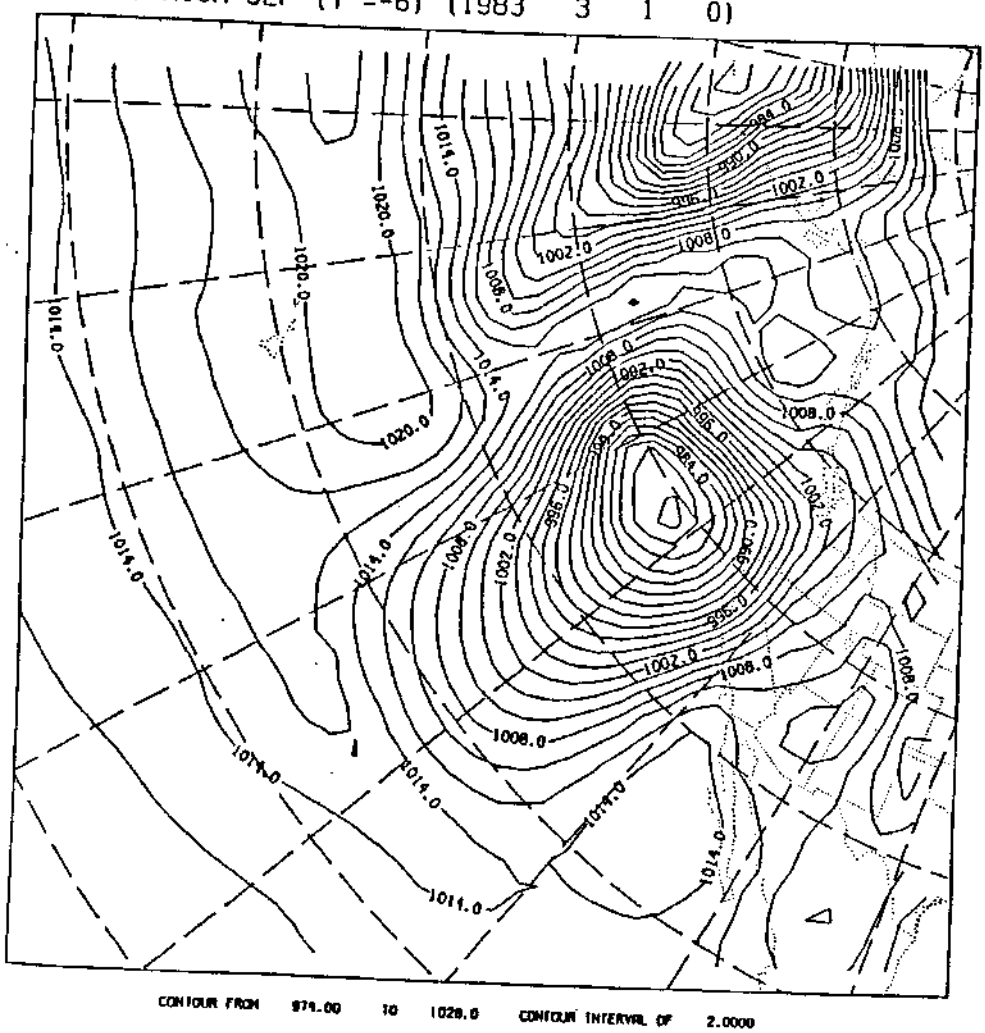

Figure 6.5b: Daily weather map, 2 March 1983.

SAN DIEGO: HIGH SLP (T =-2) (1983 3 2 0)

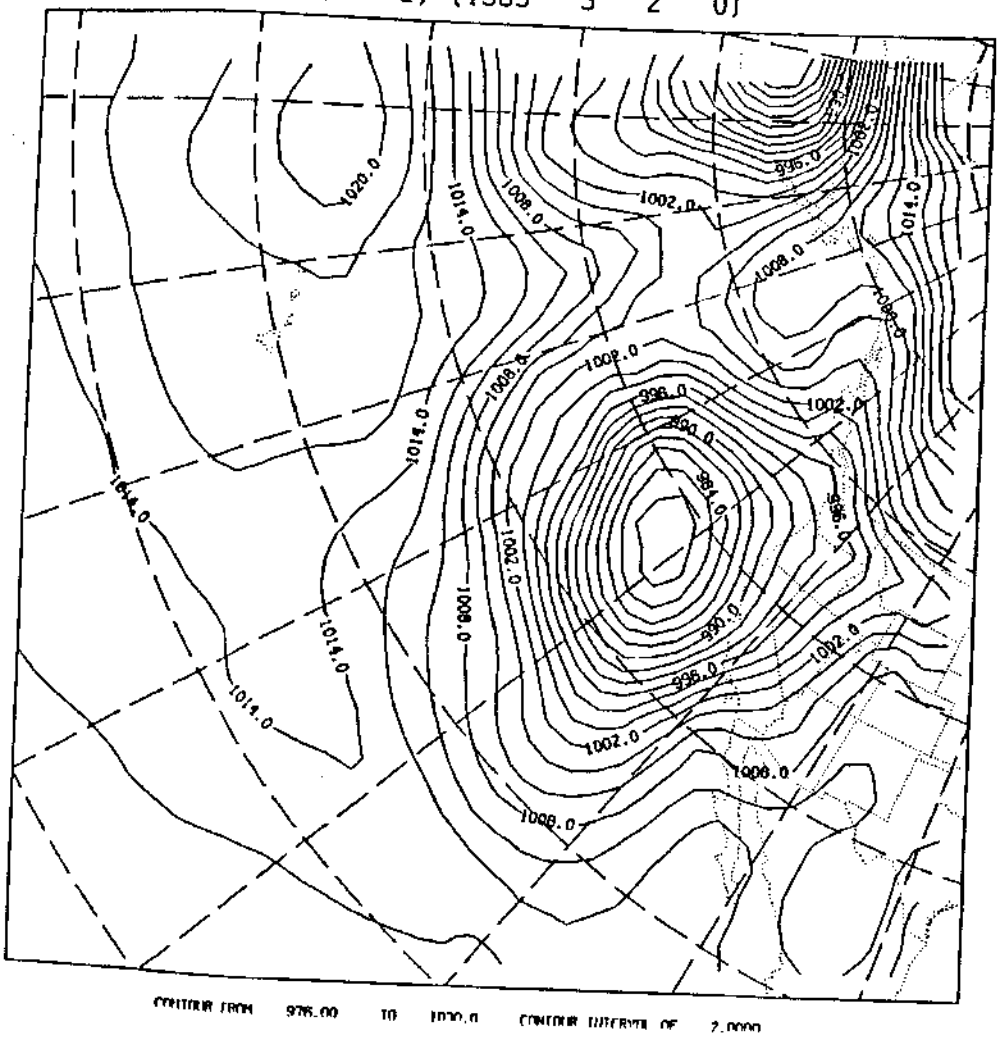

Figure 6.5c: Daily weather map, 3 March 1983.

SAN DIEGO: HIGH SLP (T = 2) (1983 3 3 0)

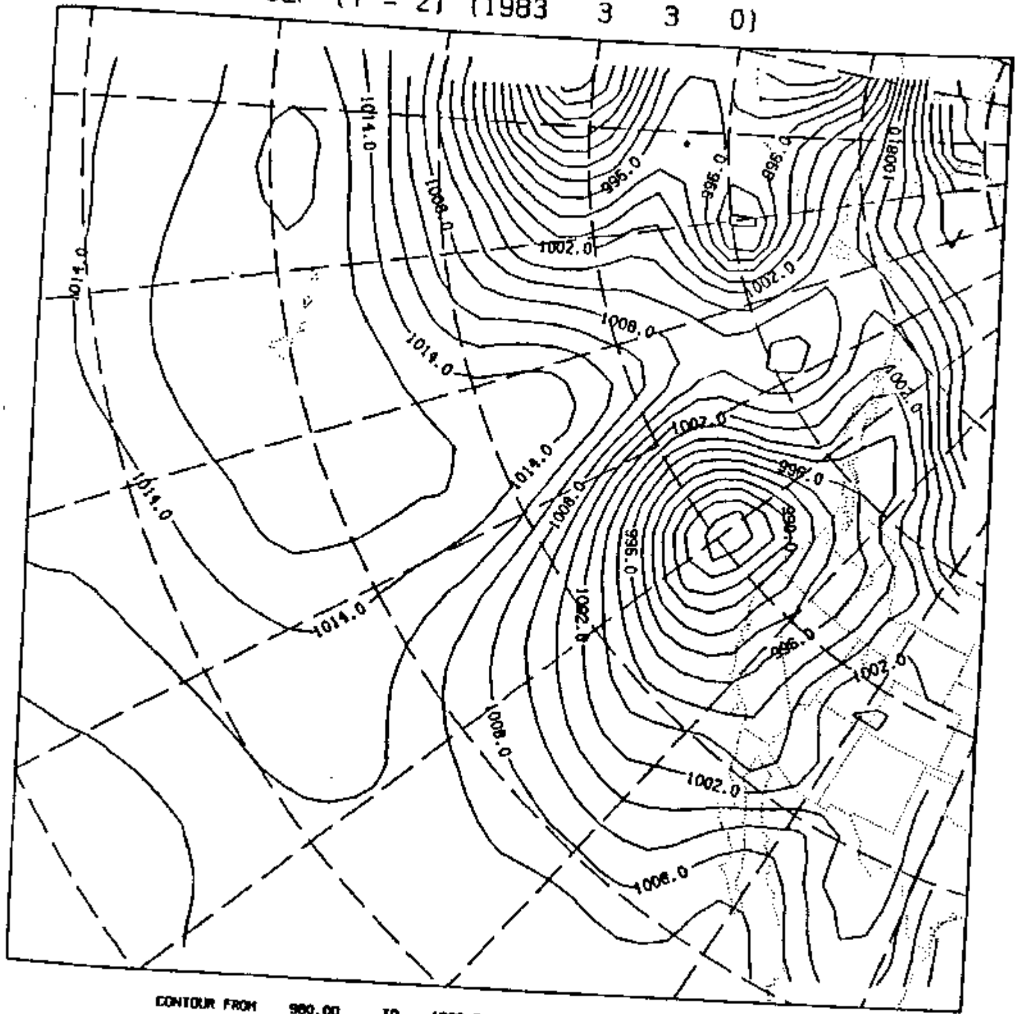

CONTOUR FROM 980.00 TO 1028.0 CONTOUR INTERVAL OF 2.0000

statistical time lag. The duration of the consistent increased wind velocity was greater than three days, and the storm duration was six days. The unusual length of time in which the storm was present over the bight can be attributed to the size of the storm and to its path and speed. The storm path had a southern component, differing it from the earlier events. The storm also seemed to stall for about a day before moving through the bight. These differences may have had an effect on the time lag between the maximum wind stress and maximum sea level.

6.7 Summary

The five storms revealed some general characteristics of the extreme sea level episodes. The events began with increased cross-shore wind stress followed by increased longshore wind stress (Figure 6.6a-e). The extreme adjusted sea levels followed just over a day after the occurrence of the cross-shore wind stress peaks. The time of occurrence of the minimum pressure was dependent upon the storm track. The episodes also revealed the importance of storm duration on the sea surface response. From the progressive wind vector plots (Figures 6.7a-e), it can be

Figure 6.6: Typical storm time series. Early March 1983. a) Cross-shore wind stress (+ from East), b) Longshore wind stress (+ from South), c) Atmospheric pressure, d) Adjusted sea level, e) Sea level. Small dash - Catalina, large dash - Newport.

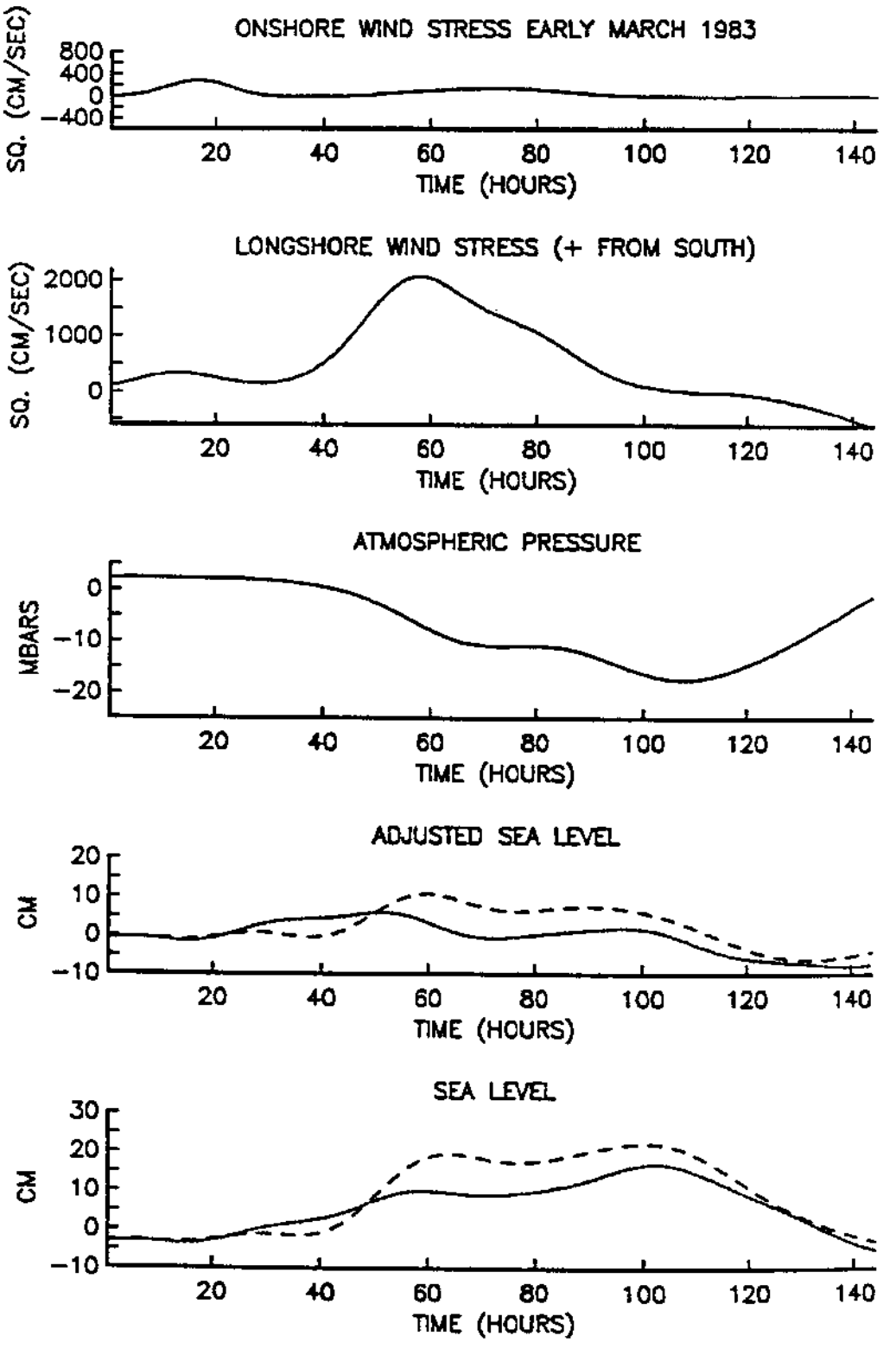
ONSHORE WIND STRESS EARLY MARCH 1983
SQ. (CM/SEC)
800
400
0
−400
20
40
60
80
100
120
140
TIME (HOURS)
LONGSHORE WIND STRESS (+ FROM SOUTH)
SQ. (CM/SEC)
2000
1000
0
20
40
60
80
100
120
140
TIME (HOURS)
ATMOSPHERIC PRESSURE
MBARS
0
−10
−20
20
40
60
80
100
120
140
TIME (HOURS)
ADJUSTED SEA LEVEL
CM
20
10
0
−10
20
40
60
80
100
120
140
TIME (HOURS)
SEA LEVEL
CM
30
20
10
0
−10
20
40
60
80
100
120
140
TIME (HOURS)

Figure 6.7a: Progressive wind vector time series, November 1982.

STATION 24 WINDS 1982

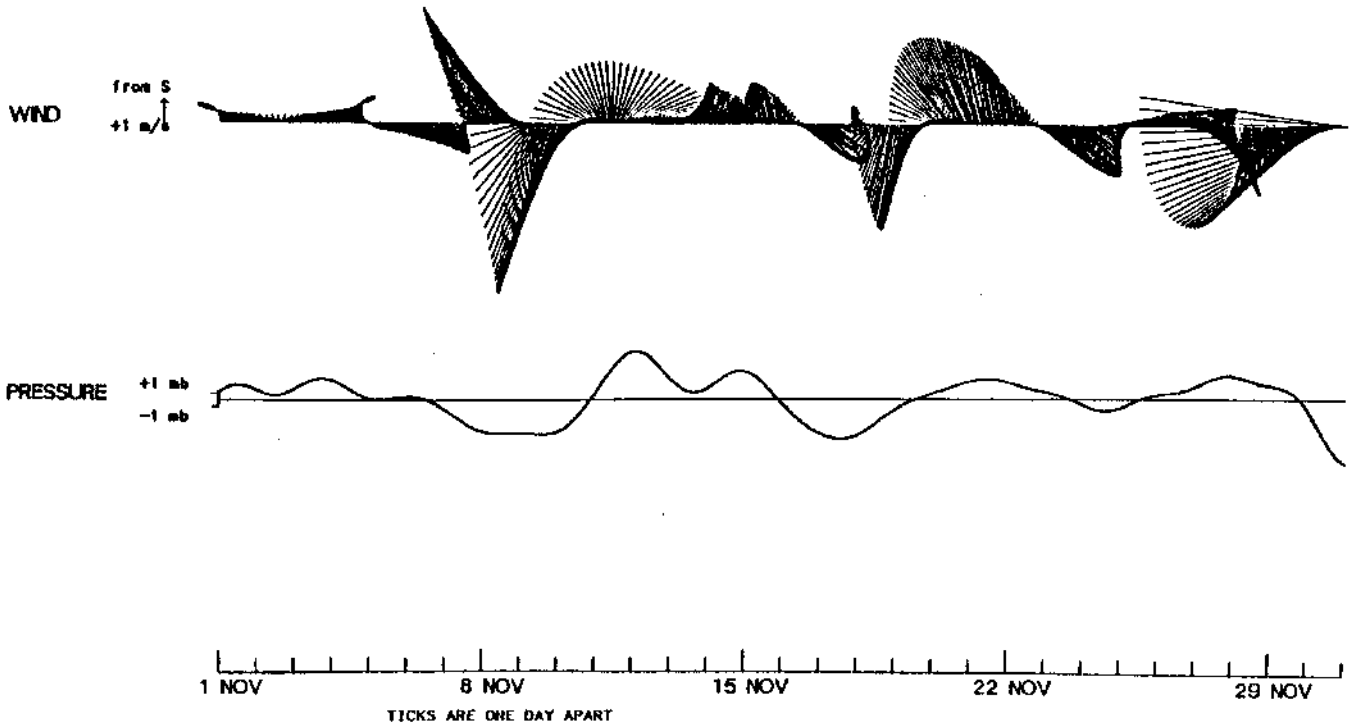

Figure 6.7b: Progressive wind vector time series, December 1982.

STATION 24 WINDS 1982

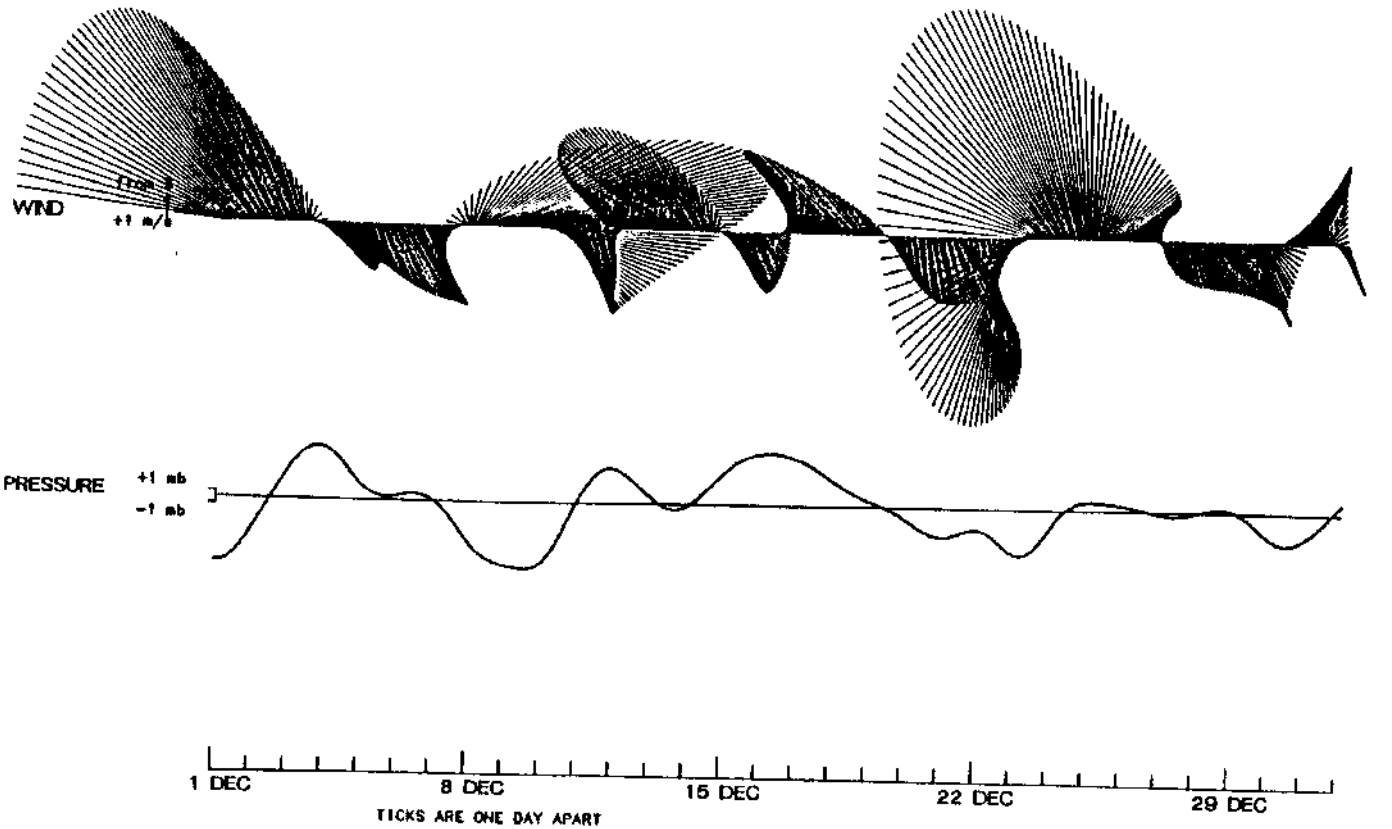

Figure 6.7c: Progressive wind vector time series, January 1983.

STATION 24 WINDS 1983

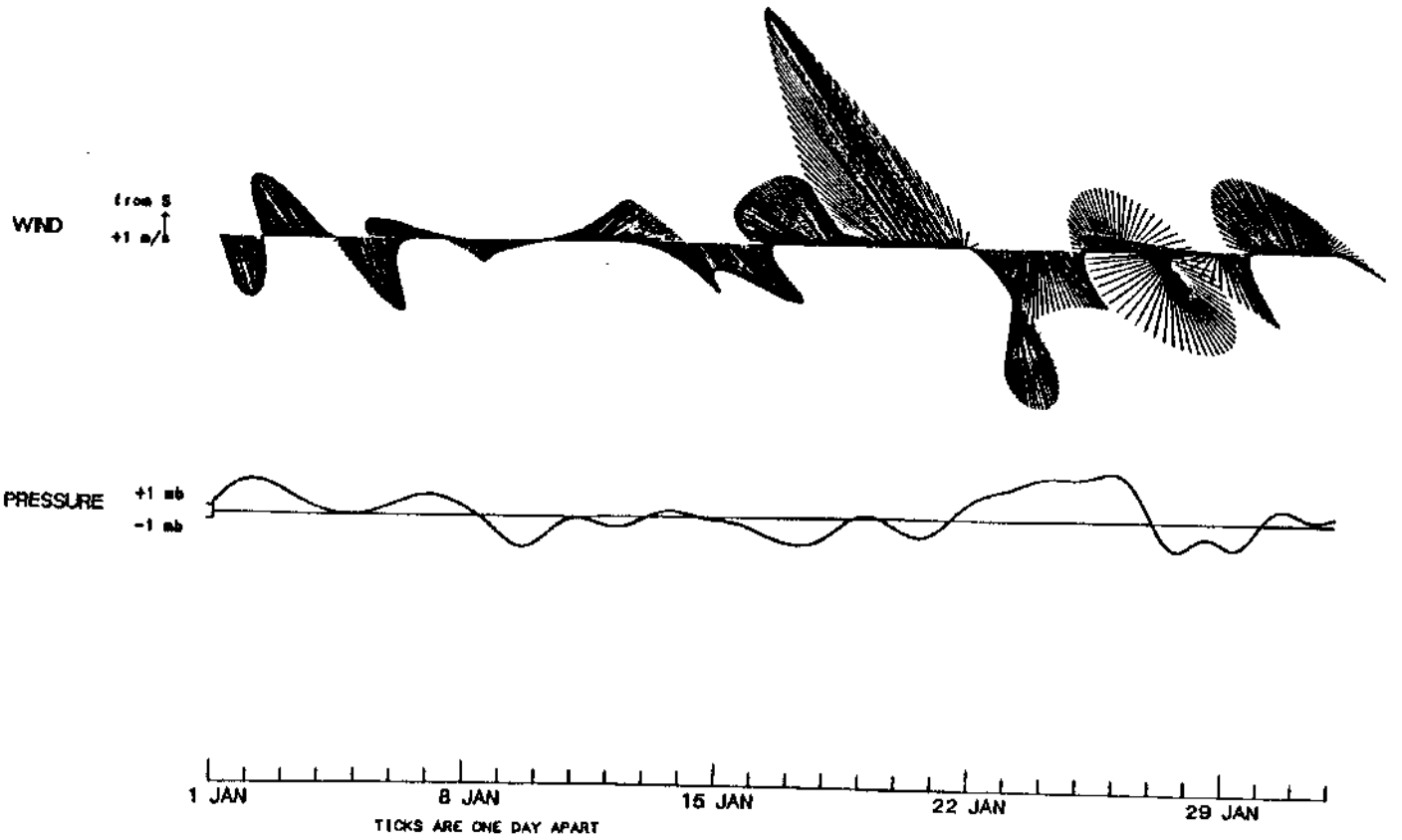

Figure 6.7d: Progressive wind vector time series, February 1983.

STATION 24 WINDS 1983

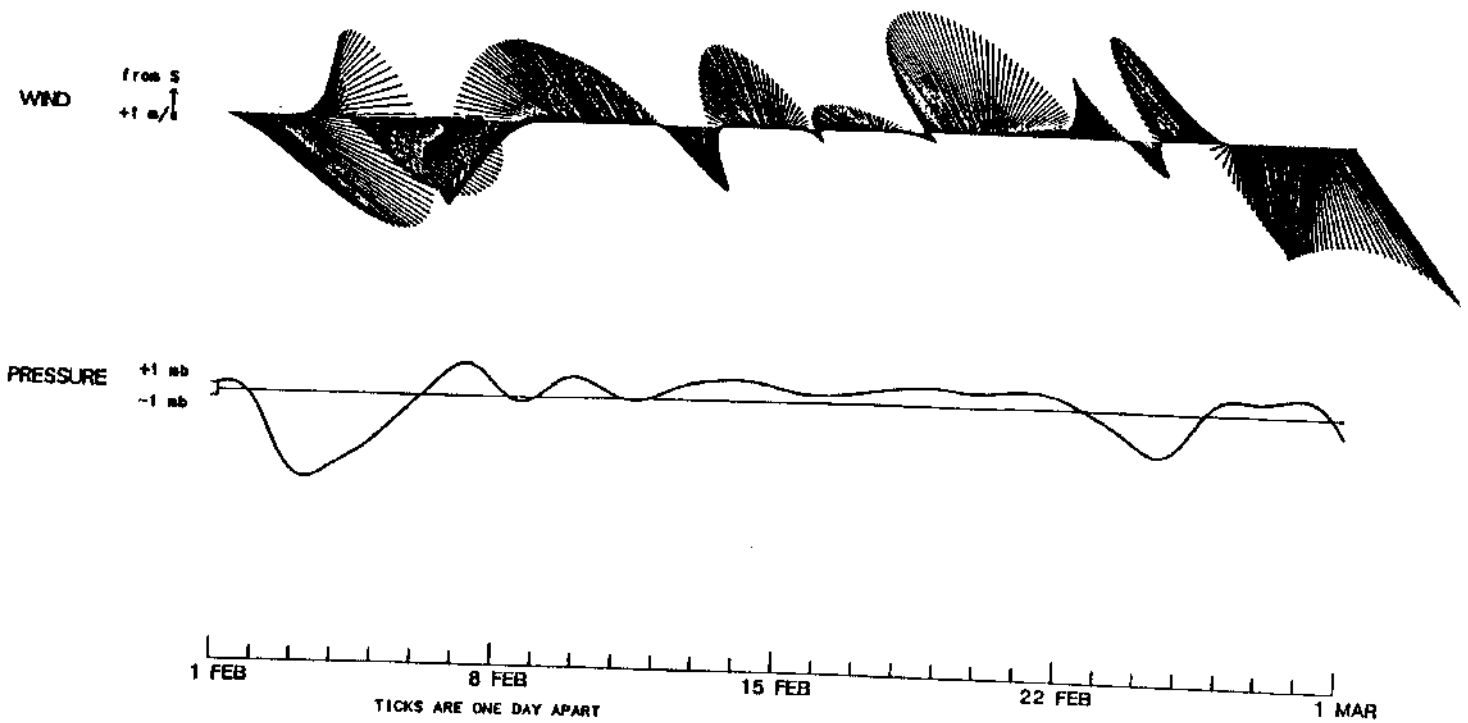

Figure 6.7e: Progressive wind vector time series, March 1983.

STATION 24 WINDS 1983

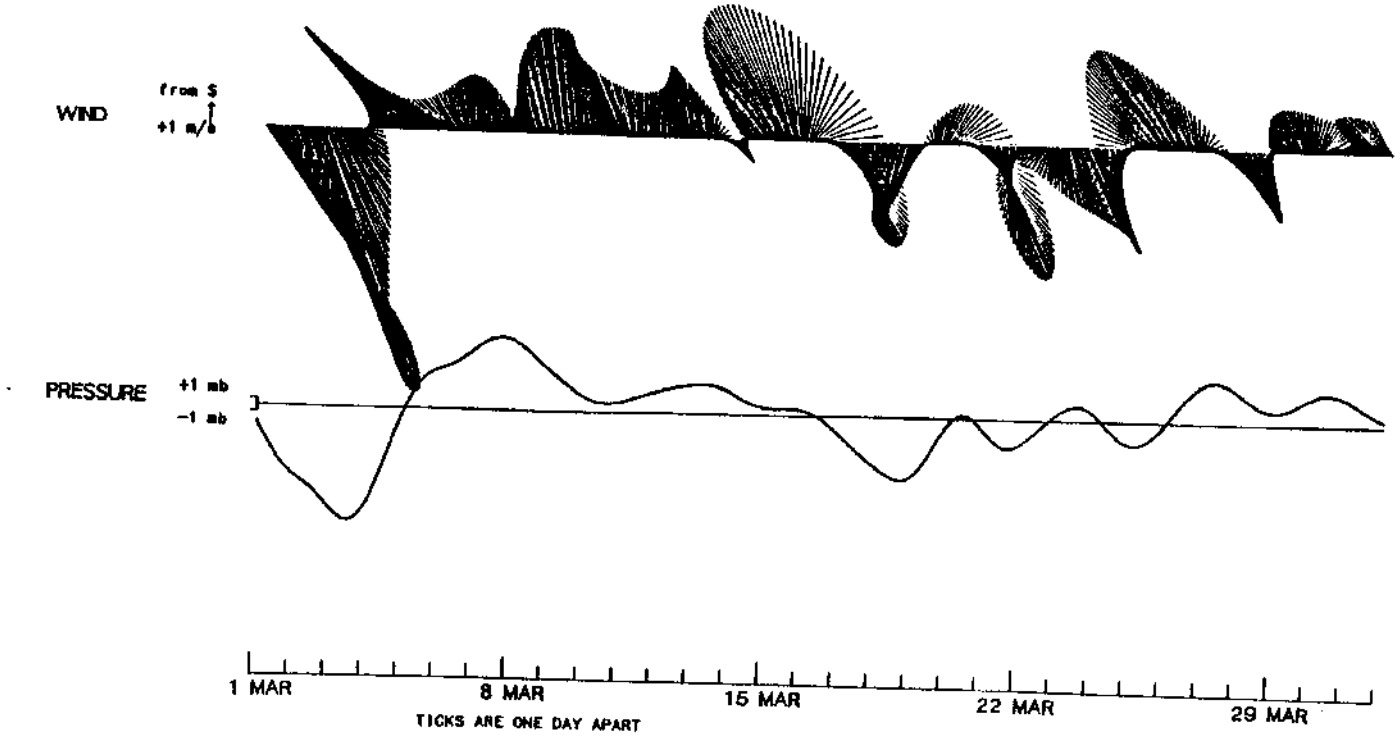

seen that the 28 November - 3 December, 20 - 25 December and 28 February - 5 March events had high wind periods of much longer duration, about twice as long as the 26 - 29 January and 1 -3 February events. The 26 - 29 January and 1 - 3 February events had slightly smaller adjusted sea level anomalies. This would seem to indicate that storm duration may play a role in determining the effectiveness of the wind stress in generating sea surface fluctuations in this frequncy range. It could also be seen how the longshore wind stress was more effective in forcing sea level variabilty than the cross-shore wind stress, confirming the statistical analysis results.

Chapter 7 Comparison of Coastal and Island Sea Level Variability

7.1 Santa Catalina Island vs. Newport Beach

Examination of filtered adjusted sea level at a coastal location, Newport Beach, CA and at the island of Santa Catalina, allows for the investigation of several physical processes. A comparison of adjusted sea level time series for Newport Beach and Santa Catalina for two time periods, the winter of 1982 - 1983 and summer of 1983, as well as a study of the meteorological conditions for the same time periods were made.

Coherency and phase spectra were computed for the adjusted sea level records at Newport Beach and Santa Catalina. In Figure 7.1a, it can be seen that the adjusted sea level signals at Santa Catalina and at Newport Beach are highly coherent (< 0.80) and in phase for the frequency range 0.8000 cpd to 0.0333 cpd, during the winter of 1982 -1983. The coherency decreased during the summer (Figure 7.1b) and the sea level at each station moved slightly out of phase. These results agreed with the results of the statistical analysis, which demonstrated that the large scale

Figure 7.1: Coherence and phase of adjusted sea level anomaly at Newport Beach and Santa Catalina island, for 26 November 1982 - 30 March 1983. When the phase < 0, Newport Beach leads Santa Catalina. Error bars provide 99% confidence limits. DOF = 72.

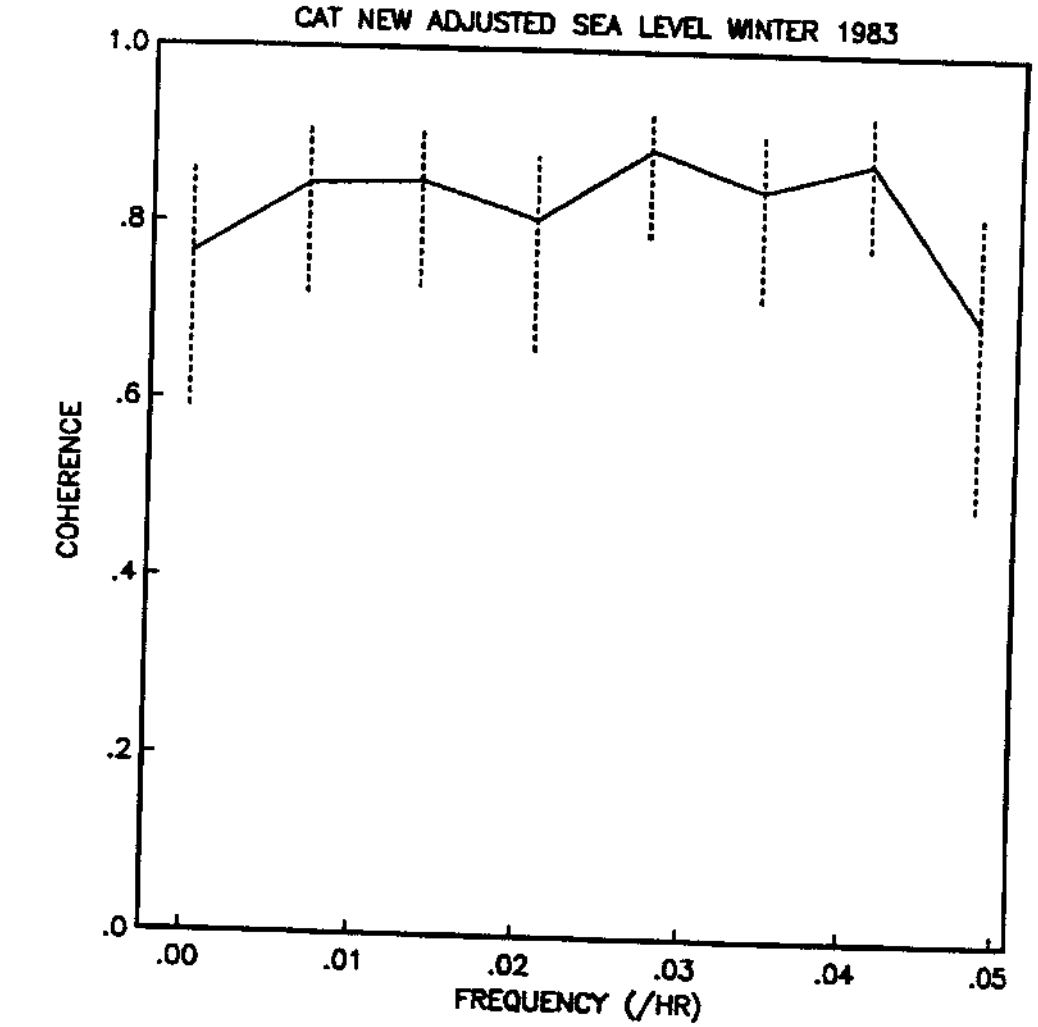
CAT NEW ADJUSTED SEA LEVEL WINTER 1983
COHERENCE
1.0
.8
.6
.4
.2
.0
.00
.01
.02
.03
.04
.05
FREQUENCY (/HR)

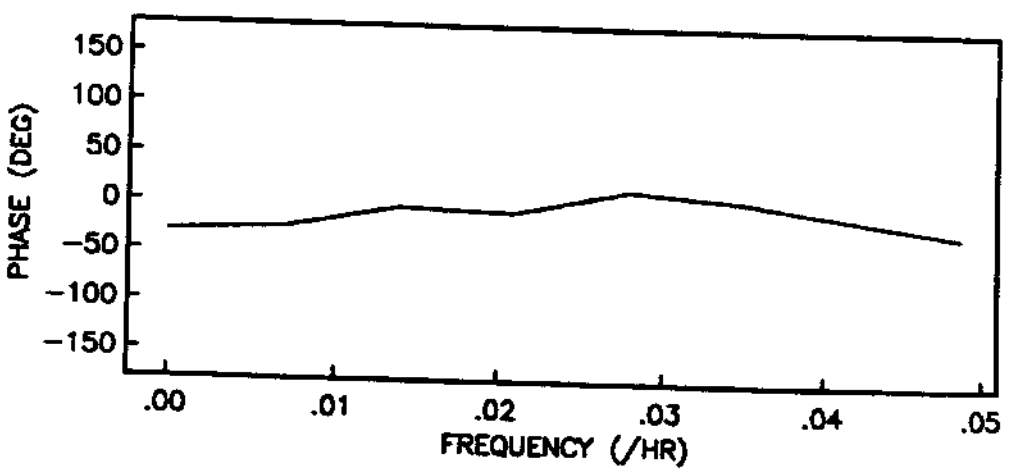
PHASE (DEG)
150
100
50
0
−50
−100
−150
.00
.01
.02
.03
.04
.05
FREQUENCY (/HR)

Figure 7.2: Coherence and phase of adjusted sea level anomaly at Newport Beach and Santa Catalina island, for 28 May 1983 - 29 September 1983. When the phase < 0, Newport Beach leads Santa Catalina. Error bars provide 99% confidence limits. DOF = 72.

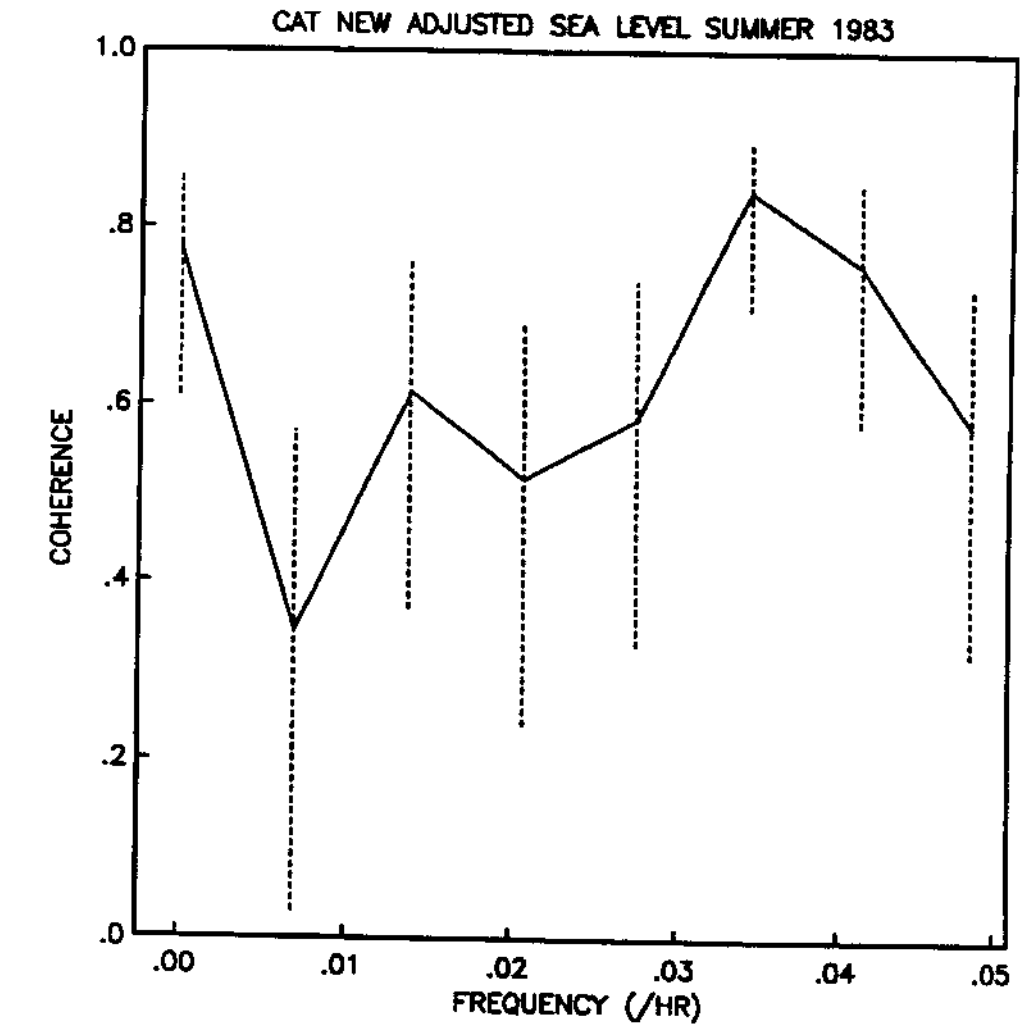
CAT NEW ADJUSTED SEA LEVEL SUMMER 1983
COHERENCE
1.0
.8
.6
.4
.2
.0
.00
.01
.02
.03
.04
.05
FREQUENCY (/HR)

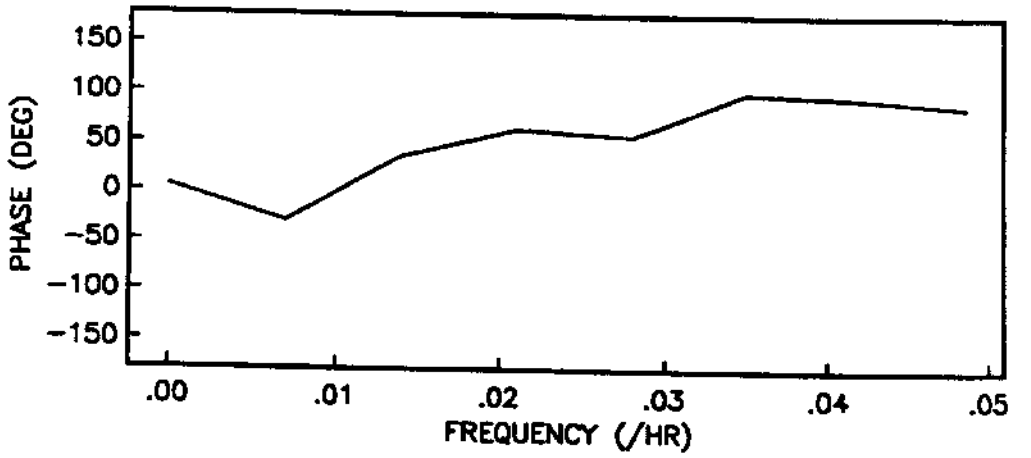
PHASE (DEG)
150
100
50
0
-50
-100
-150
.00
.01
.02
.03
.04
.05
FREQUENCY (/HR)

atmospheric pressure and wind fields play a more dominant role in forcing sea level fluctuations in the winter than in the summer. The increased influence of wind and atmospheric pressure forcing in the winter is reasonable in that the frequency of storms, with their associated high winds and pressure changes, is much higher in the winter than in the summer. The fact that the sea level was coherent at the two stations also agrees with the previous result that weather system forcing occurs at spatial scales larger than the distance between the island and the coast.

Examining the adjusted sea level at Santa Catalina and at Newport Beach and computing the difference in sea level between the two, certain large fluctuations are readily seen in the time series (Figure 7.3). The largest of these events occured in early March 1983. A total change of 12 cm in sea level difference occured over a two day period. This event began with Santa Catalina sea level 4 cm higher than Newport Beach sea level. An incoming storm caused the sea level to rise at both locations. Forty-eight hours later Santa Catalina sea level was 8 cm below Newport Beach sea level.

The maximum sea level difference reached was 8.5 cm

Figure 7.3: Time series plots of sea surface elevation difference between Santa Catalina and Newport Beach: a) 26 November 1982 - 30 March 1983, b) 28 May 1983 - 29 September 1983. When the difference > 0, Santa Catalina sea level > Newport Beach sea level.

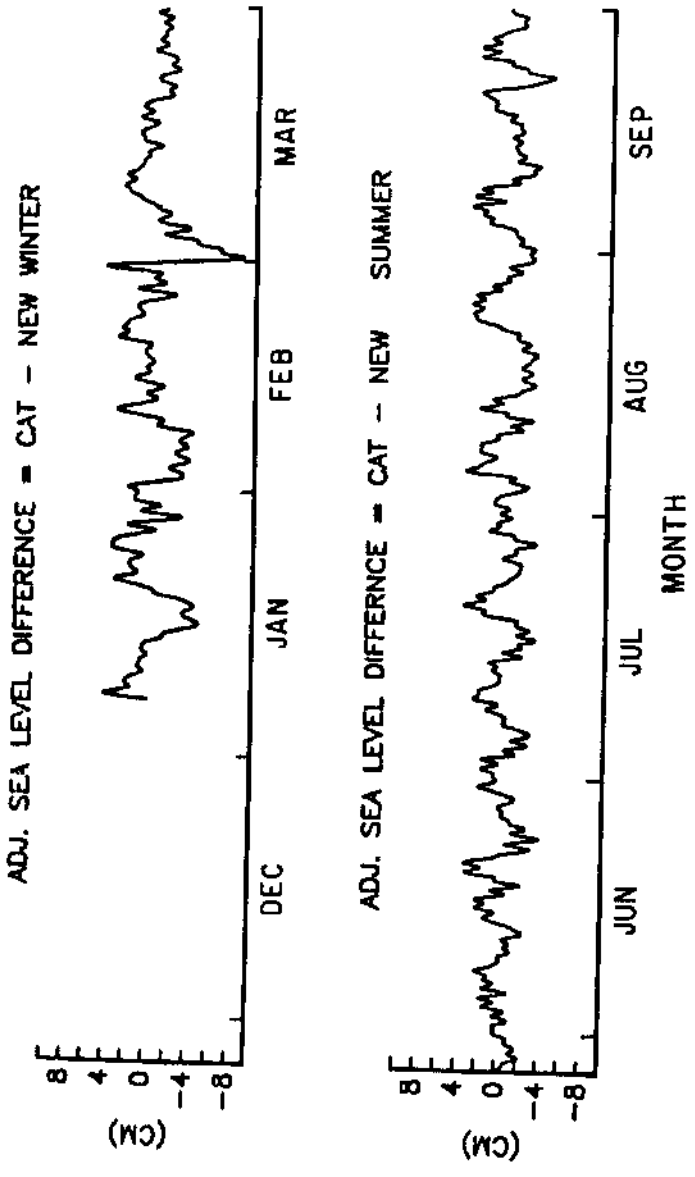
ADJ. SEA LEVEL DIFFERENCE = CAT - NEW WINTER
8
4
0
-4
-8
(CM)
DEC
JAN
FEB
MAR
ADJ. SEA LEVEL DIFFERNCE = CAT - NEW SUMMER
8
4
0
-4
-8
(CM)
JUN
JUL
AUG
SEP
MONTH

with Newport Beach sea level exceeding Santa Catalina sea level. It is generally believed that a sea surface slope of this size and spatial scale will generate a geostrophic current (Tsuchiya, 1980; Reid and Mantyla, 1976; and Reid, 1965). Assuming cross-shelf geostrophy, the speed of this current can be estimated. The cross-shelf geostrophic balance can be written:

$$fu = g\frac{\partial \eta}{\partial x} \qquad (7.1.1)$$

where: f = coriolis parameter,

g = acceleration due to gravity,

u = current speed,

η = sea surface elevation,

x = cross-shelf coordinate.

Santa Catalina Island lies approximately 50 km to the west of Newport Beach. Substituting in appropriate values for f and g, u the current speed can be calculated.

$$fu = g\frac{\partial \eta}{\partial x} = \frac{981\ cm/s}{8x10^{-5}/s} \cdot \frac{8.5\ cm}{5x10^{6} cm} = 20.8\ cm/s \qquad (7.1.2)$$

Tsuchiya (1980) and Reid (1965) computed similiar geostrophic speeds for the reversing inshore current. The inshore current flowws to the south in the summer and to the north in the winter. The sea level difference between Santa Catalina and Newport Beach is in general less than the 8.5 cm seen in early March of 1983. Though the winter is marked by several periods where Newport Beach sea level is greater than Santa Catalina sea level. These episodes seem to correspond to storm events. One possibility is that the winter storms set up the sea surface slopes which cause the inshore current to flow northward.

Examining wind velocity and atmospheric pressure records for the same time period of the large sea slope, 28 February to 8 March discussed previously, shows that a strong storm passed through the area at the same time that the sea slope developed. As the storm system entered the Southern California Bight region, wind speeds increased and were predominantly to the north. This northward flow of the wind caused a rise in sea level at both Newport Beach and Santa Catalina. As the storm neared the coast of California, wind speeds continued to increase and the direction of the winds turned to the northeast. This increase in wind speed

further increased the sea level elevations at Newport Beach and to a lesser extent at Santa Catalina. The addition of a eastward component to the wind field caused a further rise in sea level at Newport Beach that was not seen at Santa Catalina. It was this combination of both the longshore winds and cross-shore winds which caused the large difference in sea level between Santa Catalina and Newport Beach. As the storm center passed the wind speeds lessened and the wind direction reversed allowing for the the sea surface slope to relax and reverse, with Santa Catalina sea level elevation greater than Newport Beach. This sequence of events was typical for the storm episodes seen that winter. It also agrees with the regression analysis, with cross-shore wind stress leading, followed by the longshore wind stress peak and the drop in atmospheric pressure.

From this one storm event it can be readily seen that both longshore and cross-shore winds play a large role in forcing sea level fluctuations at periods longer than a day. The pressure field was seen earlier to be coherent over the spatial scales of interest and its effect at each station would be similiar. The longshore component of the wind field forces similiar sea level changes at

both Santa Catalina and Newport Beach, though to a lesser extent at the island. This would seem to support the thought that the wind forcing occurs on spatial scales larger than the island coast spacing. The onshore component of the wind behaved similarly, with a larger effect on coastal sea level than offshore. Differences in the sea level elevation at Newport Beach and Santa Catalina seem to be due to this decay in sea surface elevation in the offshore direction rather than the pile up of water against Santa Catalina. Again it seems that the sea level in the bight responds as if Santa Catalina was not present.

Chapter 8 Summary and Discussion

The winter of 1982 - 1983 was marked by the occurrence of many extreme sea level episodes. These were associated with strong North Pacific storms. Statistical analysis of the sea level anomaly, wind field, atmospheric pressure field and the sea surface temperature along with the examination of five of these extreme sea level events provides some useful insight into the generation of sea level fluctuations by meteorological forcing.

The multiple-input linear statistical analysis revealed that local meteorological forcing and sea surface temperature could explain 80% of the variance of the anomalous sea level. The results of the analysis also demonstrated agreement with the findings of Crepon (1976), to first order the inverse barometer response is accurate for the bight, although the sea surface does not exactly respond as an inverse barometer to atmospheric pressure forcing. Pressure forcing was seen to be the dominant forcing factor of sea level fluctuations in the frequency range 0.8000 cpd to 0.0333 cpd.

Sea surface temperature seemed to also play an important role in influencing sea level elevation. The above normal sea surface

temperatures characteristic of ENSO events explained up to 10% of the adjusted sea level variance in the winter of 1982 - 1983 in this frequency band and may be relatively more important at longer periods. The ENSO event was ending in the summer of 1983 and the influence of sea surface temperatures on the sea level variability reflected this, explaining only 5% of the adjusted sea level variance in the summer.

From examination and analysis of the wind fields, it was seen that wind stress could explain about 18% of the variance of the adjusted anomalous sea level record in the winter when storms were prevelent. Results for the summer showed only an 8% skill in estimating the adjusted sea level anomaly.

There were some traits which seem to be found in most of the extreme storm events. The storms were composed of peaks in both cross-shore and longshore wind stress. In the five storms examined, the cross-shore wind stress peaks lead the longshore peaks by 15 to 20 hours. Sea surface response to the wind stress peaks followed the cross-shore wind stress peak about 30 hours later. It is generally believed that longshore wind stress has a greater influence on sea level variabilty at these time scales, 1 to

30 days. This was generally true, though cross-shore wind stress effects were seen in the sea level record.

Both the statistical analysis and direct examination of the meteorological and sea level records revealed that the duration of the storm, the speed at which the storm travelled and the storm path all heavily influence how effective the storm associated winds are in causing sea level fluctuations. The spatial scale of the sea surface response to atmospheric pressure and wind was shown to be larger than the distance between the sea level stations. This was seen in the results of the statistical analysis for Santa Catalina and Newport Beach as well as from examination of the sea level record for those two stations.

Local meteorological forcing plays a major role in influencing sea level fluctuations, in the frequency range of 0.8000 cpd to 0.0333 cpd. In the winter months, when storms are common, approximately 80% of the variance can be explained by the local atmospheric pressure, wind field and sea surface temperature. In the summer the skill of the estimate drops to 45% at the coast and 60% at Santa Catalina. The remaining adjusted sea level variance is most likely due to distant

meteorologically generated sea level fluctuations which propagate into the bight from the south as coastally trapped waves.

This study was limited by the relatively short time series available at Santa Catalina island. This restricted the study to the winter of 1982-1983 and the summer of 1983. This short time series allowed for the examination of only a few storm events. This is reflected by the artificial skill of the estimates, which were approximately 0.020 for the winter of 1982-1983 and 0.04 for the summer of 1983.

The study would have been able to better examine the cross-shelf spatial scale of the sea level response if sea level data were available at more offshore locations. The geostrophic current could then be estimated at several locations throughout the bight. this would allow for a more accurate estimate as well as a more complete picture of the current to be made. At this point, current measurements within the bight, for the period of interest, would be of use for comparison between the current measurements and estimates.

A more complete study of the sea level variability should include an examination of remotely forced sea level fluctuations.

This could not be done in the present study due to the lack of sea level and meteorological data from a station south of the bight.

References

Aubrey, D. G. and K. O. Emery, 1983: Eigenanalysis of recent United States sea levels. Cont. Shelf Res., 2(1), 21-33

Barnett, T. P., 1983: Recent changes in sea level and their probable causes. Climatic Changes, 5, 15-38

Bratkovich, A., 1985: Aspects of the tidal variability observed on the Southern California continental shelf. Jour. of Phys. Ocean., 15, 225-239

Cartwright, D. E., 1982: Tidal analysis - A retrospect. Time Series Methods in Hydrosciences, 170-180

Cayan, D. R. and R. E. Flick, 1985: Extreme sea levels in San Diego, California. SIO Reference Series, 85-3, 58pp

Chelton, D. B., 1983: Effects of sampling errors in statistical estimation. Deep-Sea Research, 30(10A), 1083-1103

Chelton, D. B. and R. E. Davis, 1982: Monthly mean sea-level variability along the west coast of North America. Jour. of Phys. Ocean., 12, 757-784

Christensen, N., Jr. and N. Rodriguez, 1979: A study of sea level variations and currents off Baja California. Jour. of Phys. Ocean., 9, 631-638

Crepon, M. R., 1976: Sea level, bottom pressure and geostrophic adjustment. Memoires Societe Royale de Sciences de Liege, 10(6), 43-60

Dickson, R. E. and R. Livezey, 1984: On the contribution of major warming episodes in the tropical east Pacific to a useful prognostic relationship based on the southern oscillation. Jour. of Clim. and Appl. Meteorol., 23, 194-200

Dorman, C. E., 1982: Winds between San Diego and San Clemente Island. Jour. of Geophys. Res., 87(C12), 9636-9646

Emery, K. O. and K. Hamilton, 1985: Atmospheric forcing of interannual variability in the northeast Pacific Ocean: connections with El Nino. Jour. of Geophys. Res., 90, 857-868

Enfield D. B. and J. S. Allen, 1980: On the structure and dynamics of monthly mean sea level anomalies along the Pacific coast of North and South America. Jour. of Phys. Ocean., 10, 557-578

Enfield D. B. and J. S. Allen, 1983: The generation and propagation of sea level variability along the Pacific coast of Mexico. Jour. of Phys. Ocean., 13, 1012-1033

Estoque, M. A., 1961: A theoretical investigation of the sea breeze. Quart. Jour. of the Roy. Met. Soc., 87, 136-146

Estoque, M. A., 1962: The sea breeze as a function of the prevailing synoptic situation. Jour. Atmos. Sci., 19, 244-250

Fisher, E. L., 1977: A theoretical study of the sea breeze. Jour. Meteorol., 18, 216-233

Flather, R. A., 1976: In "Mathematical Models in Geophysics", Proc. Moscow Symp., Aug 1971. IAHS-AISH Pub. NO. 116, 215pp

Flick, R. E. , 1986: A review of conditions associated with high sea levels in Southern California. Science of the Total Environment, 55, 251-159

Flick, R. E. and D. R. Cayan, 1985: Extreme sea levelson the coast of California. Proc. of the 19th Coastal Eng. Conf., 1, 886-898

Heaps, N. S., 1965: Storm surges on a continental shelf. Phil. Trans. Roy. Soc., A257, 351-383

Kanasewich, E. R., 1981: Time sequence analysis in geophysics., The Univ. of Alberta Press, 480pp

Lentz, S. J., 1984: Subinertial motions on the Southern California continental shelf. A dissertation submitted in partial satisfaction of the requirements for the degree of Doctor of Philosophy in Oceanography at the Univ. of Calif., San Diego

Lisitzen, E., 1974: Sea level changes., Elsevier Scientific, 286pp

McIntyre, R. J., 1979: Analytic models for west coast storm surges, with application to events of January 1976. Appl. Math. Modelling, 3, 89-98

Munk, et al, 1970: Tides offshore: Transition from California coastal to deep-sea waters. Geophys. Fluid Dyn. 1, 161-235

Mysak, L. A., 1980: Recent advances in shelf dynamics. Rev. Geophys. Space Phys., 18, 211-241

Namias, J. and D. R. Cayan, 1984: El Nino: implications for forecasting. Oceanus., 27, 41-47

Quiroz, R. S. 1983: The climate of the El Nino winter of 1982-1983, a season of extraordinary climate anomalies. Mon. Weath. Rev., 3, 1685-1706

Reid, J. L. and A. W. Mantyla, 1976: The effect of the geostrophic flow upon coastal sea elevations in the northern North Pacific Ocean. Jour. Geophys. Res., 81(18), 3100-3110

Roden, G. I., 1966: Low frequency sea level oscillations along the Pacific coast of North America. Jour. Geophys. Res., 71, 4755-4775

Roed, L. P. 1979: Storm surges in stratified seas. Tellus, 31, 330-339

Seymour, R. J., R. R. Strange, D. R. Cayan and R. A. Nathan, 1984: Influence of El Ninos on California's wave climate. Proc. 19th Int. Conf. Coastal Eng., Amer. Soc. Civil Eng., 577-592

Simpson, J. J., 1983: Large-scale thermal anomalies in the California current during the 1982-1983 El Nino. Geophys. Res. Let., 10, 937-940

Simpson, J. J., 1984: El Nino - induced onshore transport in the California current during 1982-1983. Geophys. Res. Let., 11, 241-242

Tsuchiya, M., 1980: Inshore circulation in the Southern California Bight, 1974-1977. Deep-Sea Res., 27A, 99-118

Walsh, J. E., 1974: Sea breeze theory and applications. Jour. Atmos. Sci., 31, 2012-2026

Wyrtki, K., 1985: Sea level fluctuations in the Pacific during the 1982-1983 El Nino. Geophys. Res. Let., 12, 125-128

Zetler, B. D. and R. E. Flick, 1985a: Predicted extreme high tides for California, 1983-2000. Jour. Waterway, Port, Coastal and Ocean Div., ASCE, 3, 758-765

Zetler, B. D. and R. E. Flick, 1985b: Predicted extreme high tides for mixed tidal regimes. Jour. Phys. Ocean., 15, 357-359